

Response to Reviewers

Manuscript Number : acp-2015-729

Manuscript Title : Optical properties of atmospheric fine particles near Beijing during the HOPE-J³A Campaign

We thank both reviewers for their thoughtful and thorough reviews of our manuscript. Point-by-point reviewers' comments are attached below.

Response to Reviewer #1 comments

I find that the authors have done a reasonably good job of addressing the reviewer concerns. However, I believe that a few issues must be fully addressed prior to publication.

[1] P16, L30: The authors should change this such that it does not say that the n and SSA values were larger than for period 4. I see that they say now “within uncertainties,” but this is not sufficient here given that (i) the SSA values are different outside of the standard deviations (not uncertainties, technically), (ii) the n values are identical within the standard deviations and (iii) the k values are actually smaller than those reported for Period 4. Thus, this remains incorrect. The authors must be more specific here regarding each term (SSA, n and k) that is being compared.

The reviewer is correct in pointing this out. We revised this statement accordingly:

The mean values of ω_{470} , n and k were 0.86 ± 0.01 , 1.44 ± 0.03 , and 0.02 ± 0.01 , respectively. The SSA values were larger than those reported for Period 4. In general, the n values were higher and the k values lower than those seen in Period 4, although the mean values of both properties fall within the combined standard deviations of both periods.

[2] P14, L3: The authors have revised their statements regarding the increasing importance of “inorganic species” during haze periods. However, I still find this to be inconsistent with their measurements. They state “The significant increase in the concentration and fractional contribution to PM_{1.0} extinction coefficient of inorganic species, particularly nitrates (discussed in Section 4.3), indicate that inorganic species become more important during haze...” However, they observe that the fraction of PM₁ that is sulfate actually decreases. Thus, this statement is too general. It is not “particularly nitrates”, but “specifically nitrates.” The authors should make the statement specific (and avoid using terms such as “significant” unless they mean

it in a statistically significant manner): “The notable increase in the concentration and fractional contribution to PM_{1.0} extinction coefficient of nitrate (discussed in Section 4.3), indicate that nitrate becomes more important during haze...”

We think the natural interpretation in our text of “inorganic species” is “all inorganic species considered together”, in contradistinction to OM and EC. So, we see no inconsistency between our description and our measurements, as the reviewer does. The changes we observe are similar to those seen in other Chinese haze episodes, in which the OM fraction often decreases while the inorganic fraction increases. This point is missed in the reviewer’s suggested rephrasing. Nevertheless, we have adopted some of the reviewer’s suggestions to improve the clarity of our text:

The notable increase in the concentration and fractional contribution to PM_{1.0} extinction coefficient of inorganic species, and specifically nitrate and ammonium, indicate that the inorganic contribution to particulate matter becomes relatively more important than the OM fraction during haze.

[3] P21, L2: *It is not clear what is meant by “improved mass extinction efficiencies.” Improved relative to what? Do they mean their “modified” (i.e. wavelength-adjusted) values?*

We meant the IMPROVE calculation. We rewrote this sentence (to shorten the length of the paper, we removed this part to the supplement, Section S2):

With modified IMPROVE function (Eq. S7), the agreement between the measured and calculated PM_{1.0} extinctions is good (with a slope of 1.04 ± 0.04) when the measured extinction coefficient is lower than 300 Mm^{-1} (as shown in the insert of Fig. S3c).

[4] P23, L15: *The measurements do not support the notion that the “EC fraction decreased with increasing pollution level.” The values given are $4.3 \pm 3.6\%$, $4.0 \pm 2.0\%$ and $3.6 \pm 1.1\%$. These are all identical within the large uncertainties (i.e. standard deviations). This should be revised, along with the relationship with the previous sentence.*

According to comment [5], we rewrote this part. The statement of “EC fraction decreased with increasing pollution level.” was removed from the revised manuscript.

[5] P23, L20 onwards: *I find this discussion to be unclear. The authors are comparing their measured MSE and MAE values with calculated values from the IMPROVE algorithm. This is fine, but also potentially not useful. In particular, the*

IMPROVE algorithm is a crude approximation to actual behavior (it assumes some aspect of the size distribution and treats size distributions in a binary manner of “small” and “large”). It can give an idea of what is going on, but quantitative comparison is not warranted unless the goal is to develop regionally-specific coefficients for use in the algorithm based on the observations (which is where the numbers in the algorithm come from in the first place). The authors don’t really do anything with the MSE comparison, besides note that a disparity exists. I find that discussion here is still lacking. **Regarding the MAEs and the conclusions regarding “brown carbon,” the authors’ logic is now easier to follow. However, they should also consider other possibilities, such as that the absorption by EC might itself be “enhanced” due to coatings, especially since the wavelength considered here is not especially far into the blue. Regarding the Wang et al. reference, the authors should indicate the wavelength in that study.**

Related to the above comment, the authors **did not address the issue of what the MAE values are relative to EC specifically**, which is a much better metric of comparison than the MAE for PM1. From the authors’ assumption, the MAE for EC in the *IMPROVE* algorithm equals the MEE for EC, and thus is equal to 10 m²/g. First, this assumption is not really correct as the SSA of EC is not zero (more commonly, values of ~0.2 are found, indicating that the MAE values are actually about only 80% of the MEE values. This uncertainty is not accounted for in Fig. 11 or the associated discussion.) I calculate from Table 1 EC-specific MAE values of 24.2, 32.0, 33.4 and 27.4 m²/g for the four periods (clear, slightly polluted, polluted and all). From the arguments presented by the authors, I would compare these values to 10 m²/g, meaning that the observed MAE values are 2.4, 3.2, 3.3 and 2.7 times as large as the *IMPROVE* value. This would imply then that if BrC were the reason for this disparity that it contributes about 60-70% of the total absorption. These fractions would be even larger if I assumed that the MAE for EC from *IMPROVE* should only be about 8 m²/g (instead of 10). This seems very large to me given the measurement wavelength (467 nm). But perhaps it is correct. Nonetheless, **I strongly suggest that the authors present a more direct discussion of the EC-specific values (which I implied in my prior review, but perhaps I was not explicit enough). However, associated with this, I think the authors should provide some discussion as to the reasonableness of their observed EC-specific MAE values (which, again, to me seem very large but not out of the realm of possible). I think that a presentation of the EC-specific values would be much clearer than the discussion of the PM1 values as it focuses the discussion on the key measured absorbing component.**

We thank the reviewer for the constructive comment and suggestion. We provided more discussion on the EC-specific MAE values in the revised manuscript. We found that : under polluted conditions, the average mass absorption efficiencies (MAE) of EC were up to 4 times as large as the reference MAE value for freshly generated black carbon (BC). The temporal pattern of MAE values was similar to that of the OC/EC ratio, suggesting that non-BC absorption from secondary organic aerosol (SOA) also contributes to particle absorption.

Following part was added to Section 4.3 in the revised manuscript.

4.3 Mass Absorption Efficiency of EC

The mass absorption efficiency (MAE, in units of $\text{m}^2 \text{g}^{-1}$) of EC is calculated according to (Knox et al., 2009; Bond et al., 2013; Cheng et al., 2011; 2016):

$$\text{MAE} = \frac{\int_{t_1}^{t_2} \alpha_{\text{abs}} dt}{\text{EC}_m \times (t_2 - t_1)} \quad (4)$$

where α_{abs} (Mm^{-1}) is the measured value of the absorption coefficient at $\lambda = 470 \text{ nm}$, and EC_m ($\mu\text{g m}^{-3}$) is the measured EC mass concentration with the aerosol carbon analyzer. t_1 and t_2 are the start and stop times for the collection of samples with quartz filters. In this work, the integration time was determined by the quartz filter sampling period of 12 h sample^{-1} . For comparison, the MAE of freshly generated BC is $8.7 \text{ m}^2 \text{g}^{-1}$ at $\lambda = 470 \text{ nm}$ (based on a $7.5 \pm 1.2 \text{ m}^2 \text{g}^{-1}$ at $\lambda = 550 \text{ nm}$ and using the inverse wavelength dependence) (Bond et al., 2006).

Similar time profiles are seen for the measured absorption coefficient at $\lambda = 470 \text{ nm}$ and the measured mass concentrations of EC and OC (Fig. 7 (a) and (b)). Assuming that only EC contributes to aerosol absorption, the MAE of EC can be calculated using Eq. (4). The MAE values of EC at $\lambda = 470 \text{ nm}$ over the campaign period are shown in Fig. 7 (c). These values vary widely, with lower values generally seen under cleaner conditions and higher values observed under more polluted conditions. The MAE values for selected clear days (e.g. Nov. 17 - 18; Dec. 1 - Dec. 3; Dec. 29, 2014 - Jan. 1, 2015) ranged from $7 - 14 \text{ m}^2 \text{g}^{-1}$ (average of $10.3 \pm 2.7 \text{ m}^2 \text{g}^{-1}$) and are comparable to those reported in Beijing during the summer ($5 - 13 \text{ m}^2 \text{g}^{-1}$) (Cheng et al., 2011). Much higher values were seen on polluted days, where the MAE ranged from 23 to $81 \text{ m}^2 \text{g}^{-1}$ (average of $48 \pm 21 \text{ m}^2 \text{g}^{-1}$) for the period covered Dec. 23 - 28, 2014 and from 20 to $49 \text{ m}^2 \text{g}^{-1}$ (average of $42 \pm 14 \text{ m}^2 \text{g}^{-1}$) for Jan. 2

- 5, 2015. These values are comparable to those reported by Chan et al. (2011), where MAE ranged from 10 to 50 m² g⁻¹.

The average EC mass concentrations were $0.48 \pm 0.39 \mu\text{g m}^{-3}$, $1.18 \pm 0.59 \mu\text{g m}^{-3}$, and $2.72 \pm 0.87 \mu\text{g m}^{-3}$, for clear, slightly polluted, and polluted days, respectively. The corresponding mass fractions of $4.3 \pm 3.6\%$, $4.0 \pm 2.0\%$, and $3.6 \pm 1.1\%$ were approximately equal within the large variability seen on different days. The mean and standard deviations of MAE values of EC were $23.0 \pm 14.0 \text{ m}^2 \text{ g}^{-1}$, $32.7 \pm 16.0 \text{ m}^2 \text{ g}^{-1}$, and $35.0 \pm 21.7 \text{ m}^2 \text{ g}^{-1}$, respectively, for clear, slightly polluted, and polluted days. Our values suggest that EC absorption was strongly enhanced over the campaign period. Enhanced absorption (E_{abs}) could arise from the coating-enhancement of ambient BC absorption (lensing-driven enhancement), as well as absorption associated with light-absorbing organic compounds (brown carbon, BrC) (Andreae and Gelencsér 2006; Bond et al., 2013; Gustafsson, and Ramanathan, 2016). In general, light absorption from other organic species tends to be relatively small at $\lambda = 470 \text{ nm}$, whether it arises from small nitroaromatic compounds (Claeys et al., 2012) or from larger HULIS-type substances (Lorenzo and Young, 2016).

Laboratory studies report a BC enhancement factor from 1.8 to 2 for thicker coatings (Bond et al., 2013). Results from field observations are more variable (Peng et al., 2016): reported E_{abs} values ranged from 1.06 (Cappa et al. 2012; Lan et al., 2013) to 1.7 (Lack et al. 2012; Liu et al., 2015), although two recent studies (Cui et al., 2016; Peng et al., 2016) have found that for aged BC (18 h and 4.6 h after fresh emission in clear and polluted condition, respectively), E_{abs} ranged from 2 to 3. Compared to freshly emitted BC, we observe average absorption enhancements of 2.6 (clear), 3.8 (slightly polluted), and 4.0 (polluted) for different days. Our values are somewhat higher, although broadly consistent with, the Peng (2016).

Our individual MAE of EC values are often appreciably higher than has been observed in other studies (Andreae et al., 2008; Cheng et al., 2011; Wang et al., 2014). This difference may arise from either measurement uncertainties or the contribution of other absorbing species. Large MAE values could arise in part from inaccuracies in both the EC mass concentration or α_{abs} (which is itself determined from the relatively small difference between the extinction and scattering measurements). Moreover, our assumption that all particle absorption arises from EC would lead to higher MAE values if there was simultaneous absorption by other species. L. Wang et al. (2013) have recently shown that BrC was the second-largest absorbing aerosol constituent in Beijing (with a volume fraction of 5 - 25%

in the total aerosol volume) and exhibits a clear seasonal variation (dominates in late fall and winter, and extremely low in summer). The sources of BrC have been reported to be the organic components primary emitted from the combustion of biomass and fossil fuels. In a study of biomass burning particle, Lack et al. (2012) showed that the contribution of the absorption of BrC was about 27% at $\lambda = 404$ nm, while other recent studies (Nakayama et al., 2013; Moise et al., 2015) have shown that secondary organic aerosol may also act as BrC.

Our data provide some support for the suggestion that SOA is absorbing. Since primary OC and EC are mostly emitted from the same source, EC is a good tracer of primary combustion-generated carbon emissions and the OC/EC ratio can be used as an indicator for the formation of SOA (Cheng et al., 2011). Time-resolved OC and EC data provide a better understanding of the dynamics of SOA formation. In this work, the pattern of MAE coincided well with OC/EC ratio, suggesting that SOA has a non-negligible absorption on polluted days. This also implies that our MAE values reported above are upper limits, and that the absorption contribution of EC is likely to be somewhat smaller.

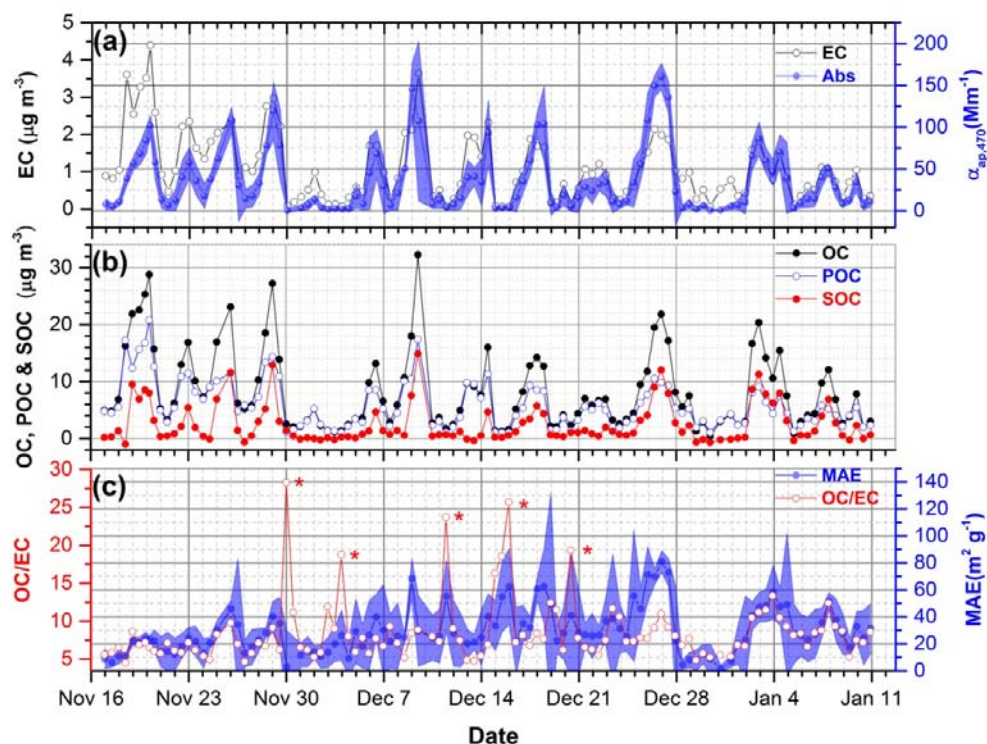


Fig. 8 Time series of (a) the measured EC mass concentrations and absorption coefficients at $\lambda = 470$ nm; (b) the measured OC mass concentrations, and the estimated primary OC (POC) and secondary OC (SOC) mass concentrations determined with the EC-tracer method (Lim and Turpin, 2002; Lin et al., 2009; Cheng et al., 2011, the details of the calculation method are given in the Supplement, Section S7.). (c) the MAE values of EC and OC to EC ratio (OC/EC). The MAE was calculated by dividing the measured absorption coefficient by the measured concentration of EC. The blue shaded areas indicate the standard deviation. The red stars associated with unusually high values in (c) may arise from artifacts arising from sampling or handling of the filter.

Following part was added to the revised supporting information.

S7 EC-tracer method for the estimation of secondary organic carbon

EC is a good tracer of primary generated organic carbon (POC). Ambient OC/EC ratios larger than the OC/EC ratio of the primary ($(OC/EC)_{pri}$) indicate the formation of secondary organic carbon (SOC). The concentrations of POC and SOC can be calculated with (Turpin and Huntzicker, 1995; Lim and Turpin, 2002; Lin et al., 2009):

$$OC_{pri} = EC \times (OC/EC)_{pri} + N$$

$$OC_{sec} = OC_{tot} - OC_{pri}$$

where OC_{sec} is the SOC and OC_{tot} is the measured ambient OC concentration. The concentration of POC (OC_{pri}) could be calculated by the product of measured EC concentration and the estimated $(OC/EC)_{pri}$. N is the contribution of POC from noncombustion sources or sample artifacts.

The estimation of $(OC/EC)_{pri}$ is based on the method used by Lim and Turpin (2002). The scattering plot of OC and EC concentrations for the full campaign is shown in Fig. S8. The lowest 20% percentile of ambient OC/EC ratios (shown in green dot points in Fig. S8) were used for the determination of $(OC/EC)_{pri}$. Time series of the estimated of POC and SOC mass concentrations are shown in Fig. S9.

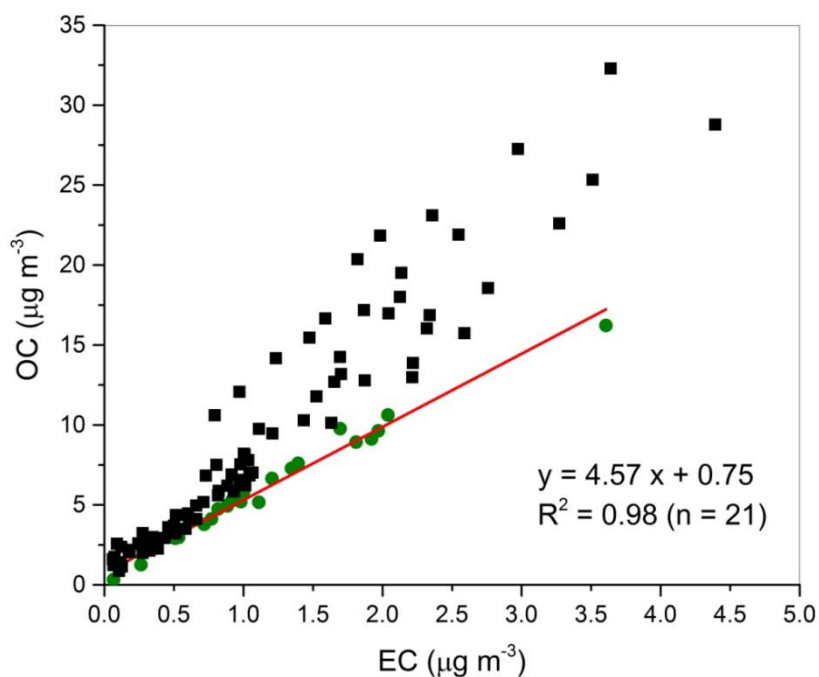


Fig. S8 Scatter plot of OC and EC concentrations. The green dot points were used to calculate the primary OC/EC.

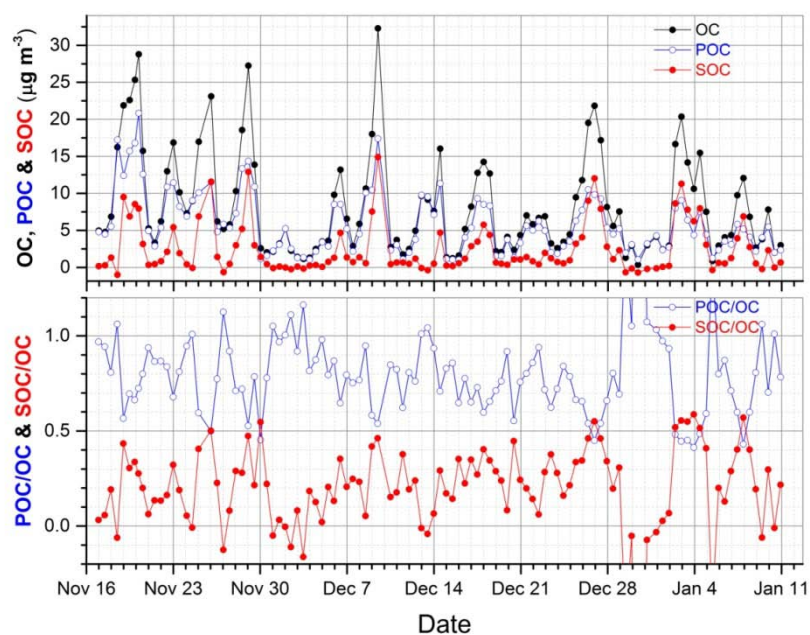


Fig. S9 Time series of (a) the measured OC mass concentrations, and the estimated primary OC (POC) and secondary OC (SOC) mass concentrations determined with EC-tracer method. (b) the percentage of POC and SOC in OC.

References:

- Andreae, M. O. and Gelencsér, A.: Black carbon or brown carbon? The nature of light-absorbing carbonaceous aerosols, *Atmos. Chem. Phys.*, 6, 3131-3148, doi:10.5194/acp-6-3131-2006, 2006.
- Andreae, M.O., Schmid, O., Yang, H., Chand, D., Yu, J.Z., Zeng, L.-M., and Zhang, Y.-H.: Optical properties and chemical composition of the atmospheric aerosol in urban Guangzhou, China, *Atmos. Environ.*, 42, 6335–6350, 2008.
- Bond, T. C., Doherty, S. J., Fahey, D. W., Forster, P. M., Berntsen, T., DeAngelo, B. J., Flanner, M. G., Ghan, S., Kärcher, B., Koch, D., Kinne, S., Kondo, Y., Quinn, P. K., Sarofim, M. C., Schultz, M. G., Schulz, M., Venkataraman, C., Zhang, H., Zhang, S., Bellouin, N., Guttikunda, S. K., Hopke, P. K., Jacobson, M. Z., Kaiser, J. W., Klimont, Z., Lohmann, U., Schwarz, J. P., Shindell, D., Storelvmo, T., Warren, S. G., and Zender C. S.: Bounding the role of black carbon in the climate system: A scientific assessment, *J. Geophys. Res. Atmos.*, 118, 5380 - 5552, doi:10.1002/jgrd.50171, 2013.
- Bond, T. C., Habib, G., and Bergstrom, R. W.: Limitations in the enhancement of visible light absorption due to mixing state, *J. Geophys. Res.*, 111(D20), 211, doi:10.1029/2006JD007315, 2006.
- Cappa, C. D., Onasch, T. B., Massoli, P., Worsnop, D. R., Bates, T. S., Cross, E. S.,

- Davidovits, P., Hakala, J., Hayden, K. L., Jobson, B. T., Kolesar, K. R., Lack, D. A., Lerner, B. M., S. M., Mellon, D., Nuaaman, I., Olfert, J. S., Petäjä, T., Quinn, P. K., Song, C., Subramanian, R., Williams, E. J., and Zaveri, R. A. : Radiative absorption enhancements due to the mixing state of atmospheric black carbon, *Science*, 337, 1078 - 1081, doi:10.1126/science.1223447, 2012.
- Cao, G., Zhang, X., Gong, S., An, X., and Wang, Y.: Emission inventories of primary particles and pollutant gases for China, *Chinese Sci. Bull.*, 56, 781 - 788, 2011.
- Chan, T. W., Brook, J. R., Smallwood, G. J., and Lu, G.: Time resolved measurements of black carbon light absorption enhancement in urban and near-urban locations of southern Ontario, Canada, *Atmos. Chem. Phys.*, 11, 10407 - 10432, doi:10.5194/acp-11-10407-2011, 2011.
- Cheng, Y., He, K.-B., Zheng, M., Duan, F.-K., Du, Z.-Y., Ma, Y.-L., Tan, J.-H., Yang, F.-M., Liu, J.-M., Zhang, X.-L., Weber, R. J., Bergin, M. H., and Russell, A. G.: Mass absorption efficiency of elemental carbon and water-soluble organic carbon in Beijing, China, *Atmos. Chem. Phys.*, 11, 11497-11510, doi:10.5194/acp-11-11497-2011, 2011.
- Cheng, Y., Engling, G., Moosmüller, H., Arnott, W.P., Chen, L.W.A., Wolde, C. E., Min Hao, W.M., and He, K.B.: Light absorption by biomass burning source emissions, *Atmos. Environ.*, 127, 347 - 354, 2016.
- Claeys, M., Vermeylen, R., Yasmeen, F., Gómez-González, Y., Chi, C., Maenhaut, W., Mészáros, T., and Salma, I.: Chemical characterisation of humic-like substances from urban, rural and tropical biomass burning environments using liquid chromatography with UV/vis photodiode array detection and electrospray ionisation mass spectrometry, *Environ. Chem.*, 9, 273-284, 2012.
- Cui, X., Wang, X., Yang, L., Chen, B., Chen, J., Andersson, A, and Gustafsson, Ö. : Radiative absorption enhancement from coatings on black carbon aerosols, *Sci. Total Environ.*, 551-552, 51 - 56, 2016.
- Di Lorenzo, R. A., and Young C. J.: Size separation method for absorption characterization in brown carbon: Application to an aged biomass burning sample, *Geophys. Res. Lett.*, 43, 458–465, doi:10.1002/2015GL066954, 2016.
- Gustafsson, Ö., and Ramanathan, V.: Convergence on climate warming by black carbon aerosols, *Proc. Nat. Acad. Sci. USA*, 113, 4243 - 4245, doi: 10.1073/pnas.1603570113, 2016.
- Knox, A., Evans, G. J., Brook, J. R., Yao, X., Jeong, C. H., Godri, K. J., Sabaliauskas, K., and Slowik, J. G. : Mass absorption cross-section of ambient black carbon aerosol in relation to chemical age, *Aerosol Sci. Technol.*, 43, 522 - 532, 2009.
- Lack, D. A., Langridge, J. M., Bahreini, R., Cappa, C. D., Middlebrook, A. M., and Schwarz, J. P. : Brown carbon and internal mixing in biomass burning particles, *Proc. Nat. Acad. Sci. USA*, 109, 14802 - 14807, 2012.

- Lan, Z.-J., Huang, X.-F., Yu, K.-Y., Sun, T.-L., Zeng, L.-W., and Hu, M.: Light absorption of black carbon aerosol and its enhancement by mixing state in an urban atmosphere in South China, *Atmos. Environ.*, 69, 118 - 123, 2013.
- Liu, S., Aiken, A.C., Gorkowski, K., Dubey, M.K., Cappa, C.D., Williams, L.R., Herndon, S.C., Massoli, P., Fortner, E.C., Chhabra, P.S., Brooks, W.A., Onasch, T.B., Jayne, J.T., Worsnop, D.R., China, S., Sharma, N., Mazzoleni, C., Xu, L., Ng, N.L., Liu, D., Allan, J.D., Lee, J.D., Fleming, Z.L., Mohr, C., Zotter, P., Szidat, S., and Prevot, A.S.H.: Enhanced light absorption by mixed source black and brown carbon particles in UK winter, *Nat. Commun.*, 6, 8435, 2015.
- Lim, H.-J., and Turpin B. J. : Origins of primary and secondary organic aerosol in Atlanta: Results of time-resolved measurements during the Atlanta supersite experiment, *Environ. Sci. Technol.*, 36, 4489–4496, 2002.
- Lin, P., Hu, M., Deng, Z., Slanina, J., Han, S., Kondo, Y., Takegawa, N., Miyazaki, Y., Zhao, Y., and Sugimoto N. : Seasonal and diurnal variations of organic carbon in PM_{2.5} in Beijing and the estimation of secondary organic carbon, *J. Geophys. Res.*, 114, D00G11, doi:10.1029/2008JD010902, 2009.
- Moise, T., Flores, J.M., and Rudich, Y.: Optical Properties of Secondary Organic Aerosols and Their Changes by Chemical Processes, *Chem. Rev.*, 115, 4400 - 4439, 2015.
- Nakayama, T., Sato, K., Matsumi, Y., Imamura, T., Yamazaki, A., and Uchiyama, A.: Wavelength and NO_x dependent complex refractive index of SOAs generated from the photooxidation of toluene, *Atmos. Chem. Phys.*, 13, 531-545, doi:10.5194/acp-13-531-2013, 2013.
- Peng, J., Hua, M., Guo, S., Du, Z., Zheng, J., Shang, D., Zamora, M. L., Zeng, L., Shao, M., Wu, Y.-S., Zheng, J., Wang, Y., Glen, C. R., Collins, D. R., Molina, M. J., and Zhang, R. : Markedly enhanced absorption and direct radiative forcing of black carbon under polluted urban environments, *Proc. Nat. Acad. Sci. USA*, 113, 4266 - 4271, doi: 10.1073/pnas.1602310113, 2016.
- Wang, Q., Huang, R.-J., Cao, J., Han, Y., Wang, G., Li, G., Wang, Y., Dai, W., Zhang, R., and Zhou, Y.: Mixing state of black carbon aerosol in a heavily polluted urban area of China: implications for light absorption enhancement, *Aerosol Sci. Technol.*, 48, 689 - 697, 2014.
- Turpin, B. J., and Huntzicker, J. J.: Identification of secondary organic aerosol episodes and quantitation of primary and secondary organic aerosol concentrations during SCAQS, *Atmos. Environ.*, 29, 3527 - 3544, 1995.

Response to Reviewer #2 comments

The authors have addressed my comments about their instrument, and they have shortened the discussion in Section 4.

Thank you for your kind consideration.

Response to Editor's comments

The paper still needs a major revision, in which it should be shortened and the discussion improved in order to make the discussion less technical and more substantial. Please shorten it, improve the discussion per the Reviewers' comments, emphasizing the important changes in aerosol scattering and absorption.

. The revised manuscript has been shortened significantly in the following places:

- **3.2 Chemical apportionment of aerosol optical properties:**

We have provided only the equation used in our study in the paper and further details of the method were removed to the supplement;

- **4.1 Temporal variations of optical properties during selected air pollution episodes:**

We have shortened this part from 5 pages to 2 pages;

- **Frequency distribution and diurnal variations of dry PM_{1.0} optical properties:**

This part was removed to the supplement;

- **Comparison of the measured aerosol optical properties to those at other locations:**

This part was removed to the supplement;

The reviewers had previously commented favorably on the clarity of the Introduction and were satisfied with the Experimental section. Accordingly, these sections are largely unchanged.

We have also improved the discussion by:

- (1) calculating the mass absorption efficiency of EC (in line with the reviewer's suggestion), and showing that our results are consistent with a several-fold absorption enhancement of EC in NCP aerosols.
- (2) On the basis of the evidence in (1), we parameterized the IMPROVE model to account for the absorption enhancement. Unsurprisingly, this greatly increases the importance of aerosol absorption, bringing the calculated extinction and SSA values into better agreement with observations. We discuss the large EC contribution to $PM_{1.0}$ extinction owing to its high absorption efficiency, and support suggestions that EC emissions should be a key target to air quality controls.
- (3) Considering the increases of nitrate in aerosols during polluted episodes, and advancing an explanation for this increase based on the molar ratios of NO_3 , NH_4 , and SO_4 .

Optical properties of atmospheric fine particles near Beijing during the HOPE-J³A Campaign

Xuezhe Xu^{1,2,3}, Weixiong Zhao^{1,2}, Qilei Zhang^{1,2,3}, Shuo Wang^{1,2,3}, Bo Fang^{1,2}, Weidong Chen⁵, Dean S. Venables^{6,7}, Xinfeng Wang⁸, Wei Pu⁹, Xin Wang⁹, Xiaoming Gao^{1,2,4}, and Weijun Zhang^{1,2,4}

¹ Key Laboratory of Atmospheric Composition and Optical Radiation, Anhui Institute of Optics and Fine Mechanics, Chinese Academy of Sciences, Hefei 230031, Anhui, China

² Laboratory of Atmospheric Physico-Chemistry, Anhui Institute of Optics and Fine Mechanics, Chinese Academy of Sciences, Hefei, 230031, Anhui, China

³ Graduate School, University of Science and Technology of China, Hefei, 230026, Anhui, China

⁴ School of Environmental Science and Optoelectronic Technology, University of Science and Technology of China, Hefei, 230026, Anhui, China

⁵ Laboratoire de Physicochimie de l'Atmosphère, Université du Littoral Côte d'Opale, 59140 Dunkerque, France

⁶ Department of Chemistry and Environmental Research Institute, University College Cork, Cork, Ireland

⁷ Leibniz Institute for Tropospheric Research, 04318 Leipzig, Germany

⁸ Environment Research Institute, Shandong University, Jinan 250100, China

⁹ Key Laboratory for Semi-Arid Climate Change of the Ministry of Education, College of Atmospheric Sciences, Lanzhou University, Lanzhou 730000, China

*Correspondence to :

Weixiong Zhao (wxzhao@aiofm.ac.cn) and Weijun Zhang (wjzhang@aiofm.ac.cn)

1 Abstract

2 The optical properties and chemical composition of PM_{1.0} particles in a suburban environment
3 (Huairou) near the mega-city of Beijing were measured during the HOPE-J³A (Haze Observation
4 Project Especially for Jing-Jin-Ji Area) field campaign. The campaign covered the period November
5 2014 to January 2015 during the winter coal heating season. The average values and standard
6 deviations of the extinction, scattering, absorption coefficients, and the aerosol single scattering
7 albedo (SSA) at $\lambda = 470$ nm during the measurement period were 201 ± 240 , 164 ± 202 , 37 ± 43
8 Mm^{-1} , and 0.80 ± 0.08 , respectively. The average values for the real and imaginary components of
9 the effective complex refractive index (CRI) over the campaign were 1.40 ± 0.06 and 0.03 ± 0.02 ,
10 while the average~~The mean~~ mass scattering ~~(MSE)~~ and absorption efficiencies ~~(MSE and MAE)~~
11 ~~efficiencies~~ of PM_{1.0} were 3.6 and $0.7 \text{ m}^2 \text{ g}^{-1}$, respectively. Highly time-resolved air pollution
12 episodes clearly show the dramatic evolution of the PM_{1.0} size distribution, extensive optical
13 properties (extinction, scattering, and absorption coefficients) and intensive optical properties (single
14 scattering albedo and ~~the effective complex refractive index, CRI~~) during haze formation,
15 development and decline. Time periods were classified into three different pollution levels (clear,
16 slightly polluted, and polluted) for further analysis. It was found that: (1) ~~The diurnal patterns of the~~
17 ~~aerosol extinction, scattering, absorption coefficients, and SSA differed for the three pollution classes.~~
18 ~~(2) The real and imaginary part of the effective CRI increased, while the SSA decreased from clear~~
19 ~~to polluted days. (3) The relative contributions of organic and inorganic species to observed aerosol~~
20 composition changed significantly from clear to polluted days: the organic mass fraction decreased
21 from 50% to 43% while the proportion of sulfates, nitrates, and ammonium increased strongly from
22 34% to 44%. (4) Chemical apportionment of extinction, ~~The fractional contribution of chemical~~
23 ~~components to extinction coefficients was calculated by~~ using the ~~modified~~ IMPROVE algorithm,
24 tended to underestimate the extinction compared to measurements. Agreement with measurements
25 was improved by modifying the parameters to account for enhanced absorption by elemental carbon
26 (EC). Organic mass was the largest contributor (58%) to the total extinction of PM_{1.0}, while EC,
27 despite its low mass concentration of ca. 4%, contributed about 17%, to extinction. When the air
28 quality deteriorated, ~~the change of the relative contribution of sulfate aerosol to the total extinction~~
29 ~~was small, but~~ the contribution of nitrate aerosol increased significantly (from 17% on clear days to
30 23% on polluted days). (5) Under polluted conditions, the average mass absorption efficiencies

1 (MAE) of EC were up to 4 times as large as the reference MAE value for freshly generated black
2 carbon (BC). The temporal pattern of MAE values was similar to that of the OC/EC ratio, suggesting
3 that non-BC absorption from secondary organic aerosol (SOA) also contributes to particle
4 absorption. ~~The observed mass scattering efficiencies of $PM_{1.0}$ increased with the extent of pollution,~~
5 ~~whereas the observed mass absorption efficiencies of $PM_{1.0}$ increased in slightly polluted conditions~~
6 ~~but decreased under polluted conditions.~~

11 **1 Introduction**

13 Atmospheric aerosols have significant effects on climate forcing (Ramanathan et al., 2001;
14 Anderson et al., 2003; Wang et al., 2010; Bahadur et al., 2012), environment (Cao et al., 2013;
15 Huang et al., 2014), and human health (Nel, 2005; S. Zheng et al., 2015). Visibility is regarded as an
16 indicator of air quality and is affected by the scattering and absorption of solar light by fine particles
17 (Watson, 2002). Uncertainties in atmospheric visibility are mainly due to the uncertainties associated
18 with the aerosols' optical properties, which depend on the physical and chemical properties of
19 atmospheric aerosol, including chemical composition, size distribution, mixing state, morphology
20 and hygroscopic properties. Understanding how these physical and chemical characteristics affect the
21 optical properties of particles is key to improve quantitative estimates of direct radiative forcing and
22 to determine the environmental effects of particles. To ascertain the relationships between these
23 parameters, many research campaigns have been performed during the past decade, including ACE-1
24 (Bates et al., 1998), ACE-2 (Raes et al., 2000), INDOEX (Eldering, 2002), ACE-Asia (Quinn, 2004;
25 Doherty et al., 2005), PRIDE-PRD2004 (Zhang et al., 2008), MILAGRO (Marley et al., 2009),
26 CAREBeijing (Jung et al., 2009; Garland et al., 2009; Wu et al., 2011) and CalNex campaign (Cahill
27 et al., 2012; Thompson et al., 2012; Ryerson et al., 2013; X. Zhang et al., 2013).

28 Rapid urbanization and economic development has brought about serious environmental
29 problems in the megacities of China (L. Han et al., 2015). The North China Plain (NCP) region in
30 northeast China has one of the highest global aerosol concentrations (Sun et al., 2013) due to the

1 dense population, the large number of vehicles, and intense industrial activity. The China National
2 Ambient Air Quality Standard designates a daily average concentration of PM_{2.5} greater than 75 µg
3 m⁻³ as harmful to health. However, PM_{2.5} concentrations in China often grossly exceed this limit –
4 for instance, daily average mass concentration of PM_{2.5} in January 2013 were higher than 500 µg m⁻³
5 for Beijing (Andersson et al., 2015). A large amount of atmospheric pollutants are emitted from
6 fossil fuel, biomass burning and urban construction (Lei et al., 2011; Zhang et al., 2011). The
7 mixture of these various emissions results in complex physical, chemical and optical properties of
8 aerosols in the NCP region.

9 In recent years, many campaigns have been conducted in Beijing ~~to study the relationships~~
10 ~~between the mass concentrations, optical properties, chemical components, hygroscopic properties,~~
11 ~~mixing state, new particle formation, light apportionment and meteorological conditions~~ (Liu et al.,
12 2013; Sun et al., 2013, 2015; Guo et al., 2014; Andersson et al., 2015; B. Han et al., 2015; Wang et
13 al., 2015; Wu et al., 2015; Xu et al., 2011; X. J. Zhao et al., 2013; G. J. Zheng et al., 2015). It is
14 worth noting that atmospheric dynamic processes differ between polluted and cleaner periods and
15 that secondary aerosols have been proposed as the major contributor to haze formation (Quan et al.,
16 2014; ~~Y.-L.~~ Sun et al., 2014). Research in the Pearl River Delta of China has shown that submicron
17 particles contribute more than 90% of the particle extinction (Cheng et al., 2008). However, few
18 studies in the NCP region have focused on light extinction contribution of submicron aerosol under
19 different air pollution conditions. Moreover, the evolution of intensive optical properties (effective
20 complex refractive index, CRI, and single scattering albedo, SSA ~~or~~ ω, the ratio of scattering to
21 extinction) in haze formation, development and decline have rarely been reported. Comprehensive
22 studies of intensive optical properties and light apportionment are necessary for a better
23 understanding of the evolution of aerosol physical and optical properties in the NCP.

24 In this paper, we report continuous measurements of the optical properties, particle size
25 distributions, and chemical composition of submicron aerosol at a suburban site (Huairou) from 16
26 November 2014 to 11 January 2015. The effective CRI for PM_{1.0} particles were retrieved with Mie
27 theory by treating the submicron aerosols as spherical particles. The fractional contribution of the
28 chemical components of particles to the total extinction coefficient were calculated by the modified
29 IMPROVE algorithm (Pitchford et al., 2007). PM_{1.0} optical properties, chemical compositions, size
30 distributions, chemical apportionment of light extinction, and mass scattering and absorption

1 efficiencies are reported for three different pollution levels (~~clear, slight polluted, and polluted days~~).
2 ~~The results show that there was a large amount of light absorbing fine particles in Beijing in the~~
3 ~~winter time over the campaign period.~~

5 2 Experimental

7 The Haze Observation Project Especially for Jing-Jin-Ji (Beijing-Tianjin-Hebei, the national
8 capital region of China) Area (HOPE-J³A) field campaign took place at the Huairou campus of the
9 University of Chinese Academy of Sciences (40°24'24.45"N, 116°40'32.95"E) from October 2014 to
10 January 2015. The goal of the HOPE-J³A campaign was to better understand the emissions, transport,
11 and evolution of atmospheric fine particles and their precursors in the Jing-Jin-Ji area. Figure 1
12 shows the map of NCP and the average distribution of the MODIS (MODerate-resolution Imaging
13 Spectroradiometer) (Chu et al., 2003) AOD (aerosol optical depth) with a resolution of 0.2°×0.2°
14 during the field campaign from 16 November 2014 to 11 January 2015. The Huairou observation site
15 (marked as a red star in Fig. 1) is situated about 60 km northeast of Beijing city center and is mainly
16 surrounded by medium density residential suburban areas.

17 The instruments were installed on the 4th floor of Teaching Building 1, with the sample inlet
18 about 2.5 m above the roof. The inlet consisted of a PM_{1.0} ambient size cut (SF-PM_{1.0}, 1.0 m³ h⁻¹,
19 Sven Leckel Ingenieurburo GmbH) with a 50% cut-point at 1.0 μm. Downstream of the inlet, the
20 sample air was dried to below 15% RH by a diffusion dryer and then passed through a copper tube (6
21 m long with an inner diameter of 1 cm) at a flow rate of 16.7 L min⁻¹.

22 The particle size distribution between 14 and 662 nm was measured every 3 min with a scanning
23 mobility particle sizer (SMPS, TSI 3936), which comprised an electrostatic classifier (TSI 3080) and
24 a condensation particle counter (TSI 3776). Diffusion losses and the effect of multicharged particles
25 were corrected by the instrument software. The SMPS was validated with laboratory-generated,
26 NIST traceable monodispersed polystyrene latex (PSL) spheres with diameters of 203 ± 5 nm
27 (Thermo Scientific 3200A) and 296 ± 6 nm (Thermo Scientific 3300A) before and after the
28 campaign (W. Zhao et al., 2013). The measured particle sizes and the certified diameters of the PSL
29 spheres agreed to within 2 %.

30 The optical properties of PM_{1.0} particles were measured with a newly developed cavity-enhanced

1 albedometer (Zhao et al., 2014a). The albedometer was based on a blue light-emitting-diode (LED)
2 incoherent broadband cavity-enhanced absorption spectroscopy (IBBCEAS) system that
3 incorporated an integrating sphere (IS). This instrument is a new tool for direct, in situ, and
4 simultaneous measurement of aerosol scattering and extinction coefficients (and thus of the
5 absorption coefficient and aerosol SSA, ω_{470}) at a mean wavelength of 470 nm. The performance of
6 the cavity-enhanced albedometer was previously evaluated using laboratory-generated, monodisperse
7 standard aerosol particles, and the scattering measurements were also found to be in close agreement
8 with TSI 3563 nephelometer measurements (Zhao et al., 2014 a, b).

9 The advantage of broadband over single wavelength measurements is its capacity to
10 simultaneously measure multiple species present in the sample (gases and particles) using a single
11 instrument. A spectral-fitting algorithm was applied from 445 to 480 nm to retrieve gas
12 concentrations based on their spectral structure and thereby to remove the contribution of gas phase
13 absorption from the aerosol extinction. The scattering signal in the IS was measured by a single
14 channel photomultiplier tube (PMT), providing an integrated result over a narrow bandwidth of ~ 9
15 nm (full-width at half maximum, FWHM) in the spectral region of 465–474 nm. Truncation
16 reduction tubes (Varma et al., 2003) were used to minimize the forward and backward truncation
17 angles to 1.2° .

18 The sample volume of the system was about 1.8 L and the flow rate of the cavity-enhanced
19 albedometer was 1.5 L min^{-1} at atmospheric pressure. The acquisition time for each measurement
20 was 9 s (for a 1.5 s integrating time per spectrum, and six-spectra averaging). The temperature and
21 relative humidity of the sample were measured with a hygrometer (Rotronic, model HC2 humidity
22 sensor). The cavity was flushed with dry zero air every hour to acquire a reference spectrum. The
23 reference spectrum was used both in the IBBCEAS retrieval (Fiedler et al., 2003) and to remove the
24 contribution of light scattering from internal surfaces and Rayleigh scattering. The mirror reflectivity
25 $R(\lambda)$ and the scaling factor (K' , the calibration coefficient that related instrument response to
26 scattering magnitude) for the scattering channel of the albedometer were determined by He, N₂ and
27 CO₂ every week. No deterioration of R and K' were observed during the campaign.

28 The detection limits for the scattering and extinction channels with 9 s integration time were
29 0.54 Mm^{-1} and 0.15 Mm^{-1} , respectively. The total uncertainty in the extinction measurement was
30 estimated to be less than 4% and arose from uncertainties in the mirror reflectivity (R) ($\sim 1\%$), the

1 ratio of cavity length to the cell length containing the air sample when the cavity mirrors were purged
2 (R_L) (~3%), and particle losses in the system (~2%). The total uncertainty in the scattering
3 measurement was about 3%, with dominant contributions from uncertainties in the experimentally
4 determined scattering calibration coefficient (K') (2%), and the uncertainty associated with particle
5 losses in the cavity (2%).

6 Based on a Mie scattering calculation, the truncated fraction of total scattering was about 0.22%
7 for a 1 μm diameter spherical particle with a complex refractive index (CRI) of $m = 1.6 + i0$ at $\lambda =$
8 470 nm. This truncation effect was therefore negligible compared to the measurement uncertainty
9 and no correction for the truncation underestimate was applied to our data.

10 Potential uncertainties associated with changes in the instrument environment were considered
11 but found to be unimportant. The instrument was located in a temperature-controlled room, the
12 temperature inside the albedometer enclosure was maintained at $28.3 \pm 0.8^\circ\text{C}$, and the sample flow
13 was controlled with a mass flow meter. Example data of the transmitted intensity measured with the
14 CCD spectrometer and the scattering signal measured with the PMT are shown in Fig. S1 in the
15 supplement. The cavity was flushed with particle-free air every hour to acquire the $I_0(\lambda)$ spectrum.
16 No obvious drift in the LED light intensity was observed even after 6 hours of measurement,
17 indicating the high stability of the instrument under these operating conditions.

18 Another $\text{PM}_{1.0}$ sampler (SF- $\text{PM}_{1.0}$, Sven Leckel Ingenieurburo GmbH) was installed on the roof
19 of the building (~ 20m above the ground) to collect $\text{PM}_{1.0}$ samples with quartz filters (47 mm,
20 MUNKTELL Corporation) for off-line aerosol chemical composition analysis. The flow rate was
21 16.7 L min^{-1} and samples were collected over the period of 16 November 2014 to 11 January 2015.
22 The collection time period was 12 h: from 08:30 to 20:30 LT for daytime samples, and from 20:30 to
23 08:30 LT for nighttime samples. Before sampling, the quartz-fiber filters were preheated for 4 h at
24 600°C in a muffle furnace, and ten filters were used as field blank samples in the sampling period. In
25 total, 114 filters were collected; these were stored at -4°C to prevent evaporation of volatilized
26 species until they were analyzed.

27 A punch of 1.5 cm^2 was taken from each filter, and then heated in inert and oxidizing
28 atmospheres to volatilize and combust the loaded carbon, respectively. The carbon (elemental carbon,
29 EC, and organic carbon, OC) concentrations were determined with a thermal/optical transmittance
30 aerosol carbon analyzer (Sunset Laboratory, Inc.) (NIOSH, 1996). The measurement principle and

1 operation of the Sunset aerosol carbon analyzer was presented in a previous study (Peterson et al.,
2 2002). Another punch with a area of 2 cm² was taken from the rest of filter, extracted into 10 mL of
3 deionized water (> 18MΩ) via 20 min sonication, filtered using a 0.22 μm PTFE syringe filter, and
4 stored in a refrigerator at 4°C until chemical analysis. Eight water-soluble ion compositions [three
5 anions: nitrate (NO₃⁻), sulfate (SO₄²⁻), and chloride (Cl⁻); five cations: ammonium (NH₄⁺), sodium
6 (Na⁺), potassium (K⁺), magnesium (Mg²⁺) and calcium (Ca²⁺)] were determined using a Dionex
7 ICS-90 Ion Chromatography system with AS14A and CS14A columns and eluents of
8 NaCO₃-NaHCO₃ and methanesulfonic acid, respectively. Further details on this analysis are given
9 elsewhere (X. F. Wang et al., 2013).

10 Meteorological parameters, including wind speed (WS) and direction (WD), temperature (*T*) and
11 relative humidity (RH), were continuously recorded at the observation site. The mass concentration
12 of PM_{2.5} for the air quality classification and concentrations of pollutant gases (SO₂, NO₂, O₃, and
13 CO) were monitored by the National Environmental Bureau and the data at Huairou were retrieved
14 from the internet (<http://113.108.142.147:20035/emcpublish/>). In this work, the PM_{2.5} pollution level
15 was divided into three categories according to the technical regulation on Ambient Air Quality Index
16 (National Environmental Protection Standard of the People's Republic of China, HJ 633–2012)
17 (http://kjs.mep.gov.cn/hjbhbz/bzwb/dqhjbh/jcg_fbz/201203/W020120410332725219541.pdf; A.
18 Zhang et al., 2013; G. J. Zheng et al., 2015): clear day (PM_{2.5} concentration ≤ 35 μg m⁻³, when the
19 corresponding individual air quality index (IAQI) of 24 hours averaged PM_{2.5} concentration ranged
20 from 0 to 50), slightly polluted day (35 μg m⁻³ < PM_{2.5} concentration ≤ 115 μg m⁻³, when IAQI of
21 PM_{2.5} ranged from 50 to 150), and polluted day (115 μg m⁻³ < PM_{2.5} concentration ≤ 350 μg m⁻³,
22 when IAQI of PM_{2.5} ranged from 150 to 400). These pollution classes are usually based on PM_{2.5}
23 concentrations averaged from 00:00 to 23:59 on a specific date. For our filter samples, however, the
24 collection time extended over two days; nevertheless, we applied the same categorization for our
25 measurements from 20:30 (day 1) to 20:30 LT (day 2).

26

27 **3 Optical data analysis method**

28

29 **3.1 Retrieval of aerosol complex refractive index**

30

1 The scattering and extinction coefficients of particles are calculated based on (Pettersson et al.,
 2 2004):

$$3 \quad \alpha_{ep,sp} = \int N(D_p) \frac{\pi}{4} D_p^2 Q_{ext,scat}(m, x) dD_p \quad (1)$$

4 where $x = \pi D_p / \lambda$ is the size parameter, $m = n + i k$ is the CRI of the particle (where n and k
 5 correspond to the real and imaginary parts of the CRI, respectively), N is the number of particles per
 6 unit volume in the size bin dD_p with mean diameter D_p , and $\frac{\pi}{4} D_p^2 Q_{ext,scat}(m, x)$ is the extinction or
 7 scattering cross section $\sigma_{ep,sp}$. The extinction or scattering efficiency, $Q_{ext,scat}$, is a function of the CRI,
 8 the morphology of the particles and the size parameter. For chemically homogeneous spherical
 9 particles, Q can be calculated from Mie theory.

10 The effective CRI is an effective property that averages over the aerosols' size, shape, mixing
 11 state and chemical composition. Simultaneous measurement of the scattering and extinction
 12 coefficients by the cavity-enhanced albedometer provides a new approach for faster retrieval of the
 13 particulate CRI (Riziq et al., 2007; Mack et al., 2010; Zhao et al., 2014a; Xu et al., 2016). Details of
 14 the CRI retrieval have been given in previous studies (Riziq et al., 2007; Mack et al., 2010). The
 15 measured extinction and scattering coefficients ($\alpha_{ep,470}$ and $\alpha_{sp,470}$) and the particle number size
 16 distribution, $N(D_p)$, were used to determine the effective CRI on the assumption that particles were
 17 spherical and that the black carbon aerosol (BC) can be treated in a volume mixing approach. The
 18 real and imaginary parts of the effective CRI were varied (between 1.3 and 1.7 for the real part and
 19 between 0 and 0.1 for the imaginary part) to calculate the extinction and scattering coefficients for
 20 each size distribution. A set of refractive indices were determined by finding the minimum of the
 21 “merit function”, χ^2 (Mack et al., 2010):

$$22 \quad \chi^2 = \frac{(\alpha_{ep} - \alpha_{ep_calc})^2}{\varepsilon_{\alpha_{ep}}^2} + \frac{(\alpha_{sp} - \alpha_{sp_calc})^2}{\varepsilon_{\alpha_{sp}}^2} \quad (2)$$

23 Here, α_{ep} and α_{sp} are the measured values of the extinction and scattering coefficients, while α_{ep_calc}
 24 and α_{sp_calc} are the corresponding calculated values. $\varepsilon_{\alpha_{ep}}$ and $\varepsilon_{\alpha_{sp}}$ are the measurement uncertainty of
 25 α_{ep} and α_{sp} , respectively. The mean standard deviations of the extinction and scattering coefficients
 26 over 3 min were taken as the measurement uncertainty for calculating χ^2 .

27 A contour plot of χ^2 versus n and k was used to estimate the standard errors of n and k . The

1 values of n and k that satisfied $\chi^2 < \chi_0^2 + 2.298$, which fell within the 1σ error bound of the best
2 measurement (with 68% confidence level of χ^2 distribution), were considered acceptable. Projections
3 of the contour lines (with a contour value of 2.298) on the n and k plane gave the standard errors Δn
4 and Δk , respectively (Dinar et al., 2008; Zhao et al., 2014a).

6 3.32 Mass scattering and absorption efficiencies

8 Mass scattering (MSE) and absorption (MAE) efficiencies are the key parameters in climate and
9 chemical transport models for estimating radiative forcing and apportioning chemical extinction
10 budgets (Bates et al., 2006; Malm and Hand, 2007). MSE and MAE (both conventionally in units of
11 $\text{m}^2 \text{g}^{-1}$) are defined as the ratio of the light scattering and absorption coefficients (Mm^{-1}) to the
12 aerosol volume mass concentration ($\mu\text{g m}^{-3}$), respectively.

$$13 \quad \text{MSE (MAE)} = \frac{\alpha_{\text{scat,abs}}}{M} \quad (73)$$

14 Knowledge of the MSEs and MAEs of each component of atmospheric aerosol is helpful for accurate
15 source apportionment and for estimating radiative forcing in climate modes. The simplest method for
16 computing MSE is by direct measurement of aerosol scattering coefficient and the mass
17 concentration. The average MSE is estimated either by dividing the average α_{scat} by the average mass
18 concentration or from the slope of a linear regression of α_{scat} and M (Hand and Malm, 2007). The
19 MAE is calculated similarly.

20 In this study, the MSEs and MAEs of $\text{PM}_{1.0}$ were estimated from the slope of a linear regression
21 of $\alpha_{\text{scat,abs}}$ and M (each data point with 3 min time resolution). The $\alpha_{\text{scat,abs}}$ was directly measured
22 with the cavity-enhanced albedometer with high time resolution, and M was calculated from the
23 average density ($\bar{\rho}$) and the volume concentrations ($V(D_p)$) measured with the SMPS
24 ($M = \bar{\rho} \int V(D_p) dD_p$). The average density was calculated from $\bar{\rho}^{-1} = \sum_j \rho_j^{-1} X_j$, where ρ_j is the
25 density of each chemical component (see Table S1 ~~in the Supplement~~), X_j is the mass concentration
26 ratio of each species to the total $\text{PM}_{1.0}$ concentration (reconstructed with equation (S68)) measured
27 from filter samples with a time resolution of 12 h sample⁻¹. If it is assumed that only EC contributes
28 to aerosol absorption, the MAE of EC can be determined (Knox et al., 2009; Bond et al., 2013;

1 [Cheng et al., 2011, 2016](#)):

$$2 \quad \text{MAE} = \frac{\int_{t_1}^{t_2} \alpha_{abs} dt}{\text{EC}_m \times (t_2 - t_1)} \quad (4)$$

3 where EC_m ($\mu\text{g m}^{-3}$) is the measured EC mass concentration with the aerosol carbon analyzer, and t_1
4 and t_2 are the start and stop times for the collection of samples with quartz filters. In this work, the
5 integration time was determined by the quartz filter sampling period of 12 h sample⁻¹. For
6 comparison, the MAE of freshly generated BC is $8.7 \text{ m}^2 \text{ g}^{-1}$ at $\lambda = 470 \text{ nm}$ (based on a $7.5 \pm 1.2 \text{ m}^2$
7 g^{-1} at $\lambda = 550 \text{ nm}$ and using the inverse wavelength dependence) (Bond et al., 2006).

9 **3.2.3 Chemical apportionment of aerosol optical properties**

10
11 Chemical apportionment of light extinction of $\text{PM}_{1.0}$ was determined with a revised IMPROVE
12 (Interagency Monitoring of Protected Visual Environments) algorithm (Pitchford et al., 2007).
13 Although the IMPROVE algorithm is a simplified predictor of extinction, it is nevertheless a useful
14 tool to estimate the contribution of different particle components to haze levels (Pitchford et al.,
15 2007). ~~Light extinction at $\lambda = 550 \text{ nm}$ can be estimated by multiplying the mass concentrations by~~
16 ~~component-specific mass extinction efficiencies (MEEs) of each of seven major components: sulfate~~
17 ~~(assumed to be ammonium sulfate), nitrate (assumed to be ammonium nitrate), organic mass (OM,~~
18 ~~based on the measured mass concentration of organic carbon, OC), elemental carbon (EC), fine soil,~~
19 ~~sea salt (chlorine, Cl), and coarse mass (the differences between $\text{PM}_{1.0}$ and $\text{PM}_{2.5}$ mass concentration).~~
20 ~~It can be expressed by the following (Pitchford et al., 2007):~~

$$21 \quad \alpha_{ext,550nm} \approx 2.2 \times f_s(\text{RH}) \times [\text{Small Sulfate}] + 4.8 \times f_L(\text{RH}) \times [\text{Large Sulfate}]$$
$$+ 2.4 \times f_s(\text{RH}) \times [\text{Small Nitrate}] + 5.1 \times f_L(\text{RH}) \times [\text{Large Nitrate}]$$
$$+ 2.8 \times [\text{Small Organic Mass}] + 6.1 \times [\text{Large Organic Mass}]$$
$$+ 10 \times [\text{Elemental Carbon}] + 1 \times [\text{Fine Soil}]$$
$$+ 1.7 \times f_{ss}(\text{RH}) \times [\text{Sea Salt}] + 0.6 \times [\text{Coarse Mass}]$$
$$+ \text{Rayleigh scattering (site specific)} + 0.33 \times [\text{NO}_2 \text{ (ppb)}]$$

22 (3)

23 where $f(\text{RH})$ is the water growth factor of inorganic components, $f_s(\text{RH})$ and $f_L(\text{RH})$ are the
24 water growth factors for the small and large particle size modes for sulfate and nitrate, respectively,

1 and $f_{ss}(RH)$ is the hygroscopic growth factor for sea salt.

2 The large and small parts are defined by the IMPROVE formula as (Pitchford et al., 2007; Cao
3 et al., 2012):

$$\begin{aligned} 4 \quad [Large\ X] &= [Total\ X]^2/20, \text{ for } [Total\ X] < 20\ \mu\text{g m}^{-3} \\ 5 \quad [Large\ X] &= [Total\ X], \text{ for } [Total\ X] \geq 20\ \mu\text{g m}^{-3} \\ 6 \quad [Small\ X] &= [Total\ X] - [Large\ X] \end{aligned} \quad (4)$$

7 where X = sulfate, nitrate or OM. The concentration of ammonium sulfate ($[(NH_4)_2SO_4]$) was
8 1.375 times the sulfate concentration ($[SO_4^{2-}]$), and the ammonium nitrate ($[NH_4NO_2]$) was 1.29
9 times the nitrate concentrations ($[NO_3^-]$). The OM concentration was estimated by multiplying the
10 reported OC concentration by a factor of 1.6 (Turpin and Lim, 2001). The sea salt mass
11 concentration was estimated by multiplying the Cl^- mass concentration by a factor of 1.8. The
12 ammonium cation was not used directly in the IMPROVE algorithm. It was assumed to be fully
13 neutralized by SO_4^{2-} and NO_3^- and treated as ammonium sulfate ($(NH_4)_2SO_4$) and ammonium
14 nitrate (NH_4NO_2), respectively.

15 The revised IMPROVE algorithm above was parameterized for atmospheric aerosol extinction at
16 $\lambda = 550\text{ nm}$. In this study, the optical properties of $PM_{1.0}$ were measured at $\lambda = 470\text{ nm}$. The
17 IMPROVE algorithm needs to be refined to better represent the chemical apportionment of light
18 extinction for $PM_{1.0}$ particles. Since dry $PM_{1.0}$ aerosols were measured, the coarse mass and the
19 hygroscopic increase of inorganic component were ignored for the inputs of the IMPROVE
20 algorithm. The fine soil component was also left out in apportioning the extinction coefficient due to
21 its small fraction of $PM_{1.0}$ particles during wintertime in Beijing (K. Sun et al., 2014).

22 Under the assumptions of the IMPROVE algorithm (in which particles are treated as separate
23 entities), the difference in the wavelength will only affect the dry mass extinction efficiency terms.
24 We modified the MEE terms in equation (3) of each individual particle components with a scaling
25 factor so as to be directly comparable to measurements at $\lambda = 470\text{ nm}$. The scaling factor was the
26 ratio of the MEEs of each species at $\lambda = 470\text{ nm}$ and $\lambda = 550\text{ nm}$ calculated with Mie theory from the
27 literature reported complex refractive index (Table S1 in the Supplement) and the measured mean
28 number size distribution. Further details are given in the Supplement, Section S2. The dry mass
29 extinction efficiencies of inorganic mass (including sulfate, nitrate and sea salt), organic mass, and
30 elemental carbon for the input of the IMPROVE formula at $\lambda = 470\text{ nm}$ should accordingly be scaled

by factors of 1.31, 1.30 and 1.08, respectively. The modified IMPROVE function for dry PM_{1.0} extinction at $\lambda = 470 \text{ nm}$ can be rewritten as following (with further details in the Supplement, Section S2):

$$\begin{aligned} \alpha_{ext,470nm,PM_{1.0}} \approx & 2.88 \times [\text{Small Sulfate}] + 6.29 \times [\text{Large Sulfate}] \\ & + 3.14 \times [\text{Small Nitrate}] + 6.68 \times [\text{Large Nitrate}] \\ & + 3.64 \times [\text{Small Organic Mass}] + 7.93 \times [\text{Large Organic Mass}] \\ & + 10.8 \times [\text{Elemental Carbon}] + 2.23 \times [\text{Sea Salt}] \end{aligned}$$

(S35)

The large and small parts are defined by the IMPROVE formula as (Pitchford et al., 2007; Cao et al., 2012):

$$\begin{aligned} [\text{Large X}] &= [\text{Total X}]^2/20, \text{ for } [\text{Total X}] < 20 \mu\text{g m}^{-3} \\ [\text{Large X}] &= [\text{Total X}], \text{ for } [\text{Total X}] \geq 20 \mu\text{g m}^{-3} \\ [\text{Small X}] &= [\text{Total X}] - [\text{Large X}] \end{aligned} \quad (4)$$

where X = sulfate, nitrate or organic mass (OM). The concentration of ammonium sulfate ($[(\text{NH}_4)_2\text{SO}_4]$) was 1.375 times the sulfate concentration ($[\text{SO}_4^{2-}]$), and the ammonium nitrate ($[\text{NH}_4\text{NO}_3]$) was 1.29 times the nitrate concentrations ($[\text{NO}_3^-]$). The OM concentration was estimated by multiplying the reported OC concentration by a factor of 1.6 (Turpin and Lim, 2001). The sea salt mass concentration was estimated by multiplying the Cl^- mass concentration by a factor of 1.8. The ammonium cation was not used directly in the IMPROVE algorithm. It was assumed to be fully neutralized by SO_4^{2-} and NO_3^- and treated as ammonium sulfate ($(\text{NH}_4)_2\text{SO}_4$) and ammonium nitrate (NH_4NO_3), respectively. The PM_{1.0} mass concentration can be reconstructed as the sum of its major chemical components (Pitchford et al., 2007):

$$\begin{aligned} \text{Reconstructed mass}_{PM_{1.0}} &= [(\text{NH}_4)_2\text{SO}_4] + [\text{NH}_4\text{NO}_3] + [\text{SS}] + [\text{OM}] + [\text{EC}] \\ &= 1.375 \times [\text{SO}_4^{2-}] + 1.29 \times [\text{NO}_3^-] + 1.8 \times [\text{Cl}^-] + 1.6 \times [\text{OC}] + [\text{EC}] \end{aligned} \quad (6)$$

4 Results and discussion

An overview of the measurement results of the aerosol optical properties, size distribution, and chemical composition of PM_{1.0} particles is shown in Table 1 and Fig. 2. There are obvious differences of the campaign average number and surface size distribution of PM_{1.0} for the three different pollution categories (Fig. 3). For clear days, the mean particle number size distributions

1 fitted by a mono-log normal function was around 41 nm. Bimodal distributions were observed on
2 slightly polluted and polluted days with modes centered at 38 and 105 nm (slightly polluted periods)
3 and at 38 and 151 nm (polluted periods). The mode of the number size distributions exhibits the
4 expected displacement toward the accumulation mode with increasing levels of particulate matter.

5 During the campaign, the measured aerosol extinction ($\alpha_{ep,470}$), scattering ($\alpha_{sp,470}$), and
6 absorption coefficient ($\alpha_{ap,470}$) ranged from 0.6–1165, 0.1–1150 and 0–276 Mm^{-1} , respectively. There
7 was no obvious correlation between extensive optical properties and wind direction (Fig. S4). ~~The~~
8 ~~time profiles of these properties also showed several periods during which the particle concentration~~
9 ~~would steadily build up, before rapid dissipation and return to fewer and smaller particles.~~ Averages
10 and standard deviations of the observed particle properties are summarized in Table 1 after grouping
11 data into the different air quality classes. There are obvious differences of the campaign average
12 number and surface size distribution of $PM_{1.0}$ for the three different pollution categories (Fig. 5a).
13 For clear days, the mean particle number size distributions fitted by a mono-log normal function was
14 around 41 nm. Bimodal distributions were observed on slightly polluted and polluted days with
15 modes centered at 38 and 105 nm (slightly polluted periods) and at 38 and 151 nm (polluted periods).
16 The mode of the number size distributions exhibits the expected displacement toward the
17 accumulation mode with increasing levels of particulate matter.

18 Optical properties

19
20 There was no obvious correlation between extensive optical properties and wind direction (Fig.
21 S4). With increasing pollutant level, the extensive optical properties ($\alpha_{ep,470}$, $\alpha_{sp,470}$ and $\alpha_{ap,470}$)
22 increased strongly, in accordance with the expected, strong dependence of particle size on light
23 scattering. –In contrast, changes in the intensive optical properties, (ω_{470}), were more modest. The
24 optical measurement data are presented as histograms of the relative frequency of occurrence of
25 $\alpha_{ep,470}$, $\alpha_{sp,470}$, $\alpha_{ap,470}$ and ω_{470} (Fig. S56); and approximately 71% of extinction and scattering
26 coefficients values were lower than $200 Mm^{-1}$ and nearly 80% of absorption coefficient values were
27 located in the range of $1.5–50 Mm^{-1}$. Approximately 90% of the ω_{470} values fell into the range of
28 0.70–0.97. Compared with polluted days, the frequency distribution of the SSA showed similar
29 patterns, and the average values were similar on clear and slightly polluted days. – diurnal variations
30 of hourly averaged extinction, scattering, absorption coefficients and SSA on clear, slightly polluted

1 and polluted days are presented in Fig. S6. Diurnal variations of the optical properties were broadly
2 similar for different pollutant levels, but tended to be more marked under clean conditions and
3 modest under polluted conditions. The Huairou site is a new suburban site at which aerosol optical
4 properties have not previously been reported. To put our observations at Huairou in context, the
5 scattering and absorption coefficients and SSA observed in this campaign are also compared (in the
6 Supplement, Section S5) to those at other locations (urban, suburban, and rural sites).

7 We present our results as follows: Firstly, selected periods are investigated in detail for showing
8 the process of haze formation, development and decline. The extensive optical properties (extinction,
9 scattering, and absorption coefficients) and intensive optical properties (SSA and effective CRI) are
10 presented for these periods. Secondly, the mass scattering and absorption efficiencies are determined.
11 And finally, the ~~diurnal variations of aerosol size distribution, optical properties and~~ chemical
12 composition on different pollution days during the campaign are considered. Chemical
13 apportionment of aerosol extinction is then studied based on the modified IMPROVE algorithm. And
14 ~~finally, the MSE and MAE of PM_{1.0} is presented for clear, slightly polluted, and polluted~~
15 ~~daysdiscussed.~~

17 **4.1 Temporal variations of optical properties during selected air pollution episodes**

18
19 The temporal variations of aerosol particle number and surface size distribution, aerosol
20 extinction, scattering, absorption coefficients, ω_{470} , and the retrieved effective CRIs from 22 to 24
21 November 2014 are presented in Fig. 34. The corresponding temporal wind direction and speed are
22 shown in the upper panel of Fig. 34, while temperature, relative humidity, pressure, and
23 concentrations of pollutant gases (SO₂, NO₂, O₃, and CO) are shown in Fig. S3-S7 in the Supplement.
24 The time series of PM_{1.0} particle number distribution during the episode varied with meteorology and
25 the sources of pollutants. To emphasize the variation of these parameters during the episode, the
26 extended air pollution episode was divided into six shorter periods. The statistical analyses of these
27 periods are summarized in Table 2. In the selected haze episode, these six periods show variations in
28 the PM_{1.0} size distribution and the extensive optical properties of particles in the process of haze
29 formation, development and decline. The evolution of intensive optical properties was related to the
30 variation of PM_{1.0} chemical components.

1 24 h back trajectories starting at 200 m a.g.l. in Huairou site calculated every 4 h (at 02:00, 6:00,
2 10:00, 14:00, 18:00 and 22:00 LT) are shown in ~~the lower panel of~~ Fig. 4–5
3 (<http://ready.arl.noaa.gov/HYSPLIT.php>). The trajectories from the northerly direction were clean air
4 masses with high transport heights and long transport pathways; trajectories from the southerly
5 direction were mainly polluted air masses with low transport heights and short transport pathways.

6 ~~According to the regulatory classification of the atmospheric pollution level, these six periods~~
7 ~~can be divided into two categories: clear day (22:00 LT 21 November–10:00 LT 22 November) and~~
8 ~~polluted day (10:00 LT 22 November–22:00 LT 22 November, 22:00 LT 22 November–10:00 LT 23~~
9 ~~November, 10:00 LT 23 November–22:00 LT 23 November, 22:00 LT 23 November–10:00 LT 24~~
10 ~~November). The mean value of the total mass concentration on clear days was $9.49 \mu\text{g m}^{-3}$, and the~~
11 ~~mean fractional contributions of OM, nitrate, and sulfate were 56% ($5.32 \mu\text{g m}^{-3}$), 12% ($1.12 \mu\text{g m}^{-3}$),~~
12 ~~and 14% ($1.34 \mu\text{g m}^{-3}$), respectively. On polluted days, the mean value of the total mass~~
13 ~~concentration was $41.64 \mu\text{g m}^{-3}$ with fractional contributions of 44% OM ($18.47 \mu\text{g m}^{-3}$), 22% nitrate~~
14 ~~($9.30 \mu\text{g m}^{-3}$), and 11% sulfate ($4.54 \mu\text{g m}^{-3}$). In summary, in going from clear to polluted days, the~~
15 ~~fractional contribution of OM to the total mass decreased by 12%, whereas the fraction of nitrate~~
16 ~~almost doubled and that of sulfate decreased slightly. Organic matter was the largest contributor to~~
17 ~~$\text{PM}_{1.0}$. The significant increase in the concentration and fractional contribution to $\text{PM}_{1.0}$ extinction~~
18 ~~coefficient of inorganic species, particularly nitrates (discussed in Section 4.3), indicate that~~
19 ~~inorganic species become more important during haze, an observation which is consistent with~~
20 ~~previously measurements during an extreme haze episode in Beijing in January 2013 (Wang et al.,~~
21 ~~2015). The difference between sulfate and nitrate likely reflects the different sources and formation~~
22 ~~mechanisms for sulfate and nitrate aerosols (G. J. Zheng et al., 2015).~~

23 ~~In the selected haze episode, these six periods show variations in the $\text{PM}_{1.0}$ size distribution and~~
24 ~~the extensive optical properties of particles in the process of haze formation, development and~~
25 ~~decline. The evolution of intensive optical properties was related to the variation of $\text{PM}_{1.0}$ chemical~~
26 ~~components.~~

28 **Period 1: First traffic-dominated pollution period (05:40–10:00 LT 22 November)**

29
30 Relatively small, light absorbing particles dominated this period. The mean diameter of the

~~number size distribution was 56 ± 6 nm, and the average number and surface concentration were $2.1 \pm 0.8 \times 10^4$ particle cm^{-3} and $3.7 \pm 1.5 \times 10^8$ $\text{nm}^2 \text{cm}^{-3}$, respectively. The mean values of $\alpha_{\text{ep},470}$, $\alpha_{\text{sp},470}$ and $\alpha_{\text{ap},470}$ were 56 ± 24 , 44 ± 10 and 12 ± 6 Mm^{-1} , respectively. The ω_{470} , real and imaginary part of effective CRI (n, k) were 0.79 ± 0.03 , 1.38 ± 0.06 and 0.03 ± 0.02 , respectively.~~

During Period 1 and Period 6~~this period~~, winds were typically from the northeast; the trajectory indicated that the air masses came from cleaner air to the north and carried pollutants from northeast areas to the observation site, with concentrations of small, light absorption particles increasing. These clean air masses showed a relatively large contribution from traffic emissions. Lower values of the SSA were found during the rush hour, in common with other studies that have similarly found minimum SSA values during the morning traffic rush hour (Garland et al., 2008; Lyamani et al., 2010).

Period 2: New particle formation period (12:40–15:00 LT 22 November)

~~This period started with clean atmospheric conditions and was characterized by the formation and growth of small particles. The mean diameter of the number size distribution was 25 ± 4 nm and the mean values of $\alpha_{\text{ep},470}$, $\alpha_{\text{sp},470}$ and $\alpha_{\text{ap},470}$ were 17 ± 5 , 16 ± 5 and 1.0 ± 0.4 Mm^{-1} , respectively. The mean values of ω_{470} , n and k were 0.94 ± 0.03 , 1.40 ± 0.06 and 0.008 ± 0.005 , respectively. These values indicated that optical extinction in these newly formed particles was dominated by scattering, although it should be noted that the uncertainties in the ω_{470} values are larger under these conditions of low scattering and extinction.~~

For Period 2, the air masses came from the north with clean air, but their reduced height resulted in entrainment of surface aerosols and transport to the observation site. The transport of clean, fresh air resulted in sharply decreased pollutant levels and promoted new particle formation. Takegawa et al. (2009) and Guo et al. (2014) showed that newly formed aitken mode particles were mainly composed of sulfate and organic matter, indicating that most components were absolute scattering species. In this case, the values of SSA and k should be close to 1 and 0, respectively. The retrieved values of SSA (0.94 ± 0.03) and k (0.008 ± 0.005) matched these expectations and indicate that the newly formed particles were predominantly scattering species.

For Periods 3 and 4, the shorter transport pathway of air masses suggested that the composition

1 was dominated by local emissions, including primary emissions and secondary formation. Period 3

2 was characterized by

3 **Period 3: Accumulated pollution period (15:30 LT 22 November–08:00 LT 23 November)**

4
5 ~~This period was characterized by~~ the dominance of larger accumulation mode particles for
6 several hours. ~~The mean diameter of number and surface size distribution was 106 ± 16 and 229 ± 16~~
7 ~~nm, respectively, which increased slowly from 15:30 LT (with a minimum value of 60 and 205 nm)~~
8 ~~to 21:40 LT (with a maximum value of 131 and 248 nm) except for a valley from 17:20–18:00 LT~~
9 ~~that coincided with the afternoon rush hour. The mean values of $\alpha_{ep,470}$, $\alpha_{sp,470}$ and $\alpha_{ap,470}$ were $179 \pm$~~
10 ~~69 , 151 ± 57 and 28 ± 12 Mm^{-1} , respectively.~~

11 In the first part of the period, the winds slowed down and turned to the south. These conditions
12 favored accumulation of local pollutants (including primary emissions and secondary productions)
13 and transportation of pollutants from southern areas. Later on, the wind speed increased and the
14 direction changed to the southeast. The accumulation of pollutants brought about the formation of
15 haze. ~~During the process, the number concentration increased about 1.7 times from 1.2×10^4 to~~
16 ~~2.0×10^4 particle cm^{-3} , and the surface concentration increased about 1.3 times from 3.2×10^8 to~~
17 ~~10.3×10^8 $nm^2 \cdot cm^{-3}$, leading to large values of $\alpha_{ep,470}$ ($285 Mm^{-1}$), $\alpha_{sp,470}$ ($235 Mm^{-1}$) and $\alpha_{ap,470}$ (50~~
18 ~~Mm^{-1}). The wind speed eventually decreased and the wind direction changed, first to northeastern,~~
19 ~~and then to southeastern directions. Another major peak in the extinction occurred during this period~~
20 ~~when a large number of small size particles were observed. The mean values of ω_{470} , and the real~~
21 ~~part and imaginary part of the effective CRI were 0.85 ± 0.01 , 1.39 ± 0.04 and 0.02 ± 0.006 ,~~
22 ~~respectively. Clearly, the air masses from northeast areas carried appreciable numbers of small, light~~
23 ~~absorbing particles.~~

24
25 **Period 4: Combined pollution period (08:30–12:00 LT 23 November)**

26
27 ~~For Periods 3 and 4, the shorter transport pathway of air masses suggested that the composition~~
28 ~~was dominated by local emissions, including primary emissions and secondary formation.~~ Large
29 numbers of small, light absorbing particles were seen during ~~period~~ Period 4, which coincided with
30 the morning rush hour. ~~The mean diameter of the number and surface size distribution was 105 ± 16~~

1 and 251 ± 15 nm, respectively, and $\alpha_{ep,470}$, $\alpha_{sp,470}$ and $\alpha_{ap,470}$ were 405 ± 60 , 321 ± 42 and 84 ± 22
2 Mm^{-1} , respectively. The mean values of ω_{470} and the imaginary part of the effective CRI were 0.79
3 ± 0.03 and 0.034 ± 0.008 , respectively, which were similar to the values in Period 1 within the
4 observed variability the first traffic-dominated pollution period. The real part of the effective CRI
5 (1.40 ± 0.03) was similar to that of the earlier traffic-dominated pollution period within the stated
6 uncertainties. During the period, weak winds from northern directions transported polluted air to the
7 observation site and resulted in higher concentrations and a greater influence of light absorbing
8 particles. The accumulation of original and newly discharged primary pollutants led to sharp
9 variations in the aerosol size distribution and extensive optical properties. However, Variations
10 variations in the aerosol intensive optical properties were slight.

12 ~~Period 5: Particle aggregation and removal period (12:30 LT 23 November 07:30 LT 24~~ 13 ~~November)~~

15 High extinction values were observed over ~~this period~~ Period 5, with a gradual increase and then
16 decrease in extinction, scattering, and absorption. ~~The mean values of $\alpha_{ep,470}$, $\alpha_{sp,470}$ and $\alpha_{ap,470}$ were~~
17 ~~330 ± 110 , 283 ± 94 and $46 \pm 16 Mm^{-1}$, respectively.~~ The mean values of ω_{470} , n and k were $0.86 \pm$
18 0.01 , 1.44 ± 0.03 , and 0.02 ± 0.01 , respectively, ~~which were larger than the values of the period 4~~
19 ~~(although within the combined uncertainties).~~ The SSA values were larger than those reported for
20 Period 4. In general, the n values were higher and the k values lower than those seen in Period 4,
21 although the mean values of both properties fall within the combined standard deviations of both
22 periods. For this period, ~~Air mass trajectories indicate that~~ the airflow started over the Beijing city
23 area and passed over the southwestern direction of the observation site. ~~Air masses following this~~
24 short path would, bringing surface air pollutants to the Huairou site and ~~contribute~~ contributing to
25 the formation of serious haze. ~~In the first part of the period, winds from the north moderated and the~~
26 wind direction changed to the northeast, favoring accumulation of local pollutants. Later on, the wind
27 changed to the southeast, with pollutants from the south contributing to the formation of serious haze.
28 Particles dispersed later after the wind speed increased and its direction became northeasterly. Both the
29 mean diameter of the number and surface size distribution (124 ± 19 and 263 ± 11 nm) and n were
30 larger in this period than in the other five periods. The light scattering efficiency increased with the

1 increment of the particle size.

2 According to the regulatory classification of the atmospheric pollution level, these six periods
3 can be divided into two categories: clear day (22:00 LT 21 November–10:00 LT 22 November) and
4 polluted day (10:00 LT 22 November–22:00 LT 22 November, 22:00 LT 22 November–10:00 LT 23
5 November, 10:00 LT 23 November–22:00 LT 23 November, 22:00 LT 23 November–10:00 LT 24
6 November). The mean value of the total mass concentration on clear days was $9.49 \mu\text{g m}^{-3}$, and the
7 mean fractional contributions of OM, nitrate, and sulfate were 56% ($5.32 \mu\text{g m}^{-3}$), 12% ($1.12 \mu\text{g m}^{-3}$),
8 and 14% ($1.34 \mu\text{g m}^{-3}$), respectively. On polluted days, the mean value of the total mass
9 concentration was $41.64 \mu\text{g m}^{-3}$ with fractional contributions of 44% OM ($18.47 \mu\text{g m}^{-3}$), 22% nitrate
10 ($9.30 \mu\text{g m}^{-3}$), and 11% sulfate ($4.54 \mu\text{g m}^{-3}$). In summary, in going from clear to polluted days, the
11 fractional contribution of OM to the total mass decreased by 12%, whereas the fraction of nitrate
12 almost doubled and that of sulfate decreased slightly. Organic matter was the largest contributor to
13 $\text{PM}_{1.0}$. The notable increase in the concentration and fractional contribution to $\text{PM}_{1.0}$ extinction
14 coefficient of inorganic species, and specifically nitrate and ammonium, indicate that the inorganic
15 contribution to particulate matter becomes relatively more important than the OM fraction during
16 haze. The chemical composition is discussed further in Section 4.3.

17 4.3.2 Mass scattering and mass absorption efficiencies

18 MSE and MAE of $\text{PM}_{1.0}$

19
20
21
22 Figure 406 shows the relationship between the scattering and absorption coefficients and $\text{PM}_{1.0}$
23 mass concentrations under different pollution levels. The $\text{PM}_{1.0}$ mass concentrations were determined
24 by multiplying the volume concentrations with the volume-weighted mass density of each filter
25 sample (Hasan and Dzubay, 1983). The scattering and (to a lesser extent) the absorption coefficients
26 were generally well correlated with the $\text{PM}_{1.0}$ mass concentrations and have small y-intercepts. (The
27 larger deviation of the y-intercept on polluted days likely stems from the smaller number of low mass
28 concentration observations on these days.)

29 The derived $\text{PM}_{1.0}$ average mass scattering and absorption efficiencies during the campaign were
30 3.60 and $0.70 \text{ m}^2 \text{ g}^{-1}$, respectively (Fig. 406d). Statistical uncertainties from the slope of the

1 regression are misleadingly small and have been omitted in the reported MSE and MAE values. The
2 MSE and MAE values are smaller than those observed by Garland et al. (2008) from suburban
3 Guangzhou in July 2006 (where the $PM_{1.0}$ mass scattering and absorption efficiency calculated with
4 assuming an average effective density of ammonium sulfate (1.7 g cm^{-3}) were 4.13 and $1.09 \text{ m}^2 \text{ g}^{-1}$,
5 respectively), the value of $PM_{2.5}$ at $\lambda = 520 \text{ nm}$ obtained in urban Beijing ($4.8 \text{ m}^2 \text{ g}^{-1}$) during
6 wintertime (Tao et al., 2015), and in Chengdu and Guangzhou ($3.9 \text{ m}^2 \text{ g}^{-1}$) (Tao et al., 2014a, b). The
7 derived mass extinction efficiency is $4.30 \text{ m}^2 \text{ g}^{-1}$, which was comparable to the reported values
8 during Aerosols 1999 ($4.1\text{--}5.4 \text{ m}^2 \text{ g}^{-1}$) (Quinn et al., 2001) and INDOEX 1999 ($4.0\text{--}5.6 \text{ m}^2 \text{ g}^{-1}$)
9 (Quinn et al., 2002).

10 In this work, the MSE of $PM_{1.0}$ was $4.16 \text{ m}^2 \text{ g}^{-1}$ during polluted days, which was 34% higher
11 than that during the slightly polluted days ($3.11 \text{ m}^2 \text{ g}^{-1}$) and 75% higher than that during the clear
12 days ($2.38 \text{ m}^2 \text{ g}^{-1}$) (Fig. 406a–c). The variability in MSE is typically more dependent on mass size
13 distribution than on density or refractive index (Hand and Malm, 2007). As shown in Fig. 5(a)3, the
14 particle diameter increased significantly with high aerosol mass concentrations. The MSEs in this
15 work increased consistently with pollution level, primarily because larger particles scatter light more
16 efficiently. Cheng et al. (2015) showed that the MSEs of ammonium nitrate, ammonium sulfate and
17 organic matter increased rapidly with increasing mass concentration at lower aerosol loadings, while
18 the MSEs of ammonium nitrate and ammonium sulfate fluctuated in a narrow range under high
19 aerosol loading conditions when the MSE of organic matter is slightly smaller. One recent study
20 (Tao et al., 2015) showed that the MSE was determined by the proportions of the dominant chemical
21 components and their size distributions under different pollution levels. The MSEs in this work
22 increased consistently with the mass concentration of particles because of the relationship between
23 size and light scattering efficiency.

24 MAE of EC

25 Similar time profiles are seen for the measured absorption coefficient at $\lambda = 470 \text{ nm}$ and the
26 measured mass concentrations of EC and OC (Fig. 7 (a) and (b)). Assuming that only EC contributes
27 to aerosol absorption, the MAE of EC can be calculated using Eq. (4). The MAE values of EC at $\lambda =$
28 470 nm over the campaign period are shown in Fig. 7 (c). These values vary widely, with lower
29 470 nm over the campaign period are shown in Fig. 7 (c). These values vary widely, with lower
30 470 nm over the campaign period are shown in Fig. 7 (c). These values vary widely, with lower

1 values generally seen under cleaner conditions and higher values observed under more polluted
2 conditions. The MAE values for selected clear days (e.g. Nov. 17 - 18; Dec. 1 - Dec. 3; Dec. 29, 2014
3 - Jan. 1, 2015) ranged from 7 - 14 m² g⁻¹ (average of 10.3 ± 2.7 m² g⁻¹) and are comparable to those
4 reported in Beijing during the summer (5 - 13 m² g⁻¹) (Cheng et al., 2011). Much higher values were
5 seen on polluted days, where the MAE ranged from 23 to 81 m² g⁻¹ (average of 48 ± 21 m² g⁻¹) for
6 the period covered Dec. 23 - 28, 2014 and from 20 to 49 m² g⁻¹ (average of 42 ± 14 m² g⁻¹) for Jan. 2
7 - 5, 2015. These values are comparable to those reported by Chan et al. (2011), where MAE ranged
8 from 10 to 50 m² g⁻¹.

9 The average EC mass concentrations were 0.48 ± 0.39 μg m⁻³, 1.18 ± 0.59 μg m⁻³, and 2.72 ±
10 0.87 μg m⁻³, for clear, slightly polluted, and polluted days, respectively. The corresponding mass
11 fractions of 4.3 ± 3.6%, 4.0 ± 2.0%, and 3.6 ± 1.1% were approximately equal within the large
12 variability seen on different days. The mean and standard deviations of MAE values of EC were 23.0
13 ± 14.0 m² g⁻¹, 32.7 ± 16.0 m² g⁻¹, and 35.0 ± 21.7 m² g⁻¹, respectively, for clear, slightly polluted, and
14 polluted days. Our values suggest that EC absorption was strongly enhanced over the campaign
15 period. Enhanced absorption (E_{abs}) could arise from the coating-enhancement of ambient BC
16 absorption (lensing-driven enhancement), as well as absorption associated with light-absorbing
17 organic compounds (brown carbon, BrC) (Andreae and Gelencsér 2006; Bond et al., 2013;
18 Gustafsson, and Ramanathan, 2016). In general, light absorption from other organic species tends to
19 be relatively small at λ = 470 nm, whether it arises from small nitroaromatic compounds (Claeys et
20 al., 2012) or from larger HULIS-type substances (Lorenzo and Young, 2016).

21 Laboratory studies report a BC enhancement factor from 1.8 to 2 for thicker coatings (Bond et
22 al., 2013). Results from field observations are more variable (Peng et al., 2016): reported E_{abs} values
23 ranged from 1.06 (Cappa et al. 2012; Lan et al., 2013) to 1.7 (Lack et al. 2012; Liu et al., 2015),
24 although two recent studies (Cui et al., 2016; Peng et al., 2016) have found that for aged BC (18 h
25 and 4.6 h after fresh emission in clear and polluted condition, respectively), E_{abs} ranged from 2 to 3.
26 Compared to freshly emitted BC, we observe average absorption enhancements of 2.6 (clear), 3.8
27 (slightly polluted), and 4.0 (polluted) for different days. Our values are somewhat higher, although
28 broadly consistent with, the Peng (2016).

29 Our individual MAE of EC values are often appreciably higher than has been observed in other
30 studies (Andreae et al., 2008; Cheng et al., 2011; Wang et al., 2014). This difference may arise from

1 either measurement uncertainties or the contribution of other absorbing species. Large MAE values
2 could arise in part from inaccuracies in both the EC mass concentration or α_{abs} (which is itself
3 determined from the relatively small difference between the extinction and scattering measurements).
4 Moreover, our assumption that all particle absorption arises from EC would lead to higher MAE
5 values if there was simultaneous absorption by other species. L. Wang et al. (2013) have recently
6 shown that BrC was the second-largest absorbing aerosol constituent in Beijing (with a volume
7 fraction of 5 - 25% in the total aerosol volume) and exhibits a clear seasonal variation (dominates in
8 late fall and winter, and extremely low in summer). The sources of BrC have been reported to be the
9 organic components primary emitted from the combustion of biomass and fossil fuels. In a study of
10 biomass burning particle, Lack et al. (2012) showed that the contribution of the absorption of BrC
11 was about 27% at $\lambda = 404$ nm, while other recent studies (Nakayama et al., 2013; Moise et al., 2015)
12 have shown that secondary organic aerosol may also act as BrC.

13 Our data provide some support for the suggestion that SOA is absorbing. Since primary OC and
14 EC are mostly emitted from the same source, EC is a good tracer of primary combustion-generated
15 carbon emissions and the OC/EC ratio can be used as an indicator for the formation of SOA (Cheng
16 et al., 2011). Time-resolved OC and EC data provide a better understanding of the dynamics of SOA
17 formation. In this work, the pattern of MAE coincided well with OC/EC ratio, suggesting that SOA
18 has a non-negligible absorption on polluted days. This also implies that our MAE values reported
19 above are upper limits, and that the absorption contribution of EC is likely to be somewhat smaller.

20 The observed MAEs of $\text{PM}_{1.0}$ were 0.61, 0.75, and $0.60 \text{ m}^2 \text{ g}^{-1}$ for clear, slightly polluted and
21 polluted days, respectively. At the same time, the EC fraction decreased with increasing pollution
22 level (clear days: $0.48 \pm 0.39 \mu\text{g m}^{-3}$ ($4.3 \pm 3.6\%$), slightly polluted days: $1.18 \pm 0.59 \mu\text{g m}^{-3}$ ($4.0 \pm$
23 2.0%) and polluted days: $2.72 \pm 0.87 \mu\text{g m}^{-3}$ ($3.6 \pm 1.1\%$). As EC is the only absorbing species in the
24 modified IMPROVE algorithm, the extinction coefficients reconstructed using equation (5) can be
25 divided into two parts: absorption caused by EC and scattering caused by the other four groups. To
26 compare with the measurement results, the reconstructed $\text{PM}_{1.0}$ mass concentration was used for the
27 calculation of the reconstructed MSEs and MAEs of $\text{PM}_{1.0}$ particles (Fig. 11). The calculated MSEs
28 were 1.64, 1.58 and 1.43 times larger than the observed MSEs for clear, slightly polluted and
29 polluted days, respectively. In contrast, the calculated MAE values were 1.41, 1.67 and 1.54 times
30 smaller than the experimental results. MSEs increased with increasing pollution level in both

1 ~~experimental and calculated results (the differences in measured and calculated MSE values were~~
2 ~~-1.53, -1.82, and -1.78 m² g⁻¹, respectively), whereas for MAEs, the experimental and calculated~~
3 ~~values increased in slightly polluted conditions, but decreased under polluted conditions (the~~
4 ~~differences in the measured and calculated values were 0.18, 0.30, and 0.21 m² g⁻¹, respectively).~~
5 ~~Even though further improvement of the calculation method is necessary, the large difference of~~
6 ~~MAE on slightly polluted days suggests aerosol absorption is incompletely represented. This~~
7 ~~discrepancy may indicate the presence of other light absorbing components such as brown carbon,~~
8 ~~BrC. Wang et al. (2013) have recently shown that BrC was the second largest absorbing aerosol~~
9 ~~constituent in Beijing (with a contribution of about 5–25%) and exhibits a clear seasonal variation~~
10 ~~(dominates in late fall and winter, and extremely low in summer).~~

11 **Period 6: Second traffic-dominated pollution period (08:00–11:10 LT 24 November)**

12
13 This period corresponded to the morning rush hour on 24 November. The mean values of $\alpha_{\text{ep},470}$,
14 $\alpha_{\text{sp},470}$ and $\alpha_{\text{ap},470}$ were 80 ± 42 , 64 ± 34 and $16 \pm 8 \text{ Mm}^{-1}$, respectively, and were slightly larger than
15 in the first traffic-dominated pollution period. The mean values of ω_{470} (0.78 ± 0.04), n and k ($1.40 \pm$
16 0.04 and 0.04 ± 0.02) were comparable to the earlier traffic period. The mean diameter of the number
17 and surface size distribution was 64 ± 12 and 226 ± 14 nm, respectively, and a larger n value was
18 found. In this period, strong winds from the north transported clean air to the observation site,
19 leading to lower particle concentrations and a greater influence of fresh local emissions.

21 **4.2.3 Aerosol size distributions, optical properties, chemical composition and light extinction** 22 **apportionment on different air pollution days**

23
24 Averages and standard deviations of the observed particle properties are summarized in Table 1
25 after grouping data into the different air quality classes. There are obvious differences of the
26 campaign average number and surface size distribution of PM_{1.0} for the three different pollution
27 categories (Fig. 5a). For clear days, the mean particle number size distributions fitted by a mono-log
28 normal function was around 41 nm. Bimodal distributions were observed on slightly polluted and
29 polluted days with modes centered at 38 and 105 nm (slightly polluted periods) and at 38 and 151 nm
30 (polluted periods). The mode of the number size distributions exhibits the expected displacement

~~toward the accumulation mode with increasing levels of particulate matter.~~

Chemical composition

Table 1 and Fig. ~~5b-68~~ show the mean mass concentration values and the mean percentile compositions of observed chemical compositions of PM_{1.0} particles under different pollution levels. The contribution of sulfate, nitrate and ammonium to the observed PM_{1.0} mass concentration increased strongly on polluted compared to clear days (from 34 to 44%). Similar trends were observed for PM_{2.5} and NR-PM_{1.0} during the January 2013 severe haze events in Beijing (Y.-L. Sun et al., 2014; Tao et al., 2015; G. J. Zheng et al., 2015).

On average, OM, nitrate, sulfate, ammonium, chloride and EC comprised 46.3% ($13.3 \pm 11.1 \mu\text{g m}^{-3}$), 18.0% ($5.2 \pm 5.5 \mu\text{g m}^{-3}$), 11.6% ($3.3 \pm 3.5 \mu\text{g m}^{-3}$), 10.3% ($3.0 \pm 3.6 \mu\text{g m}^{-3}$), 5.3% ($1.5 \pm 1.9 \mu\text{g m}^{-3}$) and 3.9% ($1.1 \pm 0.9 \mu\text{g m}^{-3}$) of observed PM_{1.0}, respectively. The organic mass was the largest proportion in PM_{1.0} particles, and the contribution of nitrate was larger than that of sulfate. Compared to summer, the mass contribution of organics was significantly higher during winter, and primary organic aerosol dominated during the coal heating season (Sun et al., 2013). Huang et al. (2014) reported that secondary organic aerosol (SOA) contributed 26% of PM_{2.5} in Beijing in the January 2013 severe haze events, and indicated the dominant effect of fossil fuel SOA formation in Beijing regions.

Compared to sulfate, the fractional composition of nitrate and ammonium aerosol increased under high levels of pollution. Similar increases in the proportion of secondary inorganic species, and particularly nitrates, have been observed during other haze episodes in the North China Plain and other Chinese megacities (Pathak et al., 2009; Jansen et al., 2014; Tian et al., 2015). Based on the relative abundances of nitrate and ammonium, these increases have been attributed to gas phase formation of nitrate from HNO₃ and NH₃. In our results, the molar ratios [NO₃]/[SO₄] and [NH₄]/[SO₄] fall between 2.1 to 2.5, and 3.0 to 5.2, respectively (based on the mean concentrations of these components), and are consistent with this explanation for an ammonium-rich regime (Pathak et al., 2009; Tian et al., 2015). It is worth noting that the increases in secondary inorganic species is not universal: some studies have reported haze episodes (or portions of such episodes) in which the

organic fraction increases substantially (Tian et al., 2015; Wang et al., 2015). This difference likely reflects the relative importance of sources and atmospheric processing in both the gas and liquid phases during such events. (Tian et al., 2016). The differences may be due to both photochemical and aqueous processing which are important in nitrate formation (Wang et al., 2015) and may play a more important role in sulfate formation during wintertime (Sun et al., 2013).

Optical properties

~~There was no obvious correlation between extensive optical properties and wind direction (Fig. S4). With increasing pollutant level, the extensive optical properties ($\alpha_{\text{sp},470}$, $\alpha_{\text{ap},470}$ and $\alpha_{\text{ep},470}$) increased strongly, in accordance with the expected, strong dependence of particle size on light scattering. In contrast, changes in the intensive optical properties (ω_{470}) were more modest. The optical measurement data are presented as histograms of the relative frequency of occurrence of $\alpha_{\text{sp},470}$, $\alpha_{\text{ap},470}$, $\alpha_{\text{ep},470}$ and ω_{470} (Fig. 6). Approximately 71% of extinction and scattering coefficients values were lower than 200 Mm^{-1} and nearly 80% of absorption coefficient values were located in the range of $1.5\text{--}50 \text{ Mm}^{-1}$. Approximately 90% of the ω_{470} values fell into the range of 0.70–0.97. Compared with polluted days, the frequency distribution of the SSA showed similar patterns, and the average values were similar on clear and slightly polluted days.~~

The Huairou site is a new suburban site at which aerosol optical properties have not previously been reported. To put our observations at Huairou in context, the scattering and absorption coefficients and SSA observed in this campaign are compared in Table 3 to those at other locations (urban, suburban, and rural sites). As would be expected given the high concentrations of particulate matter in much of China, the mean $\alpha_{\text{sp},470}$ value at Huairou was considerably higher than values observed in America and Europe, including the Los Angeles basin measurements in Pasadena (Thompson et al., 2012) and the urban site of Granada (Titos et al., 2012). Within China, the Huairou values for scattering and absorption were higher than in Shanghai (Li et al., 2013) and similar to the urban site of Guangzhou in China (Garland et al., 2008). Compared with other non-urban polluted sites in China, both $\alpha_{\text{sp},470}$ and $\alpha_{\text{ap},470}$ at Huairou were lower than Xinken (Cheng et al., 2008), Yufa (Garland et al., 2009) and much lower than Xianghe (Li et al., 2007). Moreover, the $\alpha_{\text{sp},470}$ values

were comparable to those observed at Shangdianzi, an atmospheric background site located ~150 km northeast of the urban center of Beijing (Yan et al., 2008). The average value of $\alpha_{\text{ap},470}$ at Huairou was lower than those seen at other urban and suburban locations in China, with the exceptions of Guangzhou (reflecting the lower SSA values observed in Huairou) and the rural site of Shangdianzi.

The regional differences in SSA can be considered in terms of the different sources of particles, including local primary emissions, transport emissions and secondary aerosol formations. The average value of ω_{470} at Huairou was 0.80 ± 0.08 , which was lower than suburban sites in Xinken (0.83 ± 0.05), Xianghe ($0.81-0.85$) and Yufa (0.86 ± 0.07), and rural sites in Shangdianzi (0.88 ± 0.05), and Pasadena (0.92 ± 0.08). Compared to urban sites, the Huairou SSA was similar to observations in Beijing (0.80 ± 0.09) (He et al., 2009), but considerably higher than in Shanghai (0.70 ± 0.07) (Li et al., 2013) and Granada (0.71 ± 0.07) (Titos et al., 2012). The lower SSA values probably arose from the higher contribution of vehicular emissions in Shanghai (Zhou et al., 2009) and both traffic emissions and a higher mass fraction of light absorbing particles caused by fuel-oil combustion in Granada (Titos et al., 2012).

The diurnal variations of hourly averaged extinction, scattering, absorption coefficient and SSA on clear, slightly polluted and polluted days are presented in Fig. 7. Broadly similar patterns were observed for the extensive optical properties for different pollutant levels. Extinction ($\alpha_{\text{ep},470}$) and scattering ($\alpha_{\text{sp},470}$) tended to be lower during daytime and higher at night. Emissions associated with morning rush hour are apparent in the aerosol optical properties. $\alpha_{\text{ep},470}$ and $\alpha_{\text{sp},470}$ increased slowly in the morning (07:00–09:00 LT) to peak values at 09:00 LT, indicating significant emission and formation of particles during this period; these properties then decreased slowly until about 14:00 LT. The maximum values of $\alpha_{\text{ap},470}$ occurred during the traffic rush hour and could be attributed to direct emissions of light absorbing species from vehicles. We note that the increase in $\alpha_{\text{ap},470}$ from 06:00 to the maximum at 08:00 to 09:00 LT varied from 10 to 20 Mm^{-1} and was quite consistent across different pollutant days. This observation suggests that the number and type of particles emitted during this time period is not strongly influenced by pre-existing pollutant levels; however, this is what would be expected for relatively constant daily emissions from traffic.

Chemical apportionment of aerosol optical properties

1 Over the past years, the chemical apportionment of α_{ep} or α_{sp} has been conducted in both urban
2 and non-urban regions (Malm et al., 1994; Watson, 2002; Cheung et al., 2005; Malm and Hand, 2007;
3 Yang et al., 2007; Tao et al., 2009; Cao et al., 2012; Han et al., 2014; Tao et al., 2014a; Cheng et al.,
4 2015). Ammonium sulfate was generally the largest contributor to $PM_{2.5}$ or PM_{10} α_{ep} , with a range
5 from 20–50%. However, fewer studies have been reported of the chemical contribution of different
6 chemical components to the extinction of $PM_{1.0}$ under different pollution levels. ~~Studies in other~~
7 ~~Chinese megacities, such as Shanghai (Cheng et al., 2015) and Guangzhou (Tao et al., 2014b), and~~
8 ~~data from US monitoring sites show that the revised IMPROVE algorithm underestimates the $PM_{2.5}$~~
9 ~~extinction under high aerosol loading but overestimates the values under low aerosol loading. The~~
10 ~~underestimation and overestimation ratios in different studies ranged from –11 to –26 % and +25 to~~
11 ~~+54 %, respectively (Cheng et al., 2015).~~

12 ~~In this work, $\alpha_{ep,470}$ of $PM_{1.0}$ particles was reconstructed using the modified IMPROVE~~
13 ~~algorithm based on the measured concentrations of each composition (Fig. 8a), which correlated well~~
14 ~~with the measured $\alpha_{ep,470}$ ($R^2 = 0.96$) during this campaign (Fig. 8c). With improved mass extinction~~
15 ~~efficiencies, the agreement between the measured and calculated $PM_{1.0}$ extinctions is good (with a~~
16 ~~slope of 1.04 ± 0.04) when the measured extinction coefficient is lower than $300 Mm^{-1}$ (as shown in~~
17 ~~the insert of Fig. 8c). When the observed extinction coefficients are larger than $300 Mm^{-1}$, the~~
18 ~~reconstructed values of the modified IMPROVE algorithm were 16% lower than observed values~~
19 ~~(calculated from the average of the ratios of the measured extinction to the reconstructed extinction~~
20 ~~for all points $> 300 Mm^{-1}$). The modified IMPROVE algorithm for $PM_{1.0}$ at $\lambda = 470$ nm represents~~
21 ~~the chemical apportionment of light extinction quite well. The reconstructed $PM_{1.0}$ mass~~
22 ~~concentration (Fig. 8b) using the modified IMPROVE algorithm was well correlated with the~~
23 ~~measured $PM_{1.0}$ mass concentration (the summation of the concentrations of eight water-soluble ion~~
24 ~~compositions and carbon concentration (including elemental carbon, [EC], and organic mass,~~
25 ~~$1.6 \times [OC]$)) ($R^2 = 0.99$, slope = 1.00, intercept = 0.28) (Fig. 8d), indicating that the modified~~
26 ~~IMPROVE algorithm can be used to estimate the chemical apportionment for extinction in this~~
27 ~~campaign.~~

28 In this work, the average fractional contributions of each chemical component of dry $PM_{1.0}$
29 extinction coefficient with respect to different pollution levels were calculated with the IMPROVE
30 algorithm (Fig. 9). ~~are shown in Fig. 97.~~ The optical extinction caused by OM, ammonium nitrate,

1 ammonium sulfate, elemental carbon and sea salt accounted for 57.9, 17.8, 12.5, 8.6 and 3.2 % of the
2 reconstructed $PM_{1.0}$ extinction in this campaign, respectively. The contribution of chemical
3 compositions to aerosol extinction depends mainly on their mass concentrations. The mass
4 concentrations of OM, ammonium nitrate, ammonium sulfate, element carbon and sea salt accounted
5 for 50.4, 21.2, 16.8, 4.2 and 7.4 % of the reconstructed $PM_{1.0}$ mass concentrations, respectively. The
6 organic constituents comprised a large fraction of $PM_{1.0}$ mass concentration, consistent with previous
7 studies (Yao et al., 2010; Sun et al., 2013), and ~~—~~

8 ~~OM~~ therefore made the largest contribution to the extinction of $PM_{1.0}$ particles in this study. The
9 relative contribution of OM (58 %) to the total extinction reported here was comparable to that
10 previously reported in Beijing (54 %) during an extreme haze episode in January 2013 for $PM_{1.0}$
11 scattering (Wang et al., 2015), and in Shenzhen (45 %) in the winter of 2009 for $PM_{2.5}$ extinction
12 (Yao et al., 2010). The contribution of organics in Beijing increases significantly during the winter
13 coal heating season (Sun et al., 2013). Emissions from the large number of vehicles in the
14 mega-cities of China also contributes significantly to organic aerosol (Huang et al., 2014). From
15 clear days to slightly polluted days, the relative contribution of organic mass to light extinction
16 increased by 7 %, which may due to an increasing contribution of secondary organic aerosol (SOA)
17 (Huang et al., 2014). The concentrations of nitrate and ammonium aerosol increased under high
18 levels of pollution, and the relative contribution of ammonium nitrate to $PM_{1.0}$ light extinction
19 increased by 6.7 % under these conditions ~~(Wang et al., 2015). Various anthropogenic emissions,~~
20 ~~especially coal consumption, biomass burning and vehicle exhaust, result in many sources of EC in~~
21 ~~the NCP. Although EC only comprised about 4 % of $PM_{1.0}$ mass concentration, it contributed~~
22 ~~appreciably to $PM_{1.0}$ extinction owing to its high absorption efficiency.—~~

23 The parameterization of EC extinction in the modified IMPROVE algorithm is based on the
24 optical properties of freshly emitted EC. However, Section 4.2 showed that, both in our work and in
25 previous studies, EC absorption in ambient aerosols is enhanced several-fold. Not accounting for the
26 effective absorption of EC will underestimate the extinction, as in indeed borne out in the correlation
27 between calculated and measured extinctions (Fig. S3(c)). To address this issue, we investigated
28 parameterizing the IMPROVE algorithm based on the absorption enhancement of 2.4-fold recently
29 reported by Peng et al. (2016). The BC term in the modified IMPROVE function was changed as
30 follows: (1) an absorption enhancement factor of 2.4 gave a new MAE value of $20.9 \text{ m}^2 \text{ g}^{-1}$ for BC at

$\lambda = 470$ nm; and (2) a scattering contribution from EC (based on an SSA of 0.2 (Bond and Bergstrom, 2006)), produced a MSE value of $2.18 \text{ m}^2 \text{ g}^{-1}$ for BC. The MEE term ($10.8 \text{ m}^2 \text{ g}^{-1}$) in the modified IMPROVE was replaced with the summation of the two parts ($23 \text{ m}^2 \text{ g}^{-1}$ at $\lambda = 470$ nm). These changes raised the calculated aerosol extinction by 8% (Fig. S10), thereby improving the agreement with measurements. The deviation of the correlation between calculations and measurements from unity was reduced from 23% to 15%. The revised MEE of EC doubled the contribution of EC to the total aerosol extinction from 8.7% to 17% (Fig. S11). The SSA from the IMPROVE calculations accordingly decreased from 0.91 to 0.83, in much better agreement with the mean measured SSA of 0.80. We therefore recommend implementing these changes to the MEE of EC when applying the IMPROVE algorithm, particularly in polluted environments.

The contribution of EC to the total extinction is therefore considerable, despite contributing only 4% to the total aerosol mass. Major sources of EC in the NCP include coal consumption, biomass burning and vehicle exhaust. In the context of several haze episodes in the NCP, recent modeling studies have shown that EC, as the major absorbing component of aerosols, causes local atmospheric heating and thereby exacerbates aerosol pollution by reducing the planetary boundary layer height (Ding et al., 2016; Gao et al., 2015; Gao et al., 2016). The disproportionately large effect of EC observed in our study supports the suggestion in these papers that targeting the reduction of EC emissions will pay off both in improving air quality and reducing climate impacts.

~~4.3 MSE and MAE of $\text{PM}_{1.0}$~~

~~Figure 10 shows the relationship between the scattering and absorption coefficients and $\text{PM}_{1.0}$ mass concentrations under different pollution levels. The $\text{PM}_{1.0}$ mass concentrations were determined by multiplying the volume concentrations with the volume-weighted mass density of each filter sample (Hasan and Dzubay, 1983). The scattering and (to a lesser extent) the absorption coefficients were generally well correlated with the $\text{PM}_{1.0}$ mass concentrations and have small y-intercepts. (The larger deviation of the y-intercept on polluted days likely stems from the smaller number of low mass concentration observations on these days.)~~

~~The derived $\text{PM}_{1.0}$ average mass scattering and absorption efficiencies during the campaign were 3.60 and $0.70 \text{ m}^2 \text{ g}^{-1}$, respectively (Fig. 10d). Statistical uncertainties from the slope of the regression~~

1 are misleadingly small and have been omitted in the reported MSE and MAE values. The MSE and
2 MAE values are smaller than those observed by Garland et al. (2008) from suburban Guangzhou in
3 July 2006 (where the $PM_{1.0}$ mass scattering and absorption efficiency calculated with assuming an
4 average effective density of ammonium sulfate (1.7 g cm^{-3}) were 4.13 and $1.09 \text{ m}^2 \text{ g}^{-1}$, respectively),
5 the value of $PM_{2.5}$ at $\lambda = 520 \text{ nm}$ obtained in urban Beijing ($4.8 \text{ m}^2 \text{ g}^{-1}$) during wintertime (Tao et al.,
6 2015), and in Chengdu and Guangzhou ($3.9 \text{ m}^2 \text{ g}^{-1}$) (Tao et al., 2014a, b). The derived mass
7 extinction efficiency is $4.30 \text{ m}^2 \text{ g}^{-1}$, which was comparable to the reported values during Aerosols
8 1999 ($4.1\text{--}5.4 \text{ m}^2 \text{ g}^{-1}$) (Quinn et al., 2001) and INDOEX 1999 ($4.0\text{--}5.6 \text{ m}^2 \text{ g}^{-1}$) (Quinn et al., 2002).

9 In this work, the MSE of $PM_{1.0}$ was $4.16 \text{ m}^2 \text{ g}^{-1}$ during polluted days, which was 34% higher
10 than that during the slightly polluted days ($3.11 \text{ m}^2 \text{ g}^{-1}$) and 75% higher than that during the clear
11 days ($2.38 \text{ m}^2 \text{ g}^{-1}$) (Fig. 10a–e). The variability in MSE is typically more dependent on mass size
12 distribution than on density or refractive index (Hand and Malm, 2007). As shown in Fig. 5(a), the
13 particle diameter increased significantly with high aerosol mass concentrations. The MSEs in this
14 work increased consistently with pollution level, primarily because larger particles scatter light more
15 efficiently. Cheng et al. (2015) showed that the MSEs of ammonium nitrate, ammonium sulfate and
16 organic matter increased rapidly with increasing mass concentration at lower aerosol loadings, while
17 the MSEs of ammonium nitrate and ammonium sulfate fluctuated in a narrow range under high
18 aerosol loading conditions when the MSE of organic matter is slightly smaller. One recent study
19 (Tao et al., 2015) showed that the MSE was determined by the proportions of the dominant chemical
20 components and their size distributions under different pollution levels. The MSEs in this work
21 increased consistently with the mass concentration of particles because of the relationship between
22 size and light scattering efficiency.

23 The observed MAEs of $PM_{1.0}$ were 0.61 , 0.75 , and $0.60 \text{ m}^2 \text{ g}^{-1}$ for clear, slightly polluted and
24 polluted days, respectively. At the same time, the EC fraction decreased with increasing pollution
25 level (clear days: $0.48 \pm 0.39 \mu\text{g m}^{-3}$ ($4.3 \pm 3.6\%$), slightly polluted days: $1.18 \pm 0.59 \mu\text{g m}^{-3}$ ($4.0 \pm$
26 2.0%) and polluted days: $2.72 \pm 0.87 \mu\text{g m}^{-3}$ ($3.6 \pm 1.1\%$). As EC is the only absorbing species in the
27 modified IMPROVE algorithm, the extinction coefficients reconstructed using equation (5) can be
28 divided into two parts: absorption caused by EC and scattering caused by the other four groups. To
29 compare with the measurement results, the reconstructed $PM_{1.0}$ mass concentration was used for the
30 calculation of the reconstructed MSEs and MAEs of $PM_{1.0}$ particles (Fig. 11). The calculated MSEs

~~were 1.64, 1.58 and 1.43 times larger than the observed MSEs for clear, slightly polluted and polluted days, respectively. In contrast, the calculated MAE values were 1.41, 1.67 and 1.54 times smaller than the experimental results. MSEs increased with increasing pollution level in both experimental and calculated results (the differences in measured and calculated MSE values were 1.53, 1.82, and 1.78 m² g⁻¹, respectively), whereas for MAEs, the experimental and calculated values increased in slightly polluted conditions, but decreased under polluted conditions (the differences in the measured and calculated values were 0.18, 0.30, and 0.21 m² g⁻¹, respectively). Even though further improvement of the calculation method is necessary, the large difference of MAE on slightly polluted days suggests aerosol absorption is incompletely represented. This discrepancy may indicate the presence of other light absorbing components such as brown carbon, BrC. Wang et al. (2013) have recently shown that BrC was the second largest absorbing aerosol constituent in Beijing (with a contribution of about 5–25%) and exhibits a clear seasonal variation (dominates in late fall and winter, and extremely low in summer).~~

5 Summary and conclusions

PM_{1.0} optical properties and composition at a suburban site near Beijing were measured during the HOPE-J³A campaign. Six periods were investigated in detail to study the evolution of intensive optical properties and chemical composition in PM_{1.0} during an extended haze episode. Our analysis reveals that the optical properties of aerosols change significantly during the evolution of haze.

~~New particle formation and primary emissions were apparent on clear days. The highest values of ω_{470} and the lowest values of imaginary part of the effective CRI suggest that particle extinction following new particle formation is dominated by scattering. During the formation of haze, both the size and number concentration of atmospheric fine particles increased, which increased the light scattering efficiency and the real component of the effective CRI. Traffic-dominated pollution periods were characterized by small, light absorbing particles (e.g., black carbon), leading to the lowest SSA and the highest imaginary component of the effective CRI. For the combined pollution period, the accumulation of original and newly discharged primary pollutants led to sharp variations in the aerosol size distribution and extensive optical properties.~~

The mass concentrations of sulfate, nitrate, and ammonium species were high during haze

1 episodes. Organic matter was consistently the dominant constituent by mass of the observed aerosols,
2 and light extinction apportionment indicated that was it accordingly made the largest contribution to
3 the extinction of $PM_{1.0}$. Under polluted conditions, the proportion of inorganic components,
4 especially nitrate, was higher than under clean conditions and the contribution of inorganic
5 components to visibility degradation was significant.

6 Under polluted conditions, the average MAE of EC were up to 4 times as large as the reference
7 MAE value for freshly emitted BC. The temporal pattern of MAE values was similar to that of the
8 OC/EC ratio, suggesting that some non-BC absorption from SOA also contributes to particle
9 absorption. After considering the coating enhanced absorption by EC, agreement with measurements
10 was improved with the new modified IMPROVE algorithm. Organic mass was the largest
11 contributor (52%) to the total extinction of $PM_{1.0}$, while EC, despite its mass concentration being
12 only 4%, contributed about 17%, to extinction. EC, owing to its high absorption efficiency,
13 contributed appreciably to $PM_{1.0}$ extinction and should be a key target to air quality controls.

14
15 *Acknowledgements.* The authors wish thank to Zhouqing Xie at University of Science and
16 Technology of China for providing the meteorological data used in this paper and to Jun Tao and
17 Zejian Lin at South China Institute of Environmental Science for helpful discussion. This research
18 was supported by the National Natural Science Foundation of China (41330424), the Natural Science
19 Foundation of Anhui Province (1508085J03), the Key Research Program of the Chinese Academy of
20 Sciences (KJZD-EW-TZ-G06-01), and the China Special Fund for Meteorological Research in the
21 Public Interest (GYHY201406039). The support of the CaPPA project (“Chemical and Physical
22 Properties of the Atmosphere”), funded by the French National Research Agency through the
23 “Programme d’Investissement d’Avenir” (under contract ANR-10-LABX-005), is acknowledged.

24 We thank the reviewers and editor for their constructive suggestions.

27 **References**

28
29 Abo Riziq, A., Erlick, C., Dinar, E., and Rudich, Y.: Optical properties of absorbing and
30 non-absorbing aerosols retrieved by cavity ring down (CRD) spectroscopy, *Atmos. Chem.*
31 *Phys.*, 7, 1523–1536, doi:10.5194/acp-7-1523-2007, 2007.

- 1 Anderson, T. L., Charlson, R. J., Schwartz, S. E., Knutti, R., Boucher, O., Rodhe, H., and
2 Heintzenberg, J.: Atmospheric science. Climate forcing by aerosol – a hazy picture, *Science*,
3 300, 1103–1104, 2003.
- 4 Andersson, A., Deng, J., Du, K., Zheng, M., Yan, C., Skold, M., and Gustafsson, O.:
5 Regionally varying combustion sources of the January 2013 severe haze events over eastern
6 China, *Environ. Sci. Technol.*, 49, 2038–2043, doi:10.1021/es503855e, 2015.
- 7 [Andreae, M. O. and Gelencsér, A.: Black carbon or brown carbon? The nature of light-absorbing
8 carbonaceous aerosols, *Atmos. Chem. Phys.*, 6, 3131-3148, doi:10.5194/acp-6-3131-2006,
9 2006.](#)
- 10 [Andreae, M.O., Schmid, O., Yang, H., Chand, D., Yu, J.Z., Zeng, L.-M., and Zhang, Y.-H.: Optical
11 properties and chemical composition of the atmospheric aerosol in urban Guangzhou, China,
12 *Atmos. Environ.*, 42, 6335–6350, 2008.](#)
- 13 Bahadur, R., Praveen, P. S., Xu, Y., and Ramanathan, V.: Solar absorption by elemental and brown
14 carbon determined from spectral observations, *P. Natl. Acad. Sci. USA*, 109, 17366–17371,
15 2012.
- 16 Bates, T. S., Huebert, B. J., Gras, J. L., Griffiths, F. B., and Durkee, P. A.: International Global
17 Atmospheric Chemistry (IGAC) project’s first aerosol characterization experiment (ACE 1):
18 overview, *J. Geophys. Res.*, 103, 16297–16318, doi:10.1029/97jd03741, 1998.
- 19 Bates, T. S., Anderson, T. L., Baynard, T., Bond, T., Boucher, O., Carmichael, G., Clarke, A., Erlick,
20 C., Guo, H., Horowitz, L., Howell, S., Kulkarni, S., Maring, H., McComiskey, A.,
21 Middlebrook, A., Noone, K., O’Dowd, C. D., Ogren, J., Penner, J., Quinn, P. K., Ravishankara,
22 A. R., Savoie, D. L., Schwartz, S. E., Shinozuka, Y., Tang, Y., Weber, R. J., and Wu, Y.:
23 Aerosol direct radiative effects over the northwest Atlantic, northwest Pacific, and North
24 Indian Oceans: estimates based on in-situ chemical and optical measurements and chemical
25 transport modeling, *Atmos. Chem. Phys.*, 6, 1657–1732, doi:10.5194/acp-6-1657-2006, 2006.
- 26 [Bond, T. C., Doherty, S. J., Fahey, D. W., Forster, P. M., Berntsen, T., DeAngelo, B. J., Flanner, M.
27 G., Ghan, S., Kärcher, B., Koch, D., Kinne, S., Kondo, Y., Quinn, P. K., Sarofim, M. C.,
28 Schultz, M. G., Schulz, M., Venkataraman, C., Zhang, H., Zhang, S., Bellouin, N., Guttikunda,
29 S. K., Hopke, P. K., Jacobson, M. Z., Kaiser, J. W., Klimont, Z., Lohmann, U., Schwarz, J. P.,
30 Shindell, D., Storelvmo, T., Warren, S. G., and Zender C. S.: Bounding the role of black carbon
31 in the climate system: A scientific assessment, *J. Geophys. Res. Atmos.*, 118, 5380 - 5552,
32 doi:10.1002/jgrd.50171, 2013.](#)
- 33 [Bond, T. C., Habib, G., and Bergstrom, R. W.: Limitations in the enhancement of visible light
34 absorption due to mixing state, *J. Geophys. Res.*, 111\(D20\), 211, doi:10.1029/2006JD007315,
35 2006.](#)
- 36 Cahill, J. F., Suski, K., Seinfeld, J. H., Zaveri, R. A., and Prather, K. A.: The mixing state of
37 carbonaceous aerosol particles in northern and southern California measured during CARES
38 and CalNex 2010, *Atmos. Chem. Phys.*, 12, 10989–11002, doi:10.5194/acp-12-10989-2012,
39 2012.
- 40 Cao, J., Chow, J. C., Lee, F. S. C., and Watson, J. G.: Evolution of PM_{2.5} measurements and
41 standards in the US and future perspectives for china, *Aerosol Air Qual. Res.*, 13, 1197–1211,
42 2013.
- 43 Cao, J. J., Wang, Q. Y., Chow, J. C., Watson, J. G., Tie, X. X., Shen, Z. X., Wang, P., and An, Z. S.:
44 Impacts of aerosol compositions on visibility impairment in Xi’an, China, *Atmos. Environ.*, 59,

1 559–566, doi:10.1016/j.atmosenv.2012.05.036, 2012.

2 [Cappa, C. D., Onasch, T. B., Massoli, P., Worsnop, D. R., Bates, T. S., Cross, E. S., Davidovits, P.,](#)
3 [Hakala, J., Hayden, K. L., Jobson, B. T., Kolesar, K. R., Lack, D. A., Lerner, B. M., S. M.,](#)
4 [Mellon, D., Nuaaman, I., Olfert, J. S., Petäjä, T., Quinn, P. K., Song, C., Subramanian, R.,](#)
5 [Williams, E. J., and Zaveri, R. A. : Radiative absorption enhancements due to the mixing state](#)
6 [of atmospheric black carbon, *Science*, 337, 1078 - 1081, doi:10.1126/science.1223447, 2012.](#)

7 [Chan, T. W., Brook, J. R., Smallwood, G. J., and Lu, G.: Time resolved measurements of black](#)
8 [carbon light absorption enhancement in urban and near-urban locations of southern Ontario,](#)
9 [Canada, *Atmos. Chem. Phys.*, 11, 10407 - 10432, doi:10.5194/acp-11-10407-2011, 2011.](#)

10 [Cheng, Y., He, K.-B., Zheng, M., Duan, F.-K., Du, Z.-Y., Ma, Y.-L., Tan, J.-H., Yang, F.-M., Liu,](#)
11 [J.-M., Zhang, X.-L., Weber, R. J., Bergin, M. H., and Russell, A. G.: Mass absorption](#)
12 [efficiency of elemental carbon and water-soluble organic carbon in Beijing, China, *Atmos.*](#)
13 [Chem. Phys., 11, 11497-11510, doi:10.5194/acp-11-11497-2011, 2011.](#)

14 [Cheng, Y., Engling, G., Moosmüller, H., Arnott, W.P., Chen, L.W.A., Wolde, C. E., Min Hao, W.M.,](#)
15 [and He, K.B.: Light absorption by biomass burning source emissions, *Atmos. Environ.*, 127,](#)
16 [347 - 354, 2016.](#)

17 Cheng, Y. F., Wiedensohler, A., Eichler, H., Su, H., Gnauk, T., Brüggemann, E., Herrmann, H.,
18 Heintzenberg, J., Slanina, J., Tuch, T., Hu, M., and Zhang, Y. H.: Aerosol optical properties
19 and related chemical apportionment at Xinken in Pearl River Delta of China, *Atmos. Environ.*,
20 30 42, 6351–6372, doi:10.1016/j.atmosenv.2008.02.034, 2008.

21 Cheng, Z., Jiang, J., Chen, C., Gao, J., Wang, S., Watson, J. G., Wang, H., Deng, J., Wang, B., Zhou,
22 M., Chow, J. C., Pitchford, M. L., and Hao, J.: Estimation of aerosol mass scattering
23 efficiencies under high mass loading: case study for the megacity of Shanghai, China, *Environ.*
24 *Sci. Technol.*, 49, 831–838, doi:10.1021/es504567q, 2015.

25 Cheung, H. C., Wang, T., Baumann, K., and Guo, H.: Influence of regional pollution outflow on the
26 concentrations of fine particulate matter and visibility in the coastal area of southern China,
27 *Atmos. Environ.*, 39, 6463–6474, doi:10.1016/j.atmosenv.2005.07.033, 2005.

28 Chu, D. A., Kaufman, Y. J., Zibordi, G., Chern, J. D., Mao, J. T., Li, C. C., and Holben, B. N.:
29 Global monitoring of air pollution over land from the Earth Observing System-Terra Moderate
30 Resolution Imaging Spectroradiometer (MODIS), *J. Geophys. Res.*, 108(D21), 4661, 2003.

31 [Claeys, M., Vermeylen, R., Yasmeeen, F., Gómez-González, Y., Chi, C., Maenhaut, W., Mészáros, T.,](#)
32 [and Salma, I.: Chemical characterisation of humic-like substances from urban, rural and](#)
33 [tropical biomass burning environments using liquid chromatography with UV/vis photodiode](#)
34 [array detection and electrospray ionisation mass spectrometry, *Environ. Chem.*, 9, 273-284,](#)
35 [2012.](#)

36 [Cui, X., Wang, X., Yang, L., Chen, B., Chen, J., Andersson, A. and Gustafsson, Ö. : Radiative](#)
37 [absorption enhancement from coatings on black carbon aerosols, *Sci. Total Environ.* 551-552,](#)
38 [51 - 56, 2016.](#)

39 [Di Lorenzo, R. A., and Young C. J.: Size separation method for absorption characterization in brown](#)
40 [carbon: Application to an aged biomass burning sample, *Geophys. Res. Lett.*, 43, 458–465,](#)
41 [doi:10.1002/2015GL066954, 2016.](#)

42 Dinar, E., Abo Riziq, A., Spindler, C., Erlick, C., Kiss, G., and Rudich, Y.: The complex refractive
43 index of atmospheric and model humic-like substances (HULIS) retrieved by a cavity ring
44 down aerosol spectrometer (CRD-AS), *Faraday Discuss.*, 137, 279–295, 2008.

- 1 [Ding, A. J., Huang, X., Nie, W., Sun, J. N., Kerminen, V.-M., Petäjä, T., Su, H., Cheng, Y. F., Yang,](#)
2 [X.-Q., Wang, M. H., Chi, X. G., Wang, J. P., Virkkula, A., Guo, W. D., Yuan, J., Wang, S. Y.,](#)
3 [Zhang, R. J., Wu, Y. F., Song, Y., Zhu, T., Zilitinkevich, S., Kulmala, M., and Fu, C. B.:](#)
4 [Enhanced haze pollution by black carbon in megacities in China, *Geophys. Res. Lett.*, 43, 2873](#)
5 [- 2879, doi:10.1002/2016GL067745, 2016.](#)
- 6 Doherty, S. J., Quinn, P. K., Jefferson, A., Carrico, C. M., Anderson, T. L., and Hegg, D.: A
7 comparison and summary of aerosol optical properties as observed in situ from aircraft, ship,
8 and land during ACE-Asia, *J. Geophys. Res.*, 110, D04201, doi:10.1029/2004jd004964, 2005.
- 9 Eldering, A., Ogren, J. A., Chowdhury, Z., Hughes, L. S., and Cass, G. R.: Aerosol optical properties
10 during INDOEX based on measured aerosol particle size and composition, *J. Geophys. Res.*,
11 107, 8001, doi:10.1029/2001jd001572, 2002.
- 12 Fiedler, S. E., Hese, A., and Ruth, A. A.: Incoherent broad-band cavity-enhanced absorption
13 spectroscopy, *Chem. Phys. Lett.*, 371, 284–294, 2003.
- 14 [Gao, Y., Zhang, M., Liu, Z., Wang, L., Wang, P., Xia, X., Tao, M., and Zhu, L.: Modeling the](#)
15 [feedback between aerosol and meteorological variables in the atmospheric boundary layer](#)
16 [during a severe fog-haze event over the North China Plain, *Atmos. Chem. Phys.*, 15,](#)
17 [4279-4295, doi:10.5194/acp-15-4279-2015, 2015.](#)
- 18 [Gao, M., Carmichael, G. R., Wang, Y., Saide, P. E., Yu, M., Xin, J., Liu, Z., and Wang, Z.:](#)
19 [Modeling study of the 2010 regional haze event in the North China Plain, *Atmos. Chem. Phys.*,](#)
20 [16, 1673-1691, doi:10.5194/acp-16-1673-2016, 2016.](#)
- 21 Garland, R. M., Yang, H., Schmid, O., Rose, D., Nowak, A., Achtert, P., Wiedensohler, A.,
22 Takegawa, N., Kita, K., Miyazaki, Y., Kondo, Y., Hu, M., Shao, M., Zeng, L. M., Zhang, Y. H.,
23 Andreae, M. O., and Pöschl, U.: Aerosol optical properties in a rural environment near the
24 mega-city Guangzhou, China: implications for regional air pollution, radiative forcing and
25 remote sensing, *Atmos. Chem. Phys.*, 8, 5161–5186, doi:10.5194/acp-8-5161-2008, 2008.
- 26 Garland, R. M., Schmid, O., Nowak, A., Achtert, P., Wiedensohler, A., Gunthe, S. S., Takegawa, N.,
27 Kita, K., Kondo, Y., Hu, M., Shao, M., Zeng, L. M., Zhu, T., Andreae, M. O., and Pöschl, U.:
28 Aerosol optical properties observed during Campaign of Air Quality Research in Beijing 2006
29 (CAREBeijing-2006): characteristic differences between the inflow and outflow of Beijing city
30 air, *J. Geophys. Res.*, 114, D00g04, doi:10.1029/2008jd010780, 2009.
- 31 [Gustafssona, Ö., and Ramanathan, V.: Convergence on climate warming by black carbon aerosols,](#)
32 [*Proc. Nat. Acad. Sci. USA*, doi: 10.1073/pnas.1603570113, 2016.](#)
- 33 Guo, S., Hu, M., Zamora, M. L., Peng, J., Shang, D., Zheng, J., Du, Z., Wu, Z., Shao, M., Zeng, L.,
34 Molina, M. J., and Zhang, R.: Elucidating severe urban haze formation in China, *P. Natl. Acad.*
35 *Sci. USA*, 111, 17373–17378, 2014.
- 36 Han, B., Zhang, R., Yang, W., Bai, Z., Ma, Z., and Zhang, W.: Heavy air pollution episodes in
37 Beijing during January 2013: inorganic ion chemistry and source analysis using Highly Time-
38 Resolved Measurements in an urban site, *Atmos. Chem. Phys. Discuss.*, 15, 11111–11141,
39 doi:10.5194/acpd-15-11111-2015, 2015.
- 40 Han, L., Zhou, W., and Li, W.: Increasing impact of urban fine particles (PM_{2.5}) on areas
41 surrounding Chinese cities, *Scientific Reports*, 5, 12467, doi:10.1038/srep12467, 2015.
- 42 Han, T. T., Liu, X. G., Zhang, Y. H., Qu, Y., Gu, J. W., Ma, Q., Lu, K. D., Tian, H. Z., Chen, J.,
43 Zeng, L. M., Hu, M., and Zhu, T.: Characteristics of aerosol optical properties and their
44 chemical apportionments during CAREBeijing 2006, *Aerosol Air Qual. Res.*, 14, 1431–1442,

1 2014.

2 Hand, J. L., and Malm, W. C.: Review of aerosol mass scattering efficiencies from ground-based
3 measurements since 1990, *J. Geophys. Res.*, 112, D16203, doi:10.1029/2007JD008484, 2007.

4 Hasan, H. and Dzubay, T. G.: Apportioning light extinction coefficients to chemical species in
5 atmospheric aerosol, *Atmos. Environ.*, 17, 1573–1581, 1983.

6 ~~He, X., Li, C. C., Lau, A. K. H., Deng, Z. Z., Mao, J. T., Wang, M. H., and Liu, X. Y.: An intensive
7 study of aerosol optical properties in Beijing urban area, *Atmos. Chem. Phys.*, 9, 8903–8915,
8 doi:10.5194/acp-9-8903-2009, 2009.~~

9 Huang, R. J., Zhang, Y., Bozzetti, C., Ho, K.-F., Cao, J., Han, Y., Dällenbach, K. R., Slowik, J. G.,
10 Platt, S. M., Canonaco, F., Zotter, P., Wolf, R., Pieber, S. M., Bruns, E. A., Crippa, M., Ciarelli,
11 G., Piazzalunga, A., Schwikowski, M., Abbaszade, G., Schnelle-Kreis, J., Zimmermann, R.,
12 An, Z., Szidat, S., Baltensperger, U., Haddad, I. E., and Prévôt, A. S. H.: High secondary
13 aerosol contribution to particulate pollution during haze events in China, *Nature*, 514, 218–222,
14 2014.

15 [Jansen, R.C., Shi, Y., Chen, J., Hu, Y., Xu, C., Hong, S., Li, J., and Zhang, M.: Using hourly
16 measurements to explore the role of secondary inorganic aerosol in PM_{2.5} during haze and fog
17 in Hangzhou, China, *Adv. Atmos. Sci.*, 31, 1427 - 1434, 2014.](#)

18 Jung, J., Lee, H., Kim, Y. J., Liu, X. G., Zhang, Y. H., Hu, M., and Sugimoto, N.: Optical properties
19 of atmospheric aerosols obtained by in situ and remote measurements during 2006 Campaign
20 of Air Quality Research in Beijing (CAREBeijing-2006), *J. Geophys. Res.*, 114, D00g02,
21 doi:10.1029/2008jd010337, 2009.

22 [Knox, A., Evans, G. J., Brook, J. R., Yao, X., Jeong, C. H., Godri, K. J., Sabaliauskas, K., and
23 Slowik, J. G. : Mass absorption cross-section of ambient black carbon aerosol in relation to
24 chemical age, *Aerosol Sci. Technol.*, 43, 522 - 532, 2009.](#)

25 [Lack, D. A., Langridge, J. M., Bahreini, R., Cappa, C. D., Middlebrook, A. M., and Schwarz, J. P. :
26 Brown carbon and internal mixing in biomass burning particles, *Proc. Nat. Acad. Sci. USA*,
27 109, 14802 - 14807, 2012.](#)

28 [Lan, Z.-J., Huang, X.-F., Yu, K.-Y., Sun, T.-L., Zeng, L.-W., and Hu, M.: Light absorption of black
29 carbon aerosol and its enhancement by mixing state in an urban atmosphere in South China,
30 *Atmos. Environ.*, 69, 118 - 123, 2013.](#)

31 Lei, Y., Zhang, Q., He, K. B., and Streets, D. G.: Primary anthropogenic aerosol emission trends for
32 China, 1990–2005, *Atmos. Chem. Phys.*, 11, 931–954, doi:10.5194/acp-11-931-2011, 2011.

33 [Lim, H.-J., and Turpin B. J. : Origins of primary and secondary organic aerosol in Atlanta: Results of
34 time-resolved measurements during the Atlanta supersite experiment, *Environ. Sci. Technol.*,
35 36, 4489–4496, 2002.](#)

36 [Lin, P., Hu, M., Deng, Z., Slanina, J., Han, S., Kondo, Y., Takegawa, N., Miyazaki, Y., Zhao, Y., and
37 Sugimoto N. : Seasonal and diurnal variations of organic carbon in PM_{2.5} in Beijing and the
38 estimation of secondary organic carbon, *J. Geophys. Res.*, 114, D00G11,
39 doi:10.1029/2008JD010902, 2009.](#)

40 [Liu, S., Aiken, A.C., Gorkowski, K., Dubey, M.K., Cappa, C.D., Williams, L.R., Herndon, S.C.,
41 Massoli, P., Fortner, E.C., Chhabra, P.S., Brooks, W.A., Onasch, T.B., Jayne, J.T., Worsnop,
42 D.R., China, S., Sharma, N., Mazzoleni, C., Xu, L., Ng, N.L., Liu, D., Allan, J.D., Lee, J.D.,
43 Fleming, Z.L., Mohr, C., Zotter, P., Szidat, S., and Prevot, A.S.H.: Enhanced light absorption
44 by mixed source black and brown carbon particles in UK winter, *Nat. Commun.*, 6, 8435,](#)

- 1 [2015.](#)
- 2 [Liu, X. G., Li, J., Qu, Y., Han, T., Hou, L., Gu, J., Chen, C., Yang, Y., Liu, X., Yang, T., Zhang, Y.,](#)
- 3 [Tian, H., and Hu, M.: Formation and evolution mechanism of regional haze: a case study in the](#)
- 4 [megacity Beijing, China, Atmos. Chem. Phys., 13, 4501–4514, doi:10.5194/acp-13-4501-2013,](#)
- 5 [2013.](#)
- 6 ~~[Li, C., Marufu, L. T., Dickerson, R. R., Li, Z., Wen, T., Wang, Y., Wang, P., Chen, H., and Stehr,](#)~~
- 7 ~~[J.W.: In situ measurements of trace gases and aerosol optical properties at a rural site in](#)~~
- 8 ~~[northern China during East Asian Study of Tropospheric Aerosols: an international regional](#)~~
- 9 ~~[experiment 2005, J. Geophys. Res., 112, D22S04, doi:10.1029/2006jd007592, 2007.](#)~~
- 10 ~~[Li, L., Chen, J. M., Wang, L., Melluki, W., and Zhou, H. R.: Aerosol single scattering albedo](#)~~
- 11 ~~[affected by chemical composition: an investigation using CRDS combined with MARGA,](#)~~
- 12 ~~[Atmos. Res., 124, 149–157, doi:10.1016/j.atmosres.2012.11.007, 2013.](#)~~
- 13 Lyamani, H., Olmo, F. J., and Alados-Arboledas, L.: Physical and optical properties of aerosols over
- 14 an urban location in Spain: seasonal and diurnal variability, Atmos. Chem. Phys., 10, 239–254,
- 15 doi:10.5194/acp-10-239-2010, 2010.
- 16 Mack, L. A., Levin, E. J. T., Kreidenweis, S. M., Obrist, D., Moosmüller, H., Lewis, K. A., Arnott,
- 17 W. P., McMeeking, G. R., Sullivan, A. P., Wold, C. E., Hao, W.-M., Collett Jr., J. L., and
- 18 Malm, W. C.: Optical closure experiments for biomass smoke aerosols, Atmos. Chem. Phys.,
- 19 10, 9017–9026, doi:10.5194/acp-10-9017-2010, 2010.
- 20 Malm, W. C. and Hand, J. L.: An examination of the physical and optical properties of aerosols
- 21 collected in the IMPROVE program, Atmos. Environ., 41, 3407–3427,
- 22 doi:10.1016/j.atmosenv.2006.12.012, 2007.
- 23 Malm, W. C., Sisler, J. F., Huffman, D., Eldred, R. A., and Cahill, T. A.: Spatial and seasonal trends
- 24 in particle concentration and optical extinction in the United States, J. Geophys. Res., 99,
- 25 1347–1370, doi:10.1029/93jd02916, 1994.
- 26 Marley, N. A., Gaffney, J. S., Castro, T., Salcido, A., and Frederick, J.: Measurements of aerosol
- 27 absorption and scattering in the Mexico City Metropolitan Area during the MILAGRO field
- 28 campaign: a comparison of results from the T0 and T1 sites, Atmos. Chem. Phys., 9, 189–206,
- 29 doi:10.5194/acp-9-189-2009, 2009.
- 30 [Moise, T., Flores, J.M., and Rudich, Y.: Optical Properties of Secondary Organic Aerosols and Their](#)
- 31 [Changes by Chemical Processes, Chem. Rev., 115, 4400 - 4439, 2015.](#)
- 32 [Nakayama, T., Sato, K., Matsumi, Y., Imamura, T., Yamazaki, A., and Uchiyama, A.: Wavelength and](#)
- 33 [NOx dependent complex refractive index of SOAs generated from the photooxidation of](#)
- 34 [toluene, Atmos. Chem. Phys., 13, 531-545, doi:10.5194/acp-13-531-2013, 2013.](#)
- 35 Nel, A.: Atmosphere. Air pollution-related illness: effects of particles, Science, 308, 804–806, 2005.
- 36 [Peng, J., Hua, M., Guo, S., Du, Z., Zheng, J., Shang, D., Zamora, M. L., Zeng, L., Shao, M., Wu,](#)
- 37 [Y.-S., Zheng, J., Wang, Y., Glen, C. R., Collins, D. R., Molina, M. J., and Zhang, R. : Markedly](#)
- 38 [enhanced absorption and direct radiative forcing of black carbon under polluted urban](#)
- 39 [environments, Proc. Nat. Acad. Sci. USA, doi: 10.1073/pnas.1602310113, 2016.](#)
- 40 Peterson, M. R. and Richards, M. H.: Thermal-optical-transmittance analysis for organic, elemental,
- 41 carbonate, total carbon, and OCX2 in PM_{2.5} by the EPA/NIOSH method, in: Proceedings,
- 42 Symposium on Air Quality Measurement Methods and Technology-2002, San Fran- cisco,
- 43 California, 13–15 November 2002, edited by: Winegar, E. D. and Tropp, R. J., Air and Waste
- 44 Management Association, Pittsburgh, PA, 83-1–83-19, 2002.

- 1 Pettersson, A., Lovejoy, E. R., Brock, C. A., Brown, S. S., and Ravishankara, A. R.: Measurement of
2 aerosol optical extinction at with pulsed cavity ring down spectroscopy, *J. Aerosol Sci.*, 35,
3 995–1011, 2004.
- 4 Pitchford, M., Malm, W., Schichtel, B., Kumar, N., Lowenthal, D., and Hand, J.: Revised algorithm
5 for estimating light extinction from IMPROVE particle speciation data, *J. Air Waste Manage.*,
6 57, 1326–1336, doi:10.3155/1047-3289.57.11.1326, 2007.
- 7 Quan, J. N., Tie, X., Zhang, Q., Liu, Q., Li, X., Gao, Y., and Zhao, D. L.: Characteristics of heavy
8 aerosol pollution during the 2012–2013 winter in Beijing, China, *Atmos. Environ.*, 88, 83–89,
9 doi:10.1016/j.atmosenv.2014.01.058, 2014.
- 10 Quinn, P. K.: Aerosol optical properties measured on board the Ronald H. Brown during ACEAsia as
11 a function of aerosol chemical composition and source region, *J. Geophys. Res.- Atmos*, 109,
12 D19S01, doi:10.1029/2003JD004010, 2004.
- 13 Quinn, P. K., Coffman, D. J., Bates, T. S., Miller, T. L., Johnson, J. E., Voss, K., Welton, E. J., and
14 Neususs, C.: Dominant aerosol chemical components and their contribution to extinction
15 during the aerosols cruise across the Atlantic, *J. Geophys. Res.-Atmos*, 106, 20783–20809,
16 doi:10.1029/2000jd900577, 2001.
- 17 Quinn, P. K., Coffman, D. J., Bates, T. S., Miller, T. L., Johnson, J. E., Welton, E. J., Neususs, C.,
18 Miller, M., and Sheridan, P. J.: Aerosol optical properties during INDOEX 1999: means,
19 variability, and controlling factors, *J. Geophys. Res.-Atmos*, 107, 8020,
20 doi:10.1029/2000jd000037, 2002.
- 21 Raes, F., Bates, T., McGovern, F., and Van Liedekerke, M.: The 2nd Aerosol Characterization
22 Experiment (ACE-2): general overview and main results, *Tellus B*, 52, 111–125,
23 doi:10.1034/j.1600-0889.2000.00124.x, 2000. Ramanathan, V., Crutzen, P. J., Kiehl, J. T., and
24 Rosenfeld, D.: Aerosols, climate, and the hydrological cycle, *Science*, 294, 2119–2124, 2001.
- 25 Ramanathan, V., Crutzen, P. J., Kiehl, J. T., and Rosenfeld, D.: Aerosols, Climate and the
26 Hydrological Cycle, *Science*, 294, 2119–2124, 2001.
- 27 Ryerson, T. B., Andrews, A. E., Angevine, W. M., Bates, T. S., Brock, C. A., Cairns, B., Cohen, R.
28 C., Cooper, O. R., de Gouw, J. A., Fehsenfeld, F. C., Ferrare, R. A., Fischer, M. L., Flagan, R.
29 C., Goldstein, A. H., Hair, J. W., Hardesty, R. M., Hostetler, C. A., Jimenez, J. L., Langford, A.
30 O., McCauley, E., McKeen, S. A., Molina, L. T., Nenes, A., Oltmans, S. J., Parrish, D. D.,
31 Pederson, J. R., Pierce, R. B., Prather, K., Quinn, P. K., Seinfeld, J. H., Senff, C. J., Sorooshian,
32 A., Stutz, J., Surratt, J. D., Trainer, M., Volkamer, R., Williams, E. J., and Wofsy, S. C.: The
33 2010 California Research at the Nexus of Air Quality and Climate Change (CalNex) field study,
34 *J. Geophys. Res.*, 118, 5830–5866, doi:10.1002/Jgrd.50331, 2013.
- 35 ~~Sun, K., Qu, Y., Wu, Q., Han, T. T., Gu, J. W., Zhao, J. J., Sun, Y. L., Jiang, Q., Gao, Z. Q., Hu, M.,~~
36 ~~Zhang, Y. H., Lu, K. S. D., Nordmann, S., Cheng, Y. F., Hou, L., Ge, H., Furuuchi, M., Hata,~~
37 ~~M., and Liu, X. G.: Chemical characteristics of size-resolved aerosols in winter in Beijing, *J.*~~
38 ~~*Environ. Sci.*, 26, 1641–1650, 2014.~~
- 39 Sun, Y. L., Wang, Z. F., Fu, P. Q., Yang, T., Jiang, Q., Dong, H. B., Li, J., and Jia, J. J.: Aerosol
40 composition, sources and processes during wintertime in Beijing, China, *Atmos. Chem. Phys.*,
41 13, 4577–4592, doi:10.5194/acp-13-4577-2013, 2013.
- 42 Sun, Y. L., Jiang, Q., Wang, Z. F., Fu, P. Q., Li, J., Yang, T., and Yin, Y.: Investigation of the
43 sources and evolution processes of severe haze pollution in Beijing in January 2013, *J.*
44 *Geophys. Res.-Atmos*, 119, 4380–4398, doi:10.1002/2014jd021641, 2014.

- 1 Sun, Y. L., Wang, Z. F., Du, W., Zhang, Q., Wang, Q. Q., Fu, P. Q., Pan, X. L., Li, J., Jayne, J., and
2 Worsnop, D. R.: Long-term real-time measurements of aerosol particle composition in Beijing,
3 China: seasonal variations, meteorological effects, and source analysis, *Atmos. Chem. Phys.*
4 *Discuss.*, 15, 14549–14591, doi:10.5194/acpd-15-14549-2015, 2015.
- 5 Takegawa, N., Miyakawa, T., Kuwata, M., Kondo, Y., Zhao, Y., Han, S., Kita, K., Miyazaki, Y.,
6 Deng, Z., Xiao, R., Hu, M., van Pinxteren, D., Herrmann, H., Hofzumahaus, A., Holland, F.,
7 Wahner, A., Blake, D. R., Sugimoto, N., and Zhu, T.: Variability of submicron aerosol
8 observed at a rural site in Beijing in the summer of 2006, *J. Geophys. Res.*, 114, D00g05,
9 doi:10.1029/2008jd010857, 2009.
- 10 Tao, J., Ho, K. F., Chen, L. G., Zhu, L. H., Han, J. L., and Xu, Z. C.: Effect of chemical composition
11 of PM_{2.5} on visibility in Guangzhou, China, 2007 spring, *Partic.*, 7, 68–75,
12 doi:10.1016/j.partic.2008.11.002, 2009.
- 13 Tao, J., Zhang, L., Cao, J., Hsu, S.-C., Xia, X., Zhang, Z., Lin, Z., Cheng, T., and Zhang, R.:
14 Characterization and source apportionment of aerosol light extinction in Chengdu, southwest
15 China, *Atmos. Environ.*, 95, 552–562, doi:10.1016/j.atmosenv.2014.07.017, 2014a.
- 16 Tao, J., Zhang, L., Ho, K., Zhang, R., Lin, Z., Zhang, Z., Lin, M., Cao, J., Liu, S., and Wang, G.:
17 Impact of PM_{2.5} chemical compositions on aerosol light scattering in Guangzhou—the largest
18 megacity in South China, *Atmos. Res.*, 135, 48–58, doi:10.1016/j.atmosres.2013.08.015,
19 2014b.
- 20 Tao, J., Zhang, L. S. M., Gao, J., Wang, H., Chai, F. H., Wang, S. L.: Aerosol chemical composition
21 and light scattering during a winter season in Beijing, *Atmos. Environ.*, 110, 36–44,
22 doi:10.1016/j.atmosenv.2015.03.037, 2015.
- 23 [Tian, M., Wang, H. B., Chen, Y., Yang, F. M., Zhang, X. H., Zou, Q., Zhang, R. Q., Ma, Y. L., and](#)
24 [He, K. B.: Characteristics of aerosol pollution during heavy haze events in Suzhou, China,](#)
25 [Atmos. Chem. Phys. Discuss.](#), 15, 33407–33443, doi:10.5194/acpd-15-33407-2015, 2015.
- 26 [Tian, S. L., Pan, Y. P., and Wang, Y. S.: Size-resolved source apportionment of particulate matter in](#)
27 [urban Beijing during haze and non-haze episodes, Atmos. Chem. Phys.](#), 16, 1–19,
28 [doi:10.5194/acp-16-1-2016, 2016.](#)
- 29 Thompson, J. E., Hayes, P. L., Jimenez, J. L., Adachi, K., Zhang, X., Liu, J., Weber, R. J., and
30 Buseck, P. R.: Aerosol optical properties at Pasadena, CA during CalNex 2010, *Atmos.*
31 *Environ.*, 55, 190–200, doi:10.1016/j.atmosenv.2012.03.011, 2012.
- 32 ~~Titos, G., Foyo-Moreno, I., Lyamani, H., Querol, X., Alastuey, A., and Alados-Arboledas, L.:~~
33 ~~Optical properties and chemical composition of aerosol particles at an urban location: an~~
34 ~~estimation of the aerosol mass scattering and absorption efficiencies, J. Geophys. Res.~~, 117,
35 ~~D04206, doi:10.1029/2011jd016671, 2012.~~
- 36 Turpin, B. J. and Lim, H. J.: Species contributions to PM_{2.5} mass concentrations: revisiting common
37 assumptions for estimating organic mass, *Aerosol Sci. Tech.*, 35, 602–610,
38 doi:10.1080/02786820119445, 2001.
- 39 Varma, R., Moosmüller, H., and Arnott, W. P.: Toward an ideal integrating nephelometer, *Opt. Lett.*,
40 28, 1007–1009, 2003.
- 41 Wang, L., Li, Z., Tian, Q., Ma, Y., Zhang, F., Zhang, Y., Li, D., Li, K., and Li L.: Estimate of
42 aerosol absorbing components of black carbon, brown carbon, and dust from ground-based
43 remote sensing data of sun-sky radiometers, *J. Geophys. Res. Atmos.*, 118, 6534–6543,
44 doi:10.1002/jgrd.50356, 2013.

- 1 [Wang, Q., Huang, R.-J., Cao, J., Han, Y., Wang, G., Li, G., Wang, Y., Dai, W., Zhang, R., and Zhou,](#)
2 [Y.: Mixing state of black carbon aerosol in a heavily polluted urban area of China: implications](#)
3 [for light absorption enhancement, *Aerosol Sci. Technol.*, 48, 689 - 697, 2014.](#)
- 4 Wang, X., Huang, J., Zhang, R., Chen, B., and Bi, J.: Surface measurements of aerosol properties
5 over northwest China during ARM China 2008 deployment, *J. Geophys. Res.*, 115, D00K27,
6 doi:10.1029/2009JD013467, 2010.
- 7 Wang, X. F., Wang, T., Pathak, R. K., Hallquist, M., Gao, X. M., Nie, W., Xue, L. K., Gao, J., Gao,
8 R., Zhang, Q. Z., Wang, W. X., Wang, S. L., Chai, F. H., and Chen, Y. Z.: Size distributions of
9 aerosol sulfates and nitrates in Beijing during the 2008 Olympic Games: impacts of pollution
10 control measures and regional transport, *Adv. Atmos. Sci.*, 30, 341–353, 2013.
- 11 Wang, Y. H., Liu, Z. R., Zhang, J. K., Hu, B., Ji, D. S., Yu, Y. C., and Wang, Y. S.: Aerosol
12 physicochemical properties and implications for visibility during an intense haze episode
13 during winter in Beijing, *Atmos. Chem. Phys.*, 15, 3205–3215, doi:10.5194/acp-15-3205-2015,
14 2015.
- 15 Watson, J. G.: Visibility: science and regulation, *J. Air Waste Manage.*, 52, 628–713, 2002.
- 16 Wu, Q. Z., Wang, Z. F., Gbaguidi, A., Gao, C., Li, L. N., and Wang, W.: A numerical study of
17 contributions to air pollution in Beijing during CAREBeijing-2006, *Atmos. Chem. Phys.*, 11,
18 5997–6011, doi:10.5194/acp-11-5997-2011, 2011.
- 19 Wu, Z. J., Zheng, J., Shang, D. J., Du, Z. F., Wu, Y. S., Zeng, L. M., Wiedensohler, A., and Hu, M.:
20 Particle hygroscopicity and its link to chemical composition in the urban atmosphere of Beijing,
21 China during summertime, *Atmos. Chem. Phys. Discuss.*, 15, 11495–11524,
22 doi:10.5194/acpd-15-11495-2015, 2015.
- 23 Xu, J., Ma, J. Z., Zhang, X. L., Xu, X. B., Xu, X. F., Lin, W. L., Wang, Y., Meng, W., and Ma, Z. Q.:
24 Measurements of ozone and its precursors in Beijing during summertime: impact of urban
25 plumes on ozone pollution in downwind rural areas, *Atmos. Chem. Phys.*, 11, 12241–12252,
26 doi:10.5194/acp-11-12241-2011, 2011.
- 27 Xu, X., Zhao, W., Wang, S., Zhang, Q., Qian, X., Fang, B., Venables, D. S., Chen, W., Gao, X., and
28 Zhang, W.: Retrieval of the particulate complex refractive index by using cavity enhanced
29 aerosol albedometer, in preparation, 2016.
- 30 ~~Yan, P., Tang, J., Huang, J., Mao, J. T., Zhou, X. J., Liu, Q., Wang, Z. F., and Zhou, H. G.: The~~
31 ~~measurement of aerosol optical properties at a rural site in Northern China, *Atmos. Chem.*~~
32 ~~*Phys.*, 8, 2229–2242, doi:10.5194/acp-8-2229-2008, 2008.~~
- 33 Yang, L. X., Wang, D. C., Cheng, S. H., Wang, Z., Zhou, Y., Zhou, X. H., and Wang, W. X.:
34 Influence of meteorological conditions and particulate matter on visual range impairment in
35 Jinan, China, *Sci. Total Environ.*, 383, 164–173, doi:10.1016/j.scitotenv.2007.04.042, 2007.
- 36 ~~Yang, Y. R., Liu, X. G., Qu, Y., An, J. L., Jiang, R., Zhang, Y. H., Sun, Y. L., Wu, Z. J., Zhang, F.,~~
37 ~~Xu, W. Q., and Ma, Q. X.: Characteristics and formation mechanism of continuous hazes in~~
38 ~~China: a case study during the autumn of 2014 in the North China Plain, *Atmos. Chem. Phys.*,~~
39 ~~15, 8165–8178, doi:10.5194/acp-15-8165-2015, 2015.~~
- 40 Yao, T., Huang, X., He, L., Hu, M., Sun, T., Xue, L., Lin, Y., Zeng, L., and Zhang, Y.: High time
41 resolution observation and statistical analysis of atmospheric light extinction properties and the
42 chemical speciation of fine particulates, *Sci. China Chem.*, 53, 1801–1808,
43 doi:10.1007/s11426-010-4006-z, 2010.
- 44 Zhang, A., Qi, Q. W., Jiang, L. L., Zhou, F., and Wang, J. F.: Population exposure to PM_{2.5} in the

- 1 urban area of Beijing, PLoS One, 8, e63486, 2013.
- 2 Zhang, H., Hu, D., Chen, J., Ye, X., Wang, X., Hao, J., Wang, L., Zhang, R., and An, Z.: Particle
3 size distribution and polycyclic aromatic hydrocarbons emissions from agricultural crop
4 residue burning, *Environ. Sci. Technol.*, 45, 5477–5482, 2011.
- 5 Zhang, X., Lin, Y. H., Surratt, J. D., and Weber, R. J.: Sources, composition and absorption
6 Angstrom exponent of light-absorbing organic components in aerosol extracts from the Los
7 Angeles Basin, *Environ. Sci. Technol.*, 47, 3685–3693, doi:10.1021/es305047b, 2013.
- 8 Zhang, Y. H., Hu, M., Zhong, L. J., Wiedensohler, A., Liu, S. C., Andreae, M. O., Wang, W., and
9 Fan, S. J.: Regional Integrated Experiments on Air Quality over Pearl River Delta 2004
10 (PRIDE-PRD2004): overview, *Atmos. Environ.*, 42, 6157–6173,
11 doi:10.1016/j.atmosenv.2008.03.025, 2008.
- 12 Zhao, W., Dong, M., Chen, W., Gu, X., Hu, C., Gao, X., Huang, W., and Zhang, W.:
13 Wavelengthresolved optical extinction measurements of aerosols using broad-band
14 cavity-enhanced absorption spectroscopy over the spectral range of 445–480 nm, *Anal. Chem.*,
15 85, 2260–2268, doi:10.1021/ac303174n, 2013.
- 16 Zhao, W., Xu, X., Dong, M., Chen, W., Gu, X., Hu, C., Huang, Y., Gao, X., Huang, W., and Zhang,
17 W.: Development of a cavity-enhanced aerosol albedometer, *Atmos. Meas. Tech.*, 7,
18 2551–2566, doi:10.5194/amt-7-2551-2014, 2014a.
- 19 Zhao, W., Xu, X., Dong, M., Chen, W., Gao, X., Huang, W., and Zhang, W.: Development of a
20 cavity-enhanced albedometer for simultaneous measurement of aerosol extinction and
21 scattering coefficients, in *imaging and applied optics 2014*, OSA Technical Digest (online)
22 (Optical Society of America), paper JTU4A.43, 2014b.
- 23 Zhao, X. J., Zhao, P. S., Xu, J., Meng, W., Pu, W. W., Dong, F., He, D., and Shi, Q. F.: Analysis of a
24 winter regional haze event and its formation mechanism in the North China Plain, *Atmos.*
25 *Chem. Phys.*, 13, 5685–5696, doi:10.5194/acp-13-5685-2013, 2013.
- 26 Zheng, G. J., Duan, F. K., Su, H., Ma, Y. L., Cheng, Y., Zheng, B., Zhang, Q., Huang, T., Kimoto, T.,
27 Chang, D., Pöschl, U., Cheng, Y. F., and He, K. B.: Exploring the severe winter haze in Beijing:
28 the impact of synoptic weather, regional transport and heterogeneous reactions, *Atmos. Chem.*
29 *Phys.*, 15, 2969–2983, doi:10.5194/acp-15-2969-2015, 2015.
- 30 Zheng, S., Pozzer, A., Cao, C. X., and Lelieveld, J.: Long-term (2001–2012) concentrations of fine
31 particulate matter (PM_{2.5}) and the impact on human health in Beijing, China, *Atmos. Chem.*
32 *Phys.*, 15, 5715–5725, doi:10.5194/acp-15-5715-2015, 2015.
- 33 ~~Zhou, X. H., Gao, J., Wang, T., Wu, W. S., and Wang, W. X.: Measurement of black carbon aerosols~~
34 ~~near two Chinese megacities and the implications for improving emission inventories, *Atmos.*~~
35 ~~*Environ.*, 43, 3918–3924, doi:10.1016/j.atmosenv.2009.03.062, 2009.~~
- 36
- 37
- 38
- 39

1
2
3
4
5
6
7
8
9

Table 1. List of the mean optical values (aerosol extinction, scattering, absorption coefficients, and SSA at $\lambda = 470$ nm), the effective mode diameters (particle number, surface area and volume, fitted values from the measured submicron size distribution with mono-lognormal distribution function), and chemical composition of PM_{1.0} particles observed in this campaign. These parameters were classified into three different pollution levels (clear, slightly polluted and polluted days).

Parameter	Clear	Slightly Polluted	Polluted	All days	
Optical	$\alpha_{ep,470}$ (Mm ⁻¹)	58.6±81.6	186.7±161.6	567.9±292.3	200.9±239.6
	$\alpha_{sp,470}$ (Mm ⁻¹)	47.2±64.7	148.9±131.9	477.2±255.5	163.9±201.7
	$\alpha_{ap,470}$ (Mm ⁻¹)	11.6±18.3	37.8±32.3	90.9±55.8	37.0±43.2
	ω_{470}	0.81±0.10	0.79±0.07	0.84±0.06	0.80±0.08
Size	$D_{p,n}$ (nm)	38±31	73±51	120±64	67±55
	$D_{p,s}$ (nm)	374±130	338±114	335±76	351±116
	$D_{p,v}$ (nm)	478±94	480±90	455±82	475±91
Chemical Composition ($\mu\text{g}/\text{m}^3$)	OC	3.41±2.43	8.81±4.64	20.47±6.93	8.34±6.97
	EC	0.48±0.39	1.18±0.59	2.72±0.87	1.12±0.92
	NO ₃ ⁻	1.78±1.70	5.12±3.56	14.99±6.54	5.19±5.52
	SO ₄ ²⁻	1.29±0.69	3.20±2.25	9.62±4.55	3.35±3.52
	NH ₄ ⁺	0.72±0.75	2.98±2.32	9.31±4.33	2.98±3.57
	Cl ⁻	0.52±0.96	1.48±1.41	4.46±2.26	1.52±1.88
	Ca ²⁺	0.31±0.27	0.62±0.38	0.58±0.33	0.49±0.36
	K ⁺	0.16±0.25	0.50±0.38	1.18±0.46	0.46±0.48
	Na ⁺	0.19±0.22	0.33±0.28	0.60±0.38	0.32±0.30
	Mg ²⁺	0.04±0.03	0.08±0.03	0.09±0.03	0.06±0.04

10

11 Table 2. List of aerosol mean diameters and optical properties during the selected haze episode.

12

13

14

Episode	Date (LT)	Number mean diameter (nm)	Surface mean diameter (nm)	$\alpha_{ep,470}$ (Mm ⁻¹)	$\alpha_{sp,470}$ (Mm ⁻¹)	$\alpha_{ap,470}$ (Mm ⁻¹)	ω_{470}	Real part of effective CRI (n)	Imaginary part of effective CRI (k)
Period 1	22 Nov 05:40–10:00	56±6	193±19	56±24	44±19	12±6	0.79±0.03	1.38±0.06	0.03±0.02
Period 2	22 Nov 12:40–15:00	25±4	193±17	17±5	16±5	1.0±0.4	0.94±0.03	1.40±0.06	0.008±0.005
Period 3	22 Nov 15:30–23 Nov 08:00	106±16	229±16	179±69	151±57	28±12	0.85±0.01	1.39±0.04	0.02±0.006
Period 4	23 Nov 08:30–12:00	105±16	251±15	405±60	321±42	84±22	0.79±0.03	1.40±0.03	0.034±0.008
Period 5	23 Nov 12:30–24 Nov 07:30	124±19	263±11	330±110	283±94	46±16	0.86±0.01	1.44±0.03	0.02±0.01
Period 6	24 Nov 08:00–11:10	80±42	226±14	80±42	64±34	16±8	0.78±0.04	1.40±0.04	0.04±0.02

15

16

17

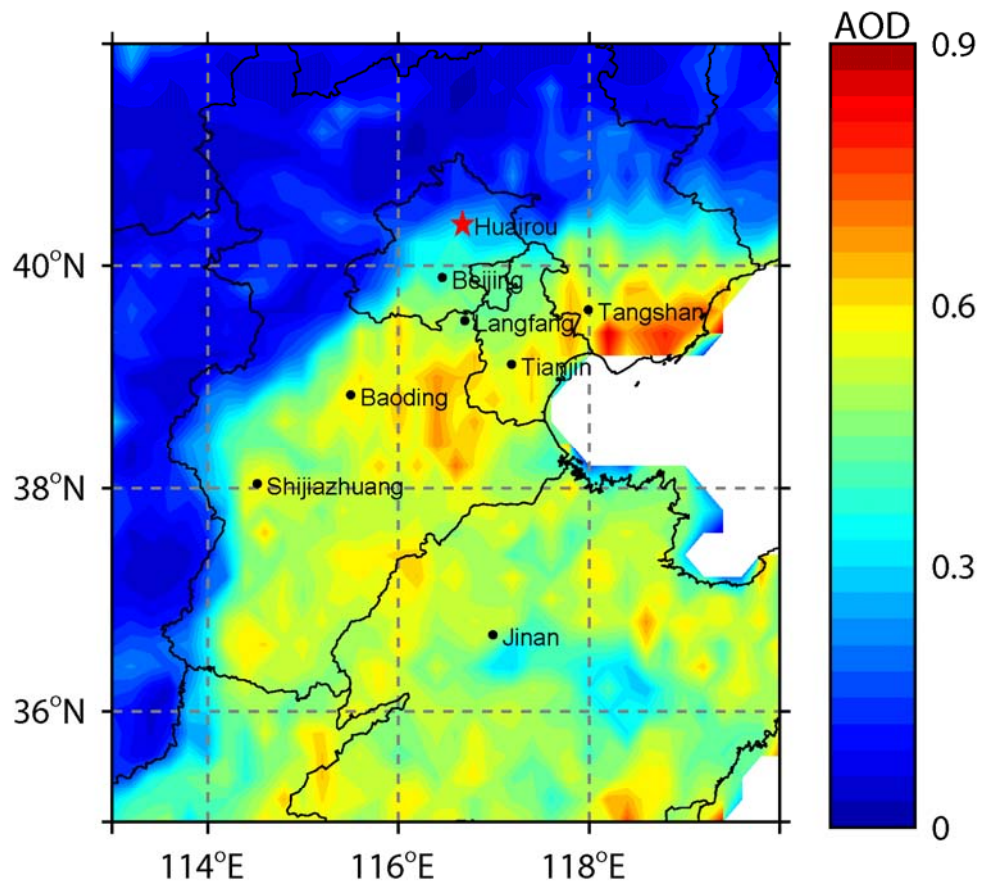
18 Table 3. List of the mean values of aerosol scattering, absorption coefficients, and single scattering albedo in this campaign and recently reported
 19 values from references.

20

Location	Date (MM/yy)	λ (nm)	α_{sp} (Mm^{-1})	α_{ap} (Mm^{-1})	ω_0	RH	Inlet	References
Granada, Spain (Urban)	03/2006–02/2007	$\alpha_{sp} \div 550$ $\alpha_{ap} \div 550$	61±25	24±9	0.71±0.07	<50%	PM ₁₀	Titos et al.(2012)
Guangzhou (Urban)	07/2006	$\alpha_{sp} \div 550$ $\alpha_{ap} \div 532$	151±103	34±27	0.82±0.07	<40%	PM ₁₀	Garland et al.(2008)
Beijing (Urban)	01/2005–12/2006	$\alpha_{sp} \div 525$ $\alpha_{ap} \div 532$	255±243	45±39	0.80±0.09	<60%	TSP	He et al.(2009)
Shanghai (Urban)	04–05/2010	$\alpha_{sp} \div 532\#$ $\alpha_{ap} \div 532$	102±74	44±35	0.70±0.07	41.2%	TSP	Li et al.(2013)
Xinken, PRD (Suburban)	10/2004–11/2004	$\alpha_{sp} \div 550$ $\alpha_{ap} \div 630$	333±138	70±42	0.83±0.05	<20%	PM ₁₀	Cheng et al.(2008)
Xianghe, Beijing (Suburban)	03/2005	$\alpha_{sp} \div 550$ $\alpha_{ap} \div 550$	468±472	65±75	0.81–0.85	<42.5%	TSP	Li et al.(2007)
Yufa, Beijing (Suburban)	08/2006–09/2006	$\alpha_{sp} \div 550$ $\alpha_{ap} \div 532$	361±295	52±37	0.86±0.07	<32%	PM ₁₀	Garland et al.(2009)
Huairou, Beijing (Suburban)	11/2014–01/2015	$\alpha_{sp} \div 470$ $\alpha_{ap} \div 470$	164±202	37±43	0.80±0.08	<15%	PM _{1.0}	This work
Shangdianzi, Beijing (Rural)	09/2003–01/2005	$\alpha_{sp} \div 525$ $\alpha_{ap} \div 525$	175±189	18±13	0.88±0.05	<60%	TSP	Yan et al.(2008)
Pasadena, US (Rural)	05/2010–06/2010	$\alpha_{sp} \div 532\#$ $\alpha_{ap} \div 532$	58±43	4±4	0.92±0.08	<50%	PM _{1.0}	Thompson et al.(2012)

21

22

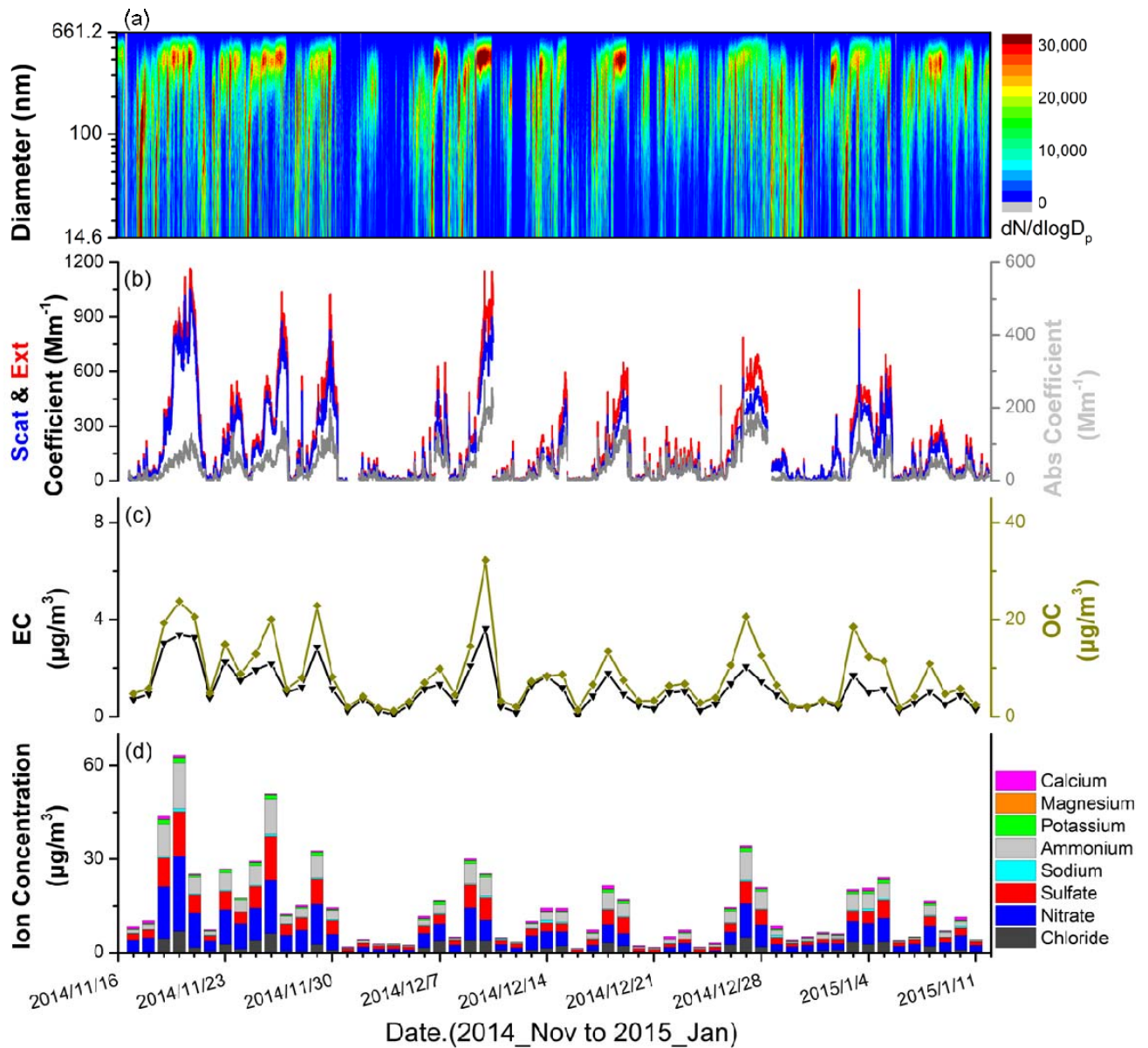


23
 24
 25
 26
 27
 28
 29
 30

Fig. 1. The map of the North China Plain. The observation site (Huairou) is marked with red star. The contour plot represents the average distribution of the MODIS AOD with $0.2^{\circ} \times 0.2^{\circ}$ resolution during the campaign (16 November 2014 to 11 January 2015).

31

32



33

34

35

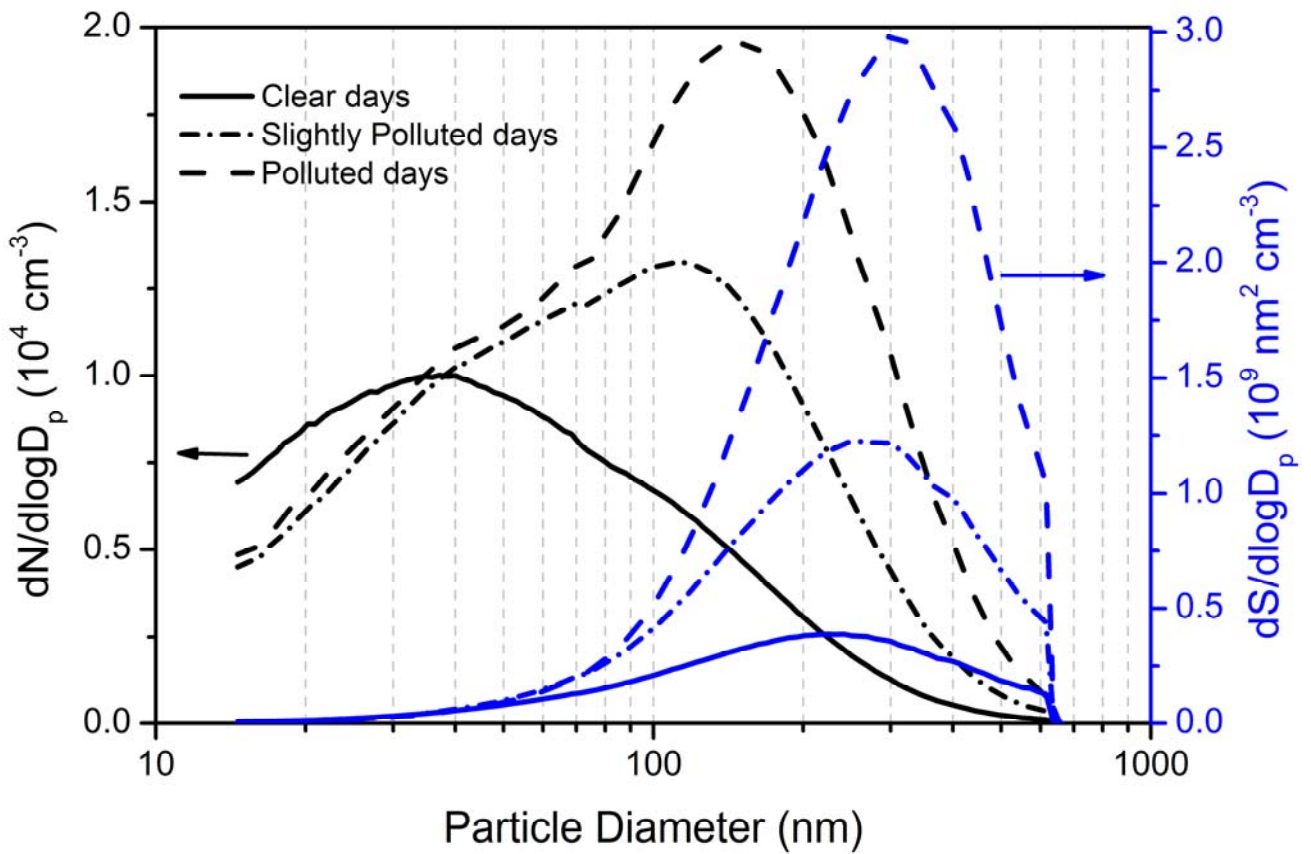
36

37 Fig. 2. Time series of (a) the aerosol number size distribution measured by SMPS, (b) the extinction,
 38 scattering and absorption coefficients at $\lambda = 470$ nm measured by cavity enhanced albedometer, (c)
 39 organic carbon and element carbon concentration measured with an off-line aerosol carbon analyzer,
 40 and (d) water-insoluble ion concentrations measured with an off-line ion chromatography of dry
 41 PM_{1.0} particles over the sampling period.

42

43

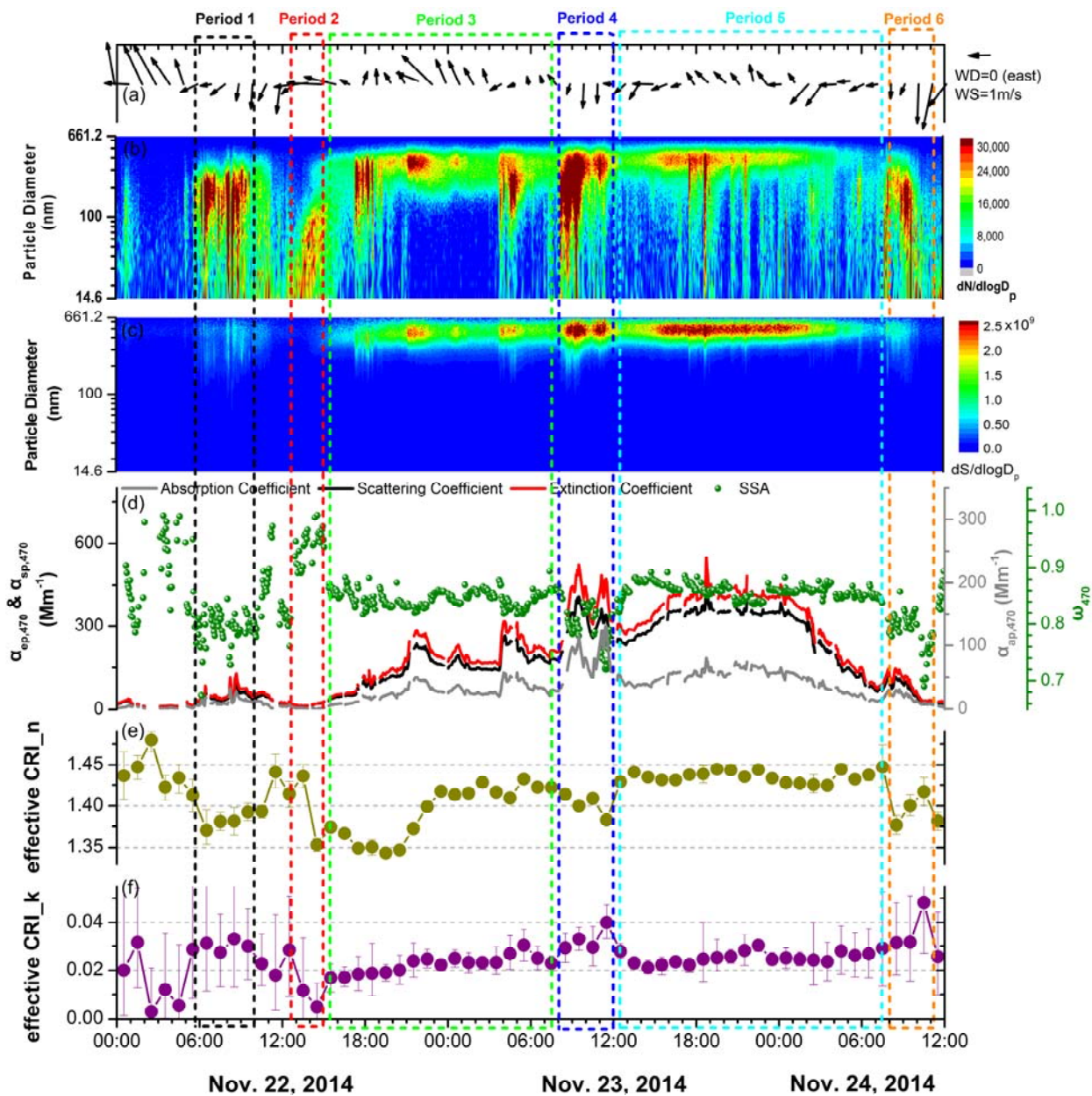
44
45
46
47
48
49
50
51
52
53



54
55
56
57
58
59
60
61
62
63

Fig. 3 The mean number and surface size distribution of ambient aerosol on clear, slightly polluted and polluted days.

64
65

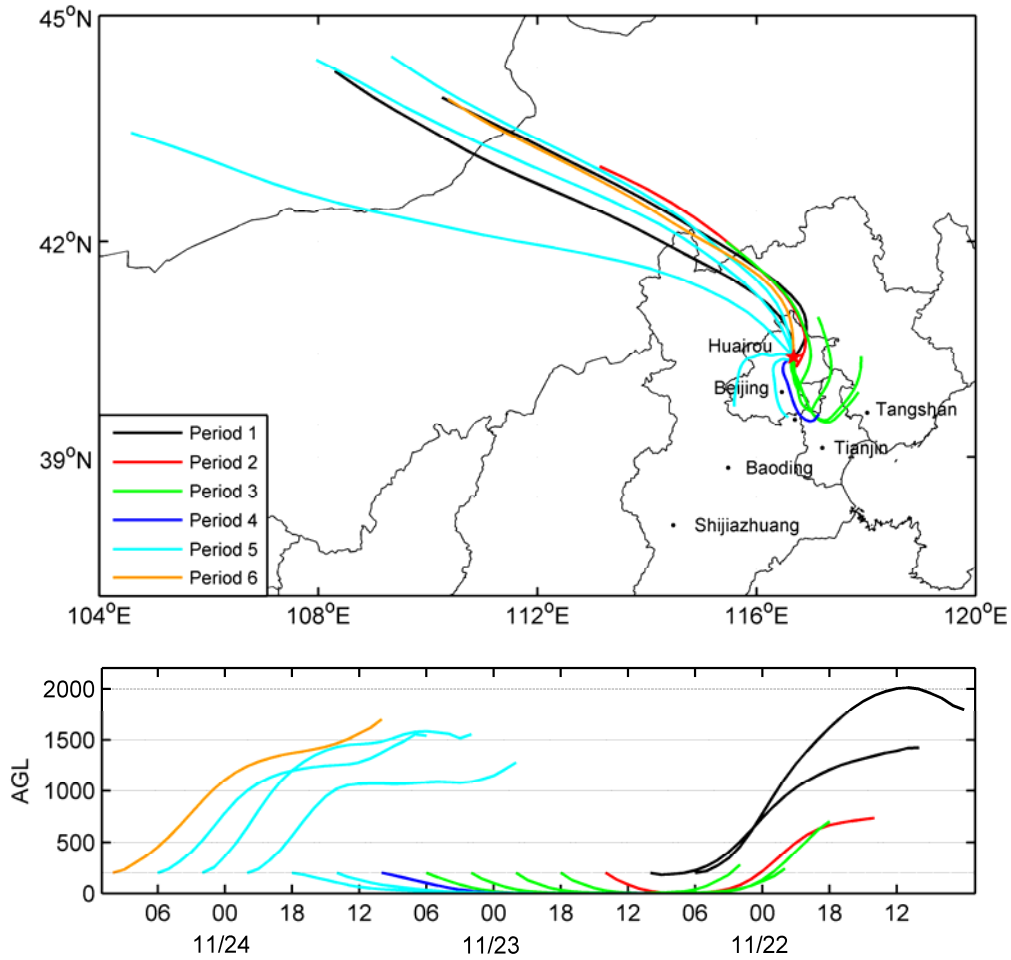


66
67
68
69

70 | Fig. 3-4 Highly time-resolved evolution of a selected air pollution episode during November 22 to 24,
71 2014. (a) particle number size distribution, (b) particle surface size distribution, (c) aerosol extinction,
72 scattering, absorption coefficients, and SSA at $\lambda = 470$ nm, (d) retrieved real part of CRI, (e)
73 retrieved imaginary part of CRI. The air pollution episode was divided into six shorter periods to
74 clearly show the evaluation of optical properties during haze formation, development and decline.

75
76

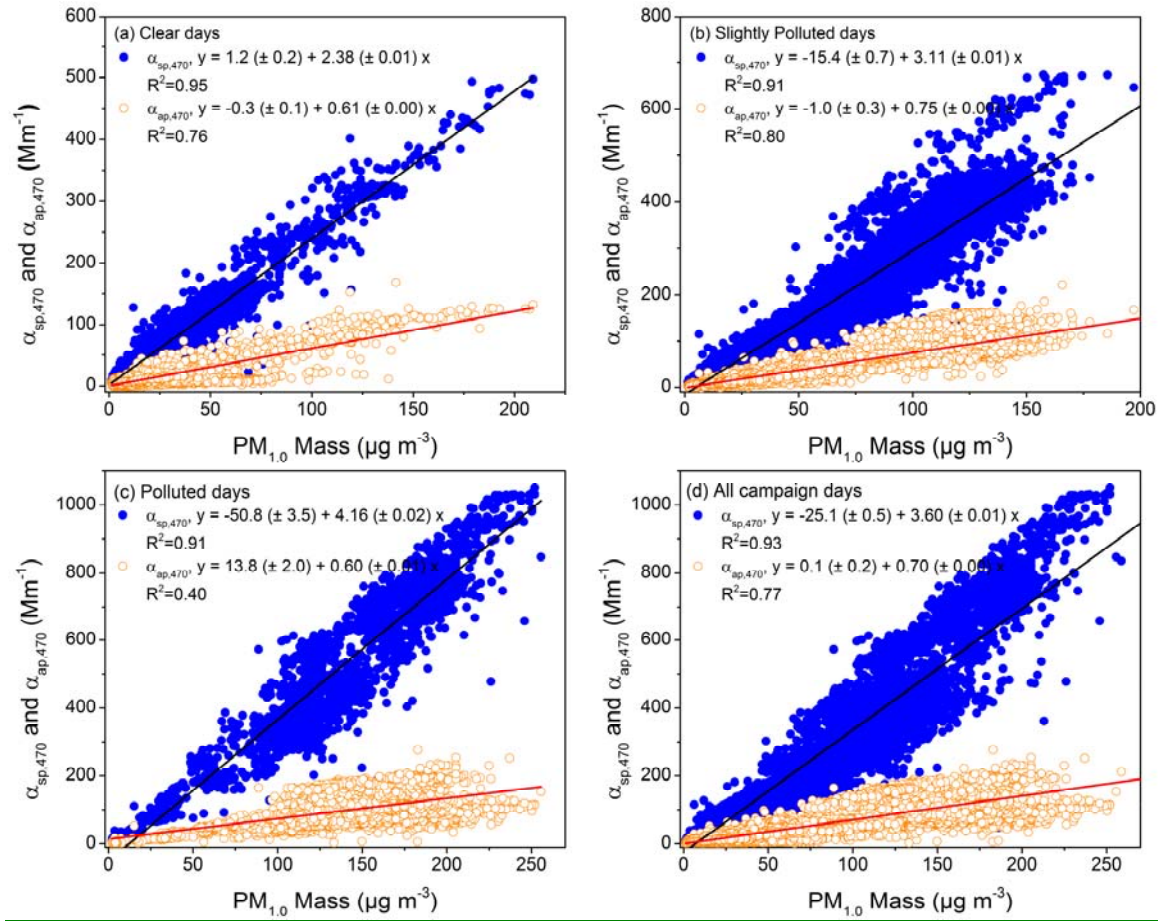
77
78
79
80



81
82
83
84
85
86
87
88
89
90
91
92
93
94

Fig. 4-5 The 24 hour back trajectories starting at 200 m above ground level in Huairou site were calculated every 4 h (at 00:00, 06:00, 12:00 and 18:00 local time) during the selected air pollution episode.

95
96
97
98
99

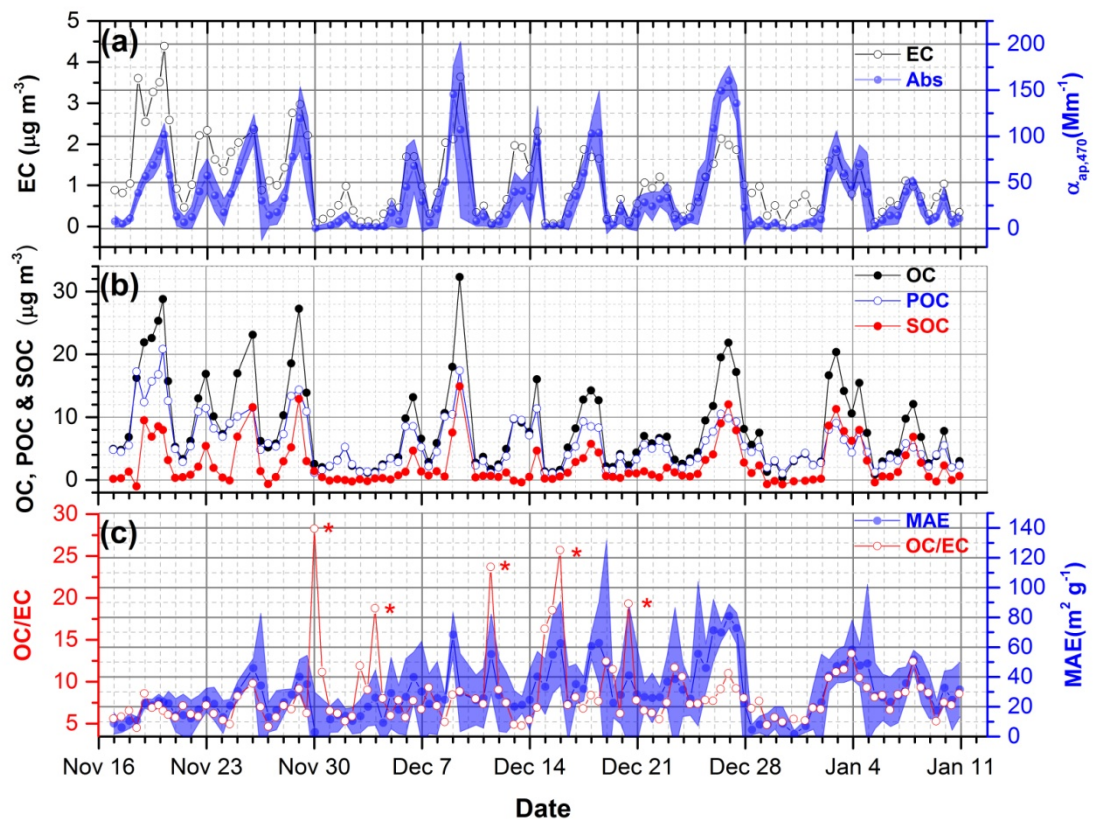


100
101
102
103
104
105
106
107

[Fig. 6](#)

108 [Scatter plots of the measured scattering and absorption coefficients at \$\lambda = 470\$ nm against \$PM_{1.0}\$ mass](#)
109 [concentrations for \$PM_{1.0}\$ particles under different pollution level.](#)

110
111
112
113
114
115
116
117
118
119

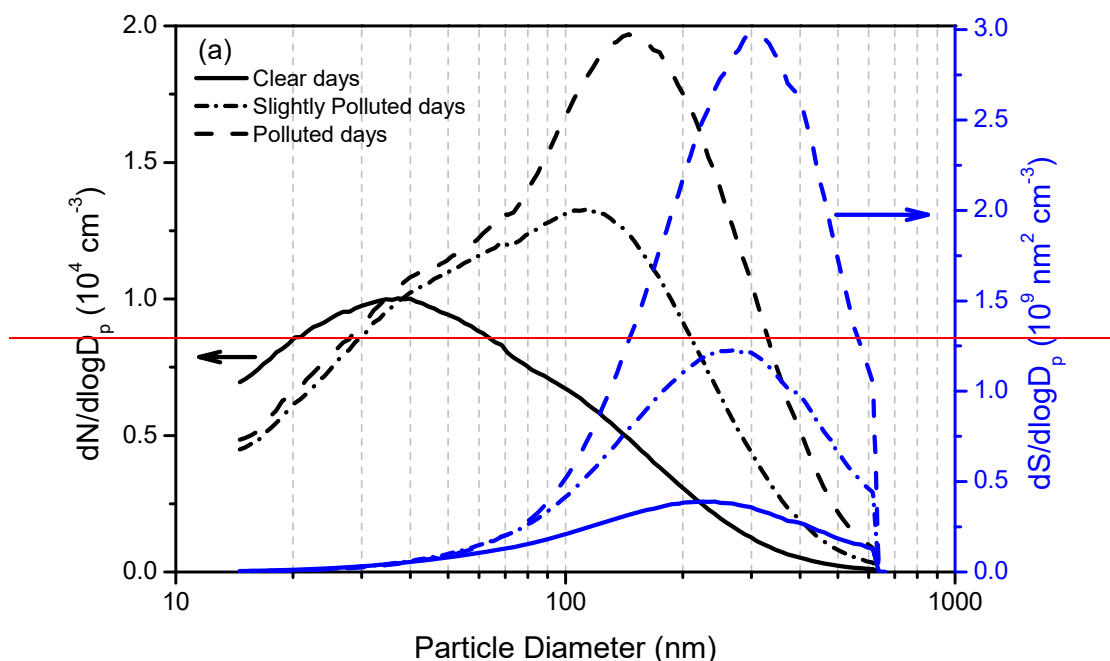


120
121
122
123
124

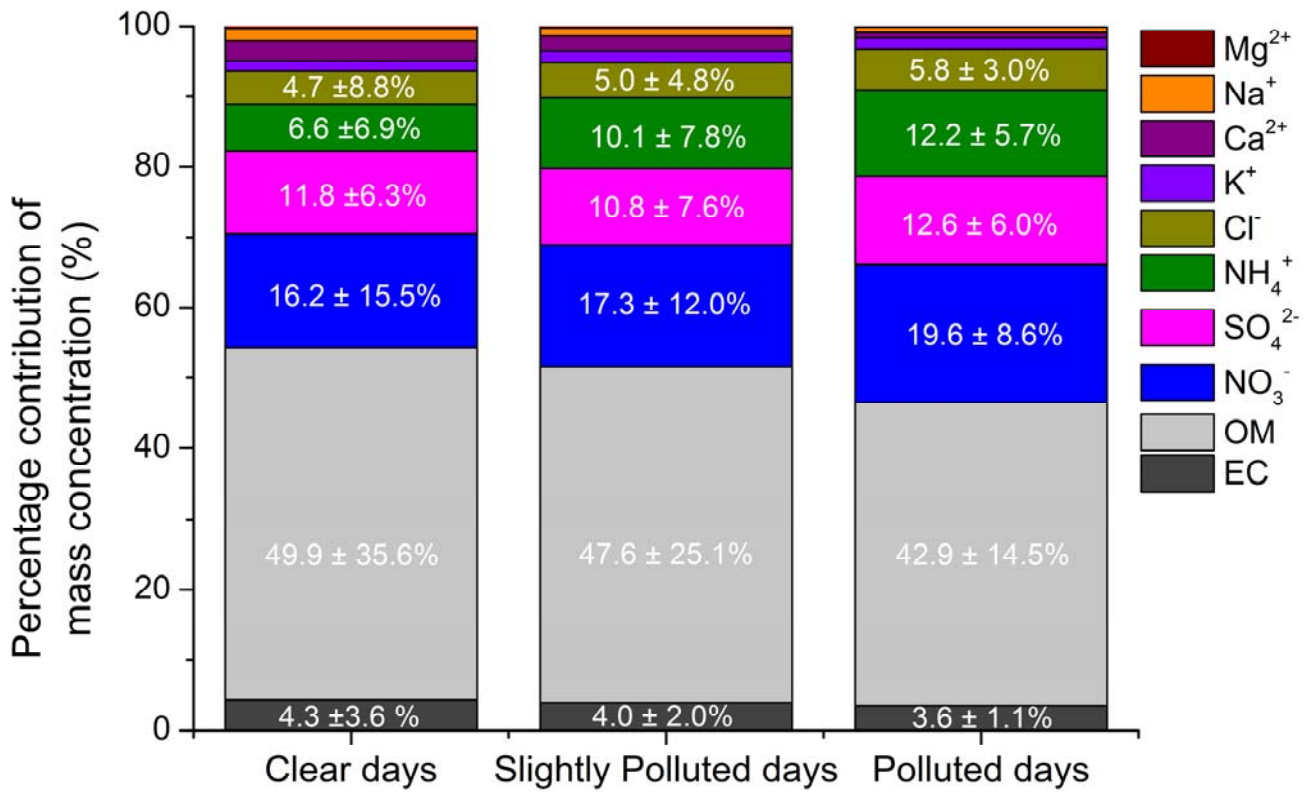
125

126 Fig. 7 Time series of (a) the measured EC mass concentrations and absorption coefficients at $\lambda = 470$
127 nm; (b) the measured OC mass concentrations, and the estimated primary OC (POC) and secondary
128 OC (SOC) mass concentrations determined with the EC-tracer method (Lim and Turpin, 2002; Lin et
129 al., 2009; Cheng et al., 2011, the details of the calculation method are given in the Supplement,
130 Section S7.). (c) the MAE values of EC and OC to EC ratio (OC/EC). The MAE was calculated by
131 dividing the measured absorption coefficient by the measured concentration of EC. The blue shaded
132 areas indicate the standard deviation. The red stars associated with unusually high values in (c) may
133 arised from artifacts arising from sampling or handling of the filter.

134



135



136

137

138

139

140

141

142

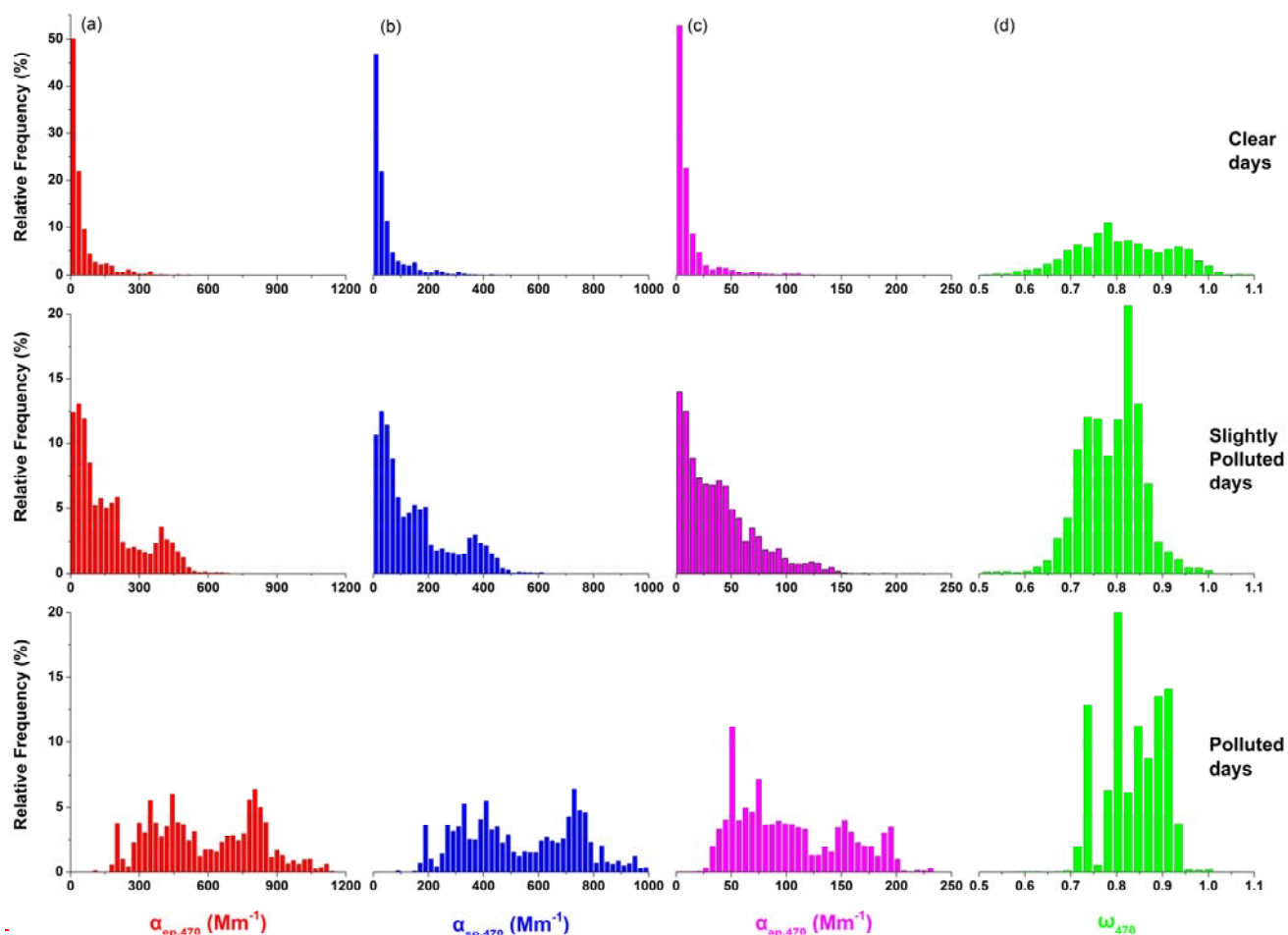
143

144 Fig. 5-8 (a) ~~The mean number and surface size distribution and (b)~~ percentage contribution of the
 145 mass concentrations of OM, EC concentrations and eight water-soluble ion components on clear,
 146 slightly polluted and polluted days.

147

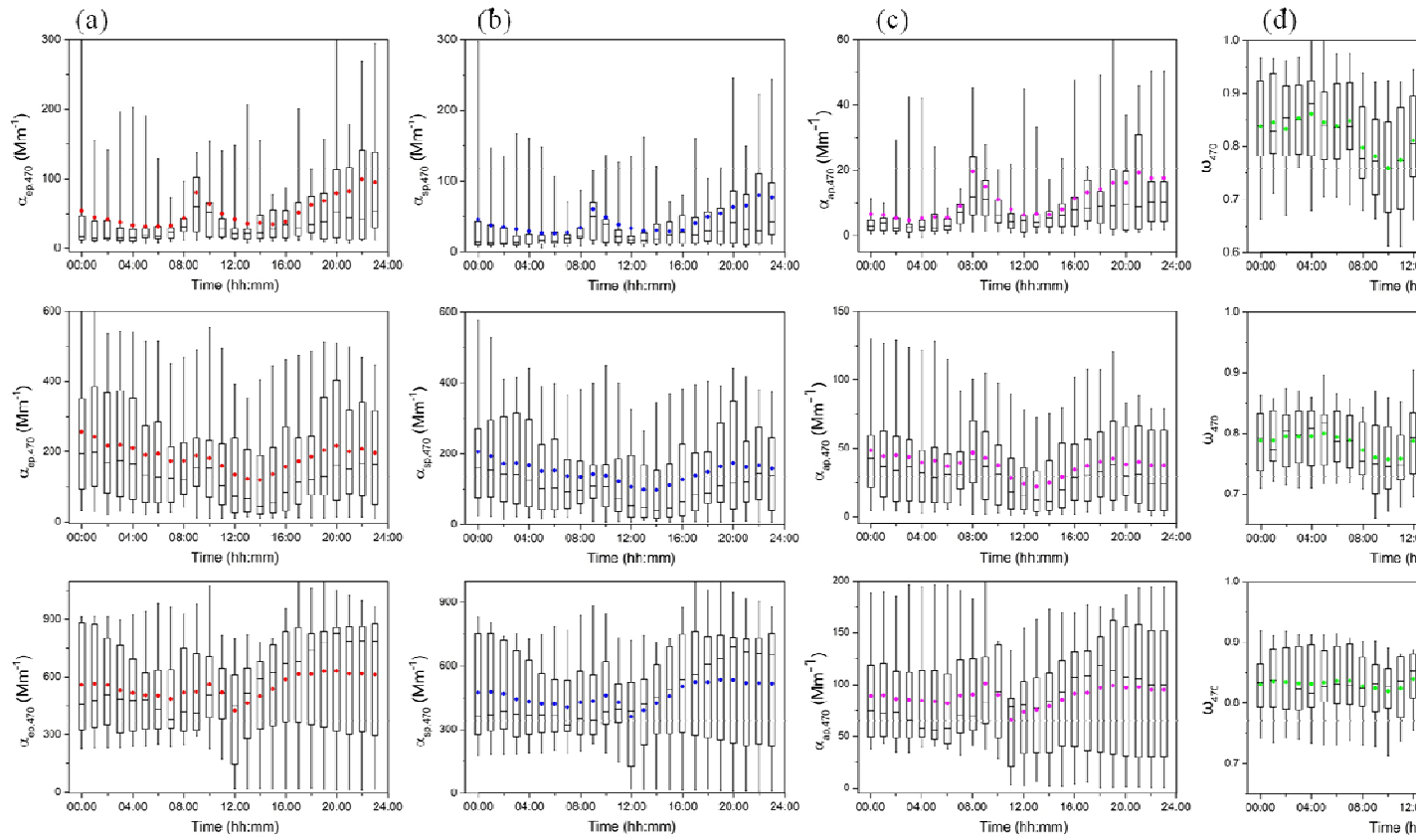
148

149
150
151



152
153
154
155
156
157
158
159
160
161

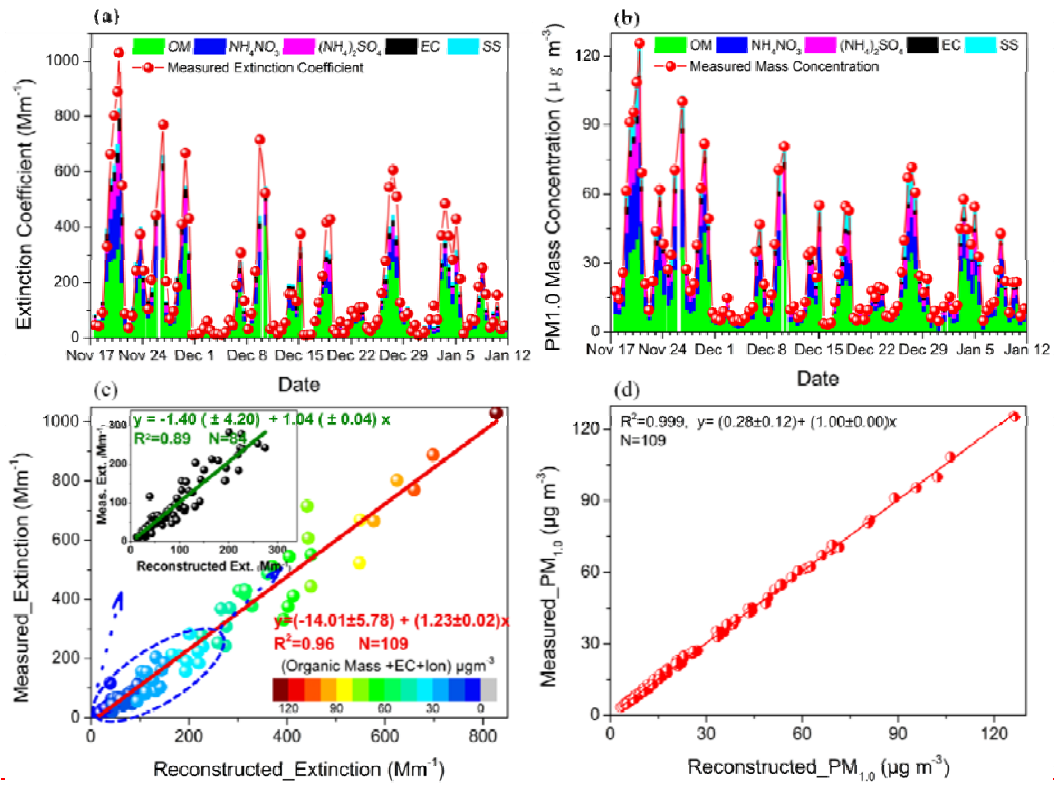
Fig 6. The frequency distributions of dry $PM_{1.0}$ optical properties at $\lambda = 470$ nm observed during the campaign. (a) extinction coefficient, (b) scattering coefficient, (c) absorption coefficient, (d) single scattering albedo on clear, slightly polluted and polluted days.



162
163
164
165
166
167

Fig. 7 Diurnal variations of hourly averaged (a) extinction coefficient, (b) scattering coefficient, (c) absorption coefficient and (d) SSA at $\lambda = 470$ nm on clear, slightly polluted and polluted days. The error bars are 5th and 95th percentiles and the limits of the boxes represent 25th and 75th percentiles.

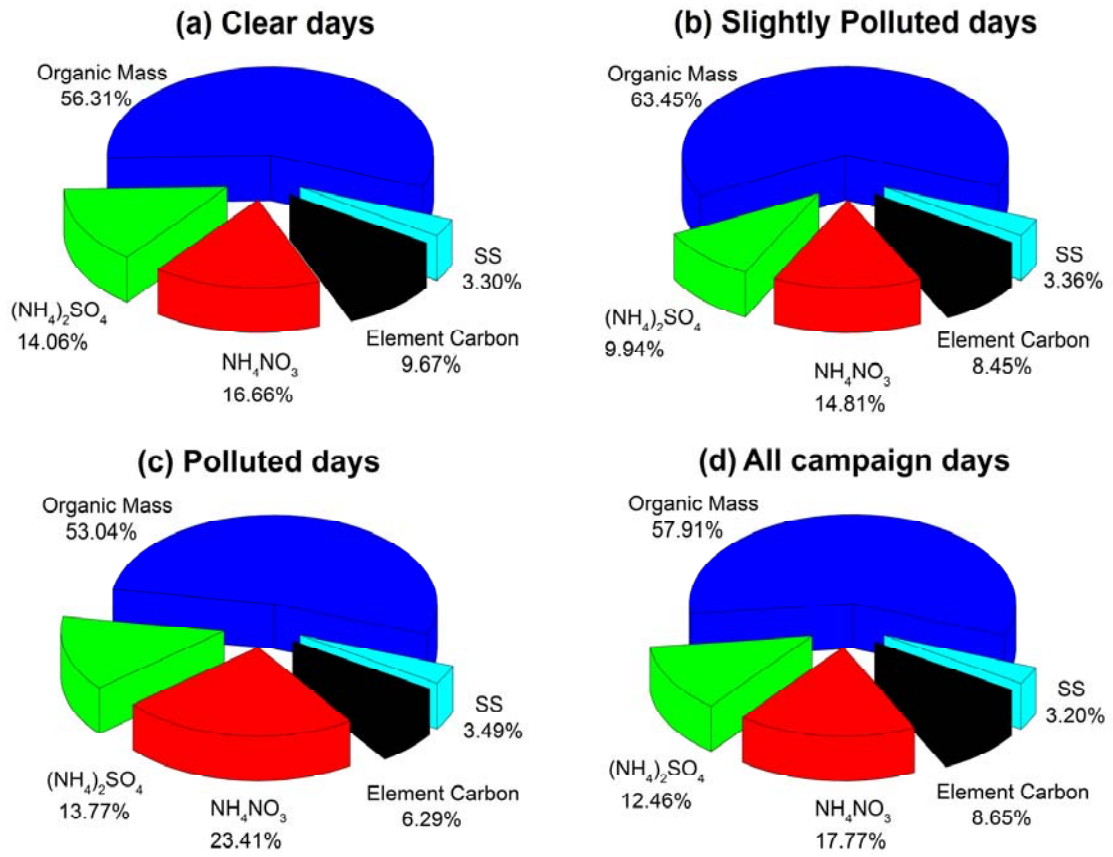
168
 169
 170
 171
 172



173
 174
 175
 176
 177
 178
 179
 180
 181
 182
 183
 184
 185

Fig. 8 (a) and (b) : The plot of measured and reconstruction value of the extinction and mass concentration, respectively; (c) and (d) : Scatter plot of the measured extinction coefficient at $\lambda = 470$ nm and $PM_{1.0}$ mass concentration against the reconstructed values with the modified IMPROVE formula. Insert of (c) shows the linear regression between measured and reconstructed extinction coefficient under lower aerosol load condition (with extinction smaller than $300 Mm^{-1}$).

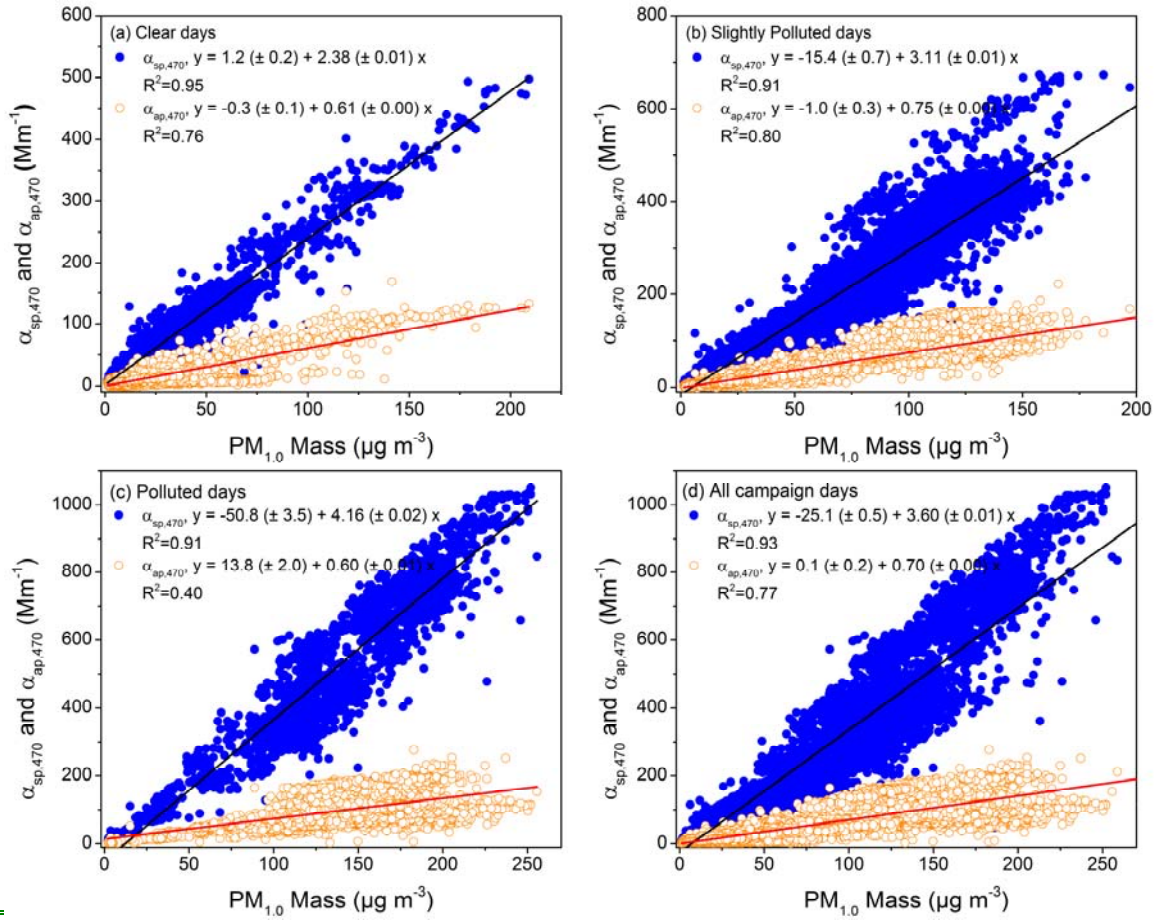
186
187
188
189



190
191
192
193
194
195
196
197
198
199
200

Fig. 9 Average fractional contribution of each chemical composition to dry $\text{PM}_{1.0}$ extinction coefficient with respect to different pollution level.

201
 202
 203
 204
 205
 206



207
 208
 209
 210
 211